REGIONAL MODEL DEVELOPMENT FOR SIMULATING ATMOSPHERIC BEHAVIOUR AND RAINFALL OVER SOUTHERN AFRICA

CJ de W Rautenbach · FA Engelbrecht · T Ndarana ·
CJ Engelbrecht · JL McGregor

WRC Report No. 1261/1/05

Water Research Commission

REGIONAL MODEL DEVELOPMENT FOR SIMULATING ATMOSPHERIC BEHAVIOUR AND RAINFALL OVER SOUTHERN AFRICA

by

C. J. de W. Rautenbach,

F.A. Engelbrecht, T. Ndarana, C.J. Engelbrecht and J.L. McGregor

Department of Geography, Geoinformatics and Meteorology

Faculty of Natural and Agricultural Sciences

University of Pretoria

Pretoria

FINAL REPORT

to the Water Research Commission

PROJECT NO. 1261/1/05
ISBN NO. 1-77005-332-8

2005

Disclaimer

This report emanates from a project financed by the Water Research Commission (WRC) and is approved for publication. Approval does not signify that the contents necessarily reflect the views and policies of the WRC or the members of the project steering committee, nor does mention of trade names or commercial products constitute endorsement or recommendation for use.

Printed by Silowa Printers: 012 804 1164

ACKNOWLEDGEMENTS

The authors of this report wishes to express their appreciation to the following people and organizations for their contribution and assistance:

1. The *Water Research Commission* for funding the research, and in particular, *Dr George Green* for his guidance.
2. The Steering Committee for their advice during the project:
   Prof B Hewitson, *Prof C Reason*, *Mr S. van Biljon*, *Mr S Naido*
3. *Dr Jack Katzfey, Dr Martin Dix* and *Dr Kim Nguyen* for their continued support and time during our many visits to the *CSIRO Atmospheric Research* in Melbourne, Australia.
4. *Ms Jennifer Jones*, *Ms Marinda Dobson*, *Dr Emsie Klopper* and *Dr Willem Landman* for their support in organizing the two workshops held as part of the project.
5. The *Centre for Environmental Studies (CFES)* at the University of Pretoria for their support and interest in the project.
6. All the *SADC delegates* (and their institutions) who not only attended the workshops, but also participated by presenting papers.
7. The *University of Pretoria* that who provided the logistics, and in particular *Ms Rita Snyders* for the research support.
8. All the students from the *Laboratory for Research and Training in Atmospheric Modelling* (*LRAM* – a project initiative) who developed project results as part of their studies in model development and climate research.

TABLE OF CONTENTS

EXECUTIVE SUMMARY

1. INTRODUCTION

Since the first attempt to utilise numerical methods for predicting weather was made by the British scientist Lewis Fry Richardson (1882-1953), many scientists accepted the challenge to produce improved methods for simulating atmospheric processes and flow. The motivation for these efforts was primarily manifested through the benefits they would hold for short-term planning (daily Numerical Weather Prediction (NWP) and air pollution modelling), seasonal risk analysis (seasonal forecasting) and early warning of the need to adapt to possible variations in the climate system (future climate change projections).

Apart from predicting the day-to-day weather, modern computerised numerical models of the atmospheric circulation have been used for many other purposes. Today numerical atmospheric models are applied in:

- Assimilation of the present state of the atmosphere for use as initial conditions in NWP models and routine air pollution research.
- Short-term NWP that involves day-to-day weather forecasting.
- Climate variability research and product generation that includes sensitivity studies and studies on longer-term forecasting, such as seasonal forecasting.
- Possible future climate change estimations, such as future climate scenarios linked to enhanced greenhouse gas concentrations.

With the training in dynamic meteorology and numerical techniques available at the University of Pretoria, and the capacity existing at South African research institutions to perform their own model simulations, the question was being asked whether South African research institutions should not also become involved in model development. The possibility of developing a unique atmospheric model on African soil by African researchers was also being mentioned. Modern atmospheric models are in an advanced stage with sophisticated numerical approaches and parameterizations. These models had been developed over years, and it would therefore not be easy to start developing a totally new model. South African scientists interested in numerical modeling would, however, benefit significantly from close collaboration with, and involvement in, international modeling efforts. These thoughts inspired the research initiatives and achievements discussed in this report.

2. AIMS OF THE PROJECT

Objectives of the research presented in this report may be summarized as follows:

- To modify the dynamic formulation and physical parameterization schemes of internationally competitive regional atmospheric circulation models in order to improve the simulation of water-related atmospheric variables over South Africa.
- To equip scientists and prospective students from the South Africa and southern African community with the necessary knowledge and skills to develop, maintain and use the regional atmospheric models by means of innovative water research training.

3. RESEARCH APPROACH

The research was conducted in collaboration with international institutions and the objectives were achieved by following two well defined research routes.

3.1 Research route 1

Research route one aimed to improve model simulated rainfall patterns over South Africa. This is in line with the research objective to improve the simulation of water related atmospheric variables over South Africa. The WRC research team performed many simulations on local workstations in order to verify different model versions on a regular basis. Model rainfall biases were identified and CSIRO-AR researchers were notified. Researchers at the CSIRO-AR then adjusted / improved rainfall parameterization schemes in the model code, where after the improved code was sent back to the WRC research team for further verification. This process of code exchange took place for almost three years, meaning that a large number of model simulations were executed on local workstations.

3.2 Research route 2

Research route two consisted of two components. (1) In the first place an unique non-hydrostatic kernel was developed by the WRC research team in South Africa. Many tests were performed in the form of the release of thermal bubbles in the model atmosphere, thereby also opening up the opportunity to add other components (radiation budget, surface characteristics, moisture and rainfall etc.) to the kernel to develop a more comprehensive model. (2) The dynamics developed were used as guideline for making C-CAM non-hydrostatic at the CSIRO-AR. This task was completed during a visit of a WRC researcher to the CSIRO-AR in February 2004.

These two research routes yielded model improvement in simulating rainfall as well as general circulation (dynamics). It also established a sustainable basis for model development in South Africa, both institutional and human related. In concluding the research, the latest version of C-CAM was used and the final simulations were verified. Model development is an ongoing process. Since the WRC project was timerestricted, it was necessary to select a cutoff point for initiating the concluding research. . Nevertheless, the concluding research did not take place before the WRC research team was convinced that significant progress had been made along the two research routes followed.

The achievements of this project, including capacity building, knowledge transfer and sustainable bilateral collaboration, not only between South Africa and the CSIRO-AR but also among African countries, proves that the research approach and routes were greatly successful.

4. FINE RESOLUTION OBSERVED RAINFALL OVER SOUTH AFRICA

Model performance is evaluated by comparing model results with observations. Many global observational fields are currently available for model verification. Coarse resolution observational fields (here regarded as coarser than 1^o x 1^o) might be useful to verify general large-scale atmospheric patterns as well as averaged climate fields, but they are not suitable for verification use in fine-resolution model-development studies where the sensitivity of the atmosphere to fine-resolution initial and boundary fields are evaluated. Global fine-resolution observational fields are not commonly available.

Many internationally available observational data sets have a relatively coarse grid resolution and important fine resolution features such as the influence of high topography on observed rainfall is smoothed out significantly. Apart from this, observed summer rainfall is significantly underestimated by some of these fields. The research team therefore decided to produce fine resolution observational data fields interpolated from 1027 South African rainfall stations. These fields were used in model verification.

5. THE STRETCHED GRID MODEL C-CAM

The research team decided to focus on the regional model C-CAM that was developed by the CSIRO Atmospheric Research (CSIRO-AR) in Australia. The advantage of C-CAM is that it is a global stretched grid model and problems related to nested modeling are therefore avoided. C-CAM employs a conformal cubic projection over a sphere instead of a traditional longitudinal-latitudinal projection. In the conformal cubic projection the model grids are expressed on six panels of a cube, which is then radially projected onto a sphere. Each panel has a user prescribed number of grid points. The grid may then be stretched with a stretch factor ranging from 0 to 1 (Schmidt factor) for full-stretch and non-stretch modes, respectively. Many model climate and sensitivity simulations were performed with C-CAM in order to improve rainfall over South Africa. The model was improved bilaterally during close collaboration with the CSIRO-AR. The latest results are a remarkable improvement on those produced at the beginning of the project.

6. A LOCALLY DEVELOPED ATMOSPHERIC MODEL

Apart from improving an international model (C-CAM), the project research also focused on the development of a unique non-hydrostatic model (equations and the associated numerical solution procedures). The aim was to develop a non-hydrostatic kernel for the hydrostatic C-CAM, which employs a semi-implicit semi-Lagrangian solution procedure. The research also focused on the development of a nonhydrostatic dynamic kernel for a new split semi-Lagrangian atmospheric model that is unique to South Africa. Significant progress has been made in the development of these models.

7. AN IMPROVED C-CAM FOR NUMERICAL WEATHER PREDICTION

In the final phase of the project a licence agreement was obtained to employ the improved C-CAM as a NWP model. NETSYS International provided office space and networking for downloading initial conditions on a daily basis. The first predictions were generated at the beginning of December 2004, and since then the model is producing predictions of four days in advance on a daily basis. Data are archived for verification purposes, and according to the license agreement predictions will be issued until December 2005. C-CAM appears to perform well as a NWP model. Model predictions are available on the following web page: http://www.up.ac.za/academic/geog/meteo

8. CONCLUSIONS

On the local front the project contributed significantly in capacity building. The two workshops that were presented as part of the project were well attended by local scientists, and the student seminar drew a lot of interest. The Laboratory for Research into Atmosheric Modelling (LRAM) was established and has served as a basis for research in atmospheric modelling over the past two years. The availability of infrastructure and models led to other modelling research activities that include:

- Long-range climate change scenario simulations for other Water Research Commission and ESKOM research projects.
- Air quality modelling with the emphasis on wind trajectory modelling for ESKOM.
- Weather forecasts for the Southern Ocean as part of research for the South African National Antarctic Programme (SANAP) funded by the Department of Environmental Affairs and Tourism (DEAT).
- Seasonal forecasting simulations with the South African Weather Service (SAWS).
- Student research as part of under and post-graduate studies.
- School projects with UP@Science

The project has assisted in establishing a strong and sustainable relationship between the project team and the CSIRO-AR. Regular contributions from the CSIRO-AR and feedback from the research team took place during the project. A number of visits strengthened this bilateral relationship. The research team and LRAM are internationally recognised as capable of performing complex atmospheric modelling simulations and of contributing to model development. The research on our own dynamic kernel has put South Africa on a higher level in the discipline of atmospheric modelling than it occupied previously.

It is recommended that the project team continue to expand the knowledge and facilities established by this project to encourage further capacity building and international recognition. The data generated through the project is available for future research.

REPORT ON CAPACITY BUILDING

The project "*Regional Model Development for Simulating Atmospheric Behaviour and Rainfall over Southern Africa*" extended over a period of three and a half years (March 2001 to December 2004) and focussed on development in the discipline of regional atmospheric modelling with emphasis on improved water related simulations. The development took place through collaboration with world leaders in the discipline of regional atmospheric modelling. Scientists, researchers and students from the South Africa and southern African community benefited from the collaboration since knowledge and skills to develop, maintain and use regional atmospheric models were transferred back to local communities.

The "*Laboratory for Research and Training in Atmospheric Modelling (LRAM)*" was launched at a student seminar.

1. PARTICIPATING ORGANISATIONS

Institutional participation

- LRAM, University of Pretoria, South Africa
- CSIRO Atmospheric Research, Melbourne, Australia
- NETSYS International, Pretoria, South Africa
- ESKOM, Johannesburg, South Africa
- Met Office Hadley Centre, United Kingdom
- University of the Witwatersrand (WITS), Johannesburg, South Africa
- South African Weather Service (SAWS) , Pretoria, South Africa
- CSAG, University of Cape Town, Cape Town, South Africa

Workshop participation

- Tanzania Meteorological Agency, Tanzania
- Mauritius Meteorological Service, Mauritius
- Physics Department, University of Botswana, Botswana
- Swaziland National Meteorological Service, Swaziland
- Zimbabwe Meteorological Services, Harare, Zimbabwe
- Drought Monitoring Centre, Harare, Zimbabwe
- Zambian Meteorological Department, Zambia
- Lesotho Meteorological Services, Lesotho
- Malawi Meteorology Service, Malawi
- Namibian Meteorology Service, Namibia
- Institute for Soil, Climate and Water, Pretoria, South Africa
- CFES, University of Pretoria, Pretoria, South Africa

2. INTERNATIONAL COLLABORATION

2.1 Visits by international researchers

2001:	August	Dr John McGregor	CSIRO, Australia
2002:	August	Dr Ian Smith	CSIRO, Australia
2002:	October	Dr John McGregor	CSIRO, Australia
2002:	November	Dr Angie Seth	IRI, United States of America
2004:	December	Dr John McGregor	CSIRO, Australia

August 2003 to November 2003: Mr Remco van de Beek from The Netherlands visited the WRC research team to work on C-CAM as part of his MSc degree. He completed two 15-year seasonal cycle simulations which he used for verification with particular emhasis on flow over Madagascar. Mr van de Beek graduated with an MSc in February 2004.

2.2 Visits to international institutions

2002:	January	Mr Francois Engelbrecht	to CSIRO, Australia
2003:	February	Prof Hannes Rautenbach	to CSIRO, Australia
2004:	January	Mr Francois Engelbrecht	to CSIRO, Australia
2004:	July	Prof Hannes Rautenbach	to CSIRO, Australia to obtain C-CAM licence

2.3 Other international modelling activities

An international student namely Mr A Beraki from Eritrea enrolled for his MSc(Meteorology) degree and used the PRECIS Regional Modelling system developed by the Hadley Centre in the United Kingdom to produce possible future climate change scenario simulations for Eritrea. 3 x 20 year runs were completed. Mr Beraki graduated with a MSc(Meteorology) in September 2005.

3. STUDENTS GRADUATED

Graduated in 2002

a) Thovakhale, B. BSc(Hons)(Meteorology) - Numerical advection schemes
b) Bopape, M-J. BSc(Hons)(Meteorology) - Climate change scenario experiments
c) Benadi, D. BSc(Meteorology) - Climate simulations over Madagascar
d) Du Pisanie, A. BSc(Meteorology) - Climate simulations over Madagascar
e) Mathee, R. BSc(Meteorology) - Climate simulations over Madagascar

Graduated in 2003

a) Du Pisanie, A. BSc(Hons)(Meteorology) - Climate change simulations
b) Ngwana, I. BSc(Hons)(Meteorology) - Inter model comparisons
c) Ndarana, T. BSc(Hons)(Meteorology) - Conformal Cubic Coordinate
d) Roux A. BSc(Meteorology) - Climate change over the Southern Ocean
e) Nake. S. BSc(Meteorology) – Climate change over Marion Island

Graduated in 2004

a) Maluta, P. BSc(Hons)(Meteorology) - Marine Forecasting
b) Van de Beek,R. MSc - Simulation of flow over Madagascar.

Enrolled MSc and PhD candidates (2004)

a) Engelbrecht, F. PhD(Meteorology) – Quasi-nonhydrostatic equations
b) Bopape, M-J. MSc(Meteorology) – Seasonal forecasting with C-CAM
c) Potgieter, C. MSc(Meteorology) – C-CAM as a short-term forecasting tool
d) Marx, E. MSc(Meteorology) – Verification of simulated short-term forecasts
e) Beraki, A. MSc(Meteorology) – PRECIS climate change simulations

3. INSTITUTIONAL DEVELOPMENT

The establishment of a "*Laboratory for Research and Training in Atmospheric Modelling (LRAM)*" at the University of Pretoria is an initiative that resulted from the WRC project.

The company NETSYS International provided space and networking infrastructure for Numerical Weather Prediction C-CAM simulations. Daily forecasts of up to four days in advanced were generated since November 2004, and results were archived for model verification purposes.

The SAWS decided to invest in C-CAM by obtaining a licence agreement for producing seasonal forecasts. The licence was negotiated with Dr John McGregor during a project visit to South Africa in December 2004.

4. PRODUCTS

The project made it possible to introduce a web page on atmospheric modelling and numerical weather prediction. The web page will make information available on the following:

a) Weather forecasts over South Africa (15km x 15km; 4-days in advance)
b) Weather forecasts over southern Africa (30km x 30km; 4-days in advance)
c) Weather forecasts over the Southern Ocean (30km x 30km; 4-days in advance)
d) Weather forecasts over Madagascar for tropical Cyclone forecasts (30km x 30km; 4-days in advance)
e) Weather forecasts over the Vaal-Gariep basin for flood management (15km x 15km; 4-days in advance)
f) Wind simulation and forecasts over the South African Highveld for pollution (15km x 15km; 4-days in advance)

The web address is: *http://www.up.ac.za/academic/geog/meteo*

KNOWLEDGE DISSEMINATION

1. PAPERS AND PRESENTATIONS

1.1 Scientific papers

Engelbrecht, F.A., Rautenbach, C.J.deW., McGregor, J.L. and Katzfey, J.J. (2002) January and July climate simulations over the SADC region using the limited-area model DARLAM. Water SA, Vol 28 No 4, 361-373.

Olwoch, J. M., Rautenbach, C. J. de W., Erasmus, B. F. N., Engelbrecht, F. A. & van Jaarsveld, A. S. (2003) Simulating tick distributions over sub-Saharan Africa: the use of observed and simulated climate surfaces. *Journal of Biogeography,* 30 no 8, 1221-1232.

1.2 Conference and other presentations

Thovhakale, B., Engelbrecht, F.A. and Rautenbach, C.J.deW. (2001) *Comparison of numerical techniques suitable for simulating moisture advection over southern Africa.* 18th Annual Conference of the South African Society for Atmospheric Sciences, Breakwater Lodge & Conference Center, Waterfront, Cape Town. (6-7 October 2001)

Engelbrecht, F.A. and Rautenbach, C.J.deW. (2001) *Full seasonally varying climate simulations over southern Africa with a limited area model.* 18th Annual Conference of the South African Society for Atmospheric Sciences, Breakwater Lodge & Conference Center, Waterfront, Cape Town. (6-7 October 2001)

Rautenbach, C.J.deW. (2002) *Model simulations of global and regional scale climate change scenarios over sub-Sahara Africa*. Climate Change Workshop, South African Sugar Technologists' Association, Mount Edgecombe, KwaZulu-Natal (28 November 2002)

Bhekizitha, M., Rautenbach, C.J.deW. and Engelbrecht, F.A. (2002) *Characteristics of cumulus parameterization schemes over southern Africa*. 19th Annual Conference of the South African Society for Atmospheric Sciences, Momentum Head Office, Centurion. (26 – 27 Augustus 2002)

Olwoch, J.M., Rautenbach, C.J.deW., Erasmus, B.F.N., Engelbrecht, F.A. and van Jaarsveld, A.S. (2002) *Simulating the spatial distribution of ticks over sub-Sahara Africa by using high-resolution climate data*. 19th Annual Conference of the South African Society for Atmospheric Sciences, Momentum Head Office, Centurion. (26 – 27 Augustus 2002)

Bopape, M., Engelbrecht, F.A. and Rautenbach, C.J.deW. (2002) *Climate change scenarios over southern Africa as simulated by the regional model DARLAM.* 19th Annual Conference of the South African Society for Atmospheric Sciences, Momentum Head Office, Centurion. (26 – 27 Augustus 2002)

Engelbrecht, F.A. (2002) *Cold bubbles and acoustically filtered non-hydrostatic equations*. 19th Annual Conference of the South African Society for Atmospheric Sciences, Momentum Head Office, Centurion. (26 – 27 Augustus 2002)

Benade, D., du Piesanie, A., Matthee R. and Engelbrecht F.A. (2002) Mesoscale model simulations over and around Madagascar. 19th Annual Conference of the South African Society for Atmospheric Sciences, Momentum Head Office, Centurion. (26 – 27 Augustus 2002)

AWARD (D.M. Kitch gold medal)
Engelbrecht, F.A. (2002) *Konvektiewe borrel eksperimente met nie-hidrostatiese vergelykings*, Studente Simposium vir die SA Akademie vir Wetenskap en Tegnologie, Pochefstroom, Oktober 2002.

Rautenbach, C.J.deW (2002) Model simulations of global and regional scale climate change scenarios over sub-Sahara Africa, Sugar Industry Workshop, Durban, October 2002.

Rautenbach, C.J.deW. and Ndarana, T. (2003) *Regional scale atmospheric modeling over southern Africa by means of a variable resolution global model*. Colloquium, South African Weather Service Head Office, Pretoria. (6 June 2003)

Opening keynote
Rautenbach, C.J.deW (2003) *The application of Australian atmospheric models in South Africa*. Annual Conference of the Australian Meteorology and Oceanography Society, Perth, Australia, February 2003.
Rautenbach, C.J.deW. (2003) *Seasonal forecasting and climate change scenario experiments for South Africa by using atmospheric models developed by the CSIRO Atmospheric Research*. CSIRO Atmospheric Research, Melbourne, Australia (14 February 2003).

Ndarana, T and Rautenbach, C.J.deW. (2003) *A conformal cubic projection on the sphere for regional atmospheric model simulations*. 20th Annual Conference of the South African Society for Atmospheric Sciences, Farm Inn, Pretoria. (13 – 14 October 2003)

Rautenbach, C.J.deW. (2003) *The influence of variable horizontal resolution in the conformal cubic model on atmospheric simulations over Africa*. 20th Annual Conference of the South African Society for Atmospheric Sciences, Farm Inn, Pretoria. (13 – 14 October 2003)

Ngwana, I and Rautenbach, C.J.deW. (2003) *Regional climate simulations by the C-CAModel over southern Africa*. 20th Annual Conference of the South African Society for Atmospheric Sciences, Farm Inn, Pretoria. (13 – 14 October 2003)

Du Pisani, A and Engelbrecht, F.A. (2003) *Simulations of climate change over southern Africa using a variable resolution model*. 20th Annual Conference of the South African Society for Atmospheric Sciences, Farm Inn, Pretoria. (13 – 14 October 2003)

Engelbrecht, F.A. (2003) *A non-hydrostatic terrain-following coordinate model*. 20th Annual Conference of the South African Society for Atmospheric Sciences, Farm Inn, Pretoria. (13 – 14 October 2003)
With researchers at ESKOM the project leader made significant progress in convincing ESKOM to establish a Centre of Excellence in Air Quality Modelling at the University of Pretoria.

2. Project Workshops

REGIONAL ATMOSPHERIC MODELLING: NUMERICAL TECHNIQUES WORKSHOP #1
University of Pretoria, South Africa
13-16 August 2001

BACKGROUND:
This workshop forms part of a *Water Research Commission (WRC)* funded research project entitled "Regional Model Development for Simulating Atmospheric Behaviour and Rainfall Over Southern Africa". The project aims to promote and develop the discipline of regional atmospheric modelling in southern Africa, and eventually to improve local simulations of such models over the region. A series of three workshops during 2001-2002 are being funded by the WRC and will be collaboratively presented by:

- *University of Pretoria (Centre for Environmental Studies and the Laboratory for Post Graduate Research in Atmospheric Modelling - LRAM)*
- *South African Weather Bureau (Prediction, Research and Development*)
- *University of Cape Town (Climate System Analysis Group)*

All candidates interested in learning more about regional modelling are invited to participate. As the series will build upon each preceding workshop, it is *required that candidates attend all three of the series*. All the major regional models used in the Southern African region will be investigated, including Research Models (DARLAM, MM5) and Operational Models (ETA, MM5).

DETAILS:
Workshop 1 will focus on the introduction of numerical techniques and the basic parameterisation schemes. The two follow-up workshops will deal primarily with more advanced modelling issues, and both are tentatively due to be presented during 2002.

Participants and presenters of the workshop will consist of varied researchers and professionals, including Dr. John McGregor, a world-renowned scientist in numerical modelling from the CSIRO Atmospheric Research, Australia.

PREREQUISITES:
Please note that participants must meet the following prerequisites:
- BSc in Mathematics or Physics or a Class 1 Meteorologist

TRAVEL AND ACCOMODATION:
Workshop 1 will be hosted by The Centre for Environmental Studies at The University of Pretoria, and will be presented at a university venue from 13-16 August 2001.

LIST OF DELEGATES

Adedoyin, A.	adedoyin@mopipi.ub.bw	University of Botswana, Botswana
Baloi, B.M.	bmbaloi@hotmail.com	Private, South Africa
Banitz, E.	estelle@weathersa.co.za	South African Weather Service, South Africa
Bopape, M.J.	mbopape@yahoo.com	University of Pretoria, South Africa
Bruyere, C.	bruyere@weathersa.co.za	South African Weather Service, South Africa
Bulane, L.	bulane@lesoff.co.za	Lesotho Meteorological Services, Lesotho
Chikoore, H.	hchikoore@weather.utande.co.zw	Zimbabwe Meteorological Services, Zimbabwe
Engelbrecht, F.A.	fengelbr@postino.up.ac.za	University of Pretoria, South Africa
Gertenbach, J.	jgertenb@postino.up.ac.za	University of Pretoria, South Africa
Jack, C.	jack@egs.uct.ac.za	University of Cape Town, South Africa
Jordaan, W.	wjordaan@weathersa.co.za	South African Weather Service, South Africa
Kgakatsi, I.B.	kgakatsi@weathersa.co.za	South African Weather Service, South Africa
Kitshoff, E.	elizmakitshoff@hotmail.com	South African Weather Service, South Africa

Mahahabsa, M.	moshmet@lesoff.co.za	Lesotho Meteorological Services, Lesotho
Makarau, A.	makarau@science.uz.ac.zw	University of Zimbabwe, Zimbabwe
Malherbe, J.	johan@iscw.agric.za	Institute: Soil, Climate and Water, South Africa
Manhique, A.J	atanasiomanhique@hotmail.com	Drought Monitoring Center, Zimbabwe
Masimini, L.	hrautenb@postino.up.ac.za	University of Pretoria, South Africa, South Africa
McGregor, J.	mcg130@dar.csiro.au	CSIRO Atmospheric Research, Australia
Mkhize, B.M.	bheki@ananzi.co.za	South African Weather Service, South Africa
Movalo, S.	shirley@weathersa.co.za	South African Weather Service, South Africa
Nkomoki, J.	jnkomoki@hotmail.com	Zambian Meteorological Department, Zambia
Pathack, B.	meteo@intnet.mu	Mauritius Meteorological Services, Mauritius
Phahlane, A.	agnes@weathersa.co.za	South African Weather Service, South Africa
Pienaar, E.	estellep@weathersa.co.za	South African Weather Service, South Africa
Pyuzza, N.D.	met@meteo-tz.org	Tanzania Meteorological Agency, Tanzania
Raboqha, S.	sraboqha@leo.co.ls	Lesotho Meteorological Services, Lesotho
Rautenbach, C.J.	hrautenb@postino.up.ac.za	University of Pretoria, South Africa
Riphagen, H.	hilarie@weathersa.co.za	South African Weather Service, South Africa
Seyama, E.	weather@africaonline.co.sz	Swaziland National Met. Service, Swaziland
Sigulda, L.	luckynsigudla@hotmail.com	Swaziland National Met. Service, Swaziland
Thovhakale, B.	tbridget81@yahoo.co.uk	University of Pretoria, South Africa
Tsukulu, S.	moshmet@lesoff.co.za	Lesotho Meteorological Services, Lesotho
Van Hemert, L.	vhemert@weathersa.co.za	South African Weather Service, South Africa
Vevha, R.	rvevha@weather.utande.co.zw	Drought Monitoring Center, Zimbabwe

INTRODUCTION TO REGIONAL ATMOSPHERIC MODELLING - WORKSHOP #1
University of Pretoria, South Africa, 13-16 August 2001

SUNDAY, 12 August 2001	
Arrival of delegates - *Please arrange with Jen Jones:* jljones@zoology.up.ac.za	
MONDAY, 13 AUGUST 2001	
08:00 – 09:00	Registration; Venue: Ground floor, Zoology Building, University of Pretoria
09:00 – 09:30	Welcome Venue: Room 2-45, Zoology Building, University of Pretoria *Prof Robin Crewe* *(Dean, Faculty of Natural and Agricultural Sciences, University of Pretoria)* *Dr Winifred Jordaan* *(Deputy Director: Training, South African Weather Service)* SESSION 1; Venue: Room 3-12, Zoology Building, University of Pretoria Chair: *Akintayo Adedoyin (University of Botswana, Botswana)* *Hannes Rautenbach (University of Pretoria, South Africa)*
09:30 – 10:00	The climate of southern Africa *Amos Makarau (University of Zimbabwe, Zimbabwe)*
10:00 – 10:30	Meso-scale weather systems *Estelle Banitz (South African Weather Service, South Africa)*
10:30 – 11:00	Why regional atmospheric modelling *John McGregor (CSIRO Atmospheric Research, Australia)*
11:00 – 11:30	Tea Research models:
11:30 – 11:50	DARLAM (CSIRO Atmospheric Research) *John McGregor (CSIRO Atmospheric Research, Australia)*
11:50 - 12:10	MM5 (UCT) *Chris Jack (University of Cape Town, South Africa)* Operational models:
12:10 – 12:30	ETA (South African Weather Bureau) *Hilarie Riphagen (South African Weather Service, South Africa)*
12:30 – 13:00	ETA (Tanzania Meteorological Agency) *Nelson Pyuzza (Tanzania Meteorological Agency, Tanzania)*

13:00 – 13:20	MM5 (South African Weather Bureau) *Cindy Bruyere (South African Weather Service, South Africa)*
13:20 – 13:30	Discussion
13:30 - 15:00	Lunch
	<u>SESSION 2; Venue: Room 3-12, Zoology Building, University of Pretoria</u> <u>Chair:</u> *Chris Jack (CSAG, University of Cape Town, South Africa)* *Estelle Banitz (South African Weather Service, South Africa)*
15:00 - 15:20	An introduction to the Atmospheric Equations *Francois Engelbrecht (Meteorology, University of Pretoria, South Africa)*
15:20 – 15:40	Dynamics of convective systems; Introductory remarks about a new limited area model *Akintayo Adedoyin (University of Botswana, Botswana)*
15:40 – 16:00	Cumulus convection schemes in Atmospheric Models *Bhekizitha Mkhize (South African Weather Service, South Africa)*
TUESDAY, 14 August 2001	
	<u>SESSION 3; Venue: Room 3-12, Zoology Building, University of Pretoria</u> <u>Chair:</u> *Nelson Pyuzza (Tanzania Meteorological Agency, Tanzania)* *Ikalafeng Kgakatsi (South African Weather Service, South Africa)*
09:00 - 09:30	Introduction to Numerical Techniques (finite difference methods) *Hannes Rautenbach (Meteorology, University of Pretoria, South Africa)*
09:30 - 10:30	Introduction to Numerical techniques (semi-Lagrangian methods and the application of numerical techniques in regional models) *John McGregor (CSIRO Atmospheric Research, Australia)*
10:30 – 11:00	Comparison of techniques and stability experiments *Francois Engelbrecht (Meteorology, University of Pretoria, South Africa)*
11:00 – 11:30	Tea
11:30 – 11:50	The advection term *Francois Engelbrecht (Meteorology, University of Pretoria, South Africa)*
11:50 – 12:00	Discussion
12:00 – 13:30	Lunch
	<u>SESSION 4; Venue: Room 3-12, Zoology Building, University of Pretoria</u> <u>Chair:</u> *Beenay Pathack (Mauritius Meteorological Service, Mauritius)* *Amos Makarau (University of Zimbabwe, Zimbabwe)*
13:30 – 15:00	Numerical representations of the advection term: Finite Differences and the Semi-Lagrangian techniques *Francois Engelbrecht (Meteorology, University of Pretoria, South Africa)* *John McGregor (CSIRO Atmospheric Research, Australia)*
15:00 – 15:30	Discussion
WEDNESDAY, 15 August 2001	
	<u>SESSION 5; Practical work session</u> <u>Venue: Computer room 3-39.1, Zoology Building, University of Pretoria</u>
09:00 – 10:00	Introduction to FORTRAN programming *Louis van Heemert (South African Weather Services, South Africa)* *Hannes Rautenbach (Meteorology, University of Pretoria, South Africa)*
10:00 – 11:00	FORTRAN programming: Data for GrADS *Francois Engelbrecht, Bridget Thovhakale (Meteorology, University of Pretoria, South Africa)*
11:00 – 11:30	Tea
11:30 – 12:30	FORTRAN programming: Practical examples *Bridget Thovhakale, Hannes Rautenbach and Francois Engelbrecht (Meteorology, University of Pretoria, South Africa)*
12:30 – 14:00	Lunch
14:00 – 16:00	A moisture advection model *Bridget Thovhakale (Meteorology, University of Pretoria, South Africa)*
18:30 for 19:00	Workshop Braai; Venue: Uitspan Terrein, University of Pretoria
THURSDAY, 16 August 2001	
	<u>SESSION 6; Practical work session</u>

	Venue: Computer room 3-39.1, Zoology Building, University of Pretoria
10:00 – 11:00	Graphical representation of model results (GrADS) *Jan Gertenbach (South African Weather Service, South Africa)*
11:00 – 11:30	Tea
11:30 – 12:30	Interpretation and limitations of results *John McGregor (CSIRO Atmospheric Research, Australia)* *Bridget Thovhakale (Meteorology, University of Pretoria, South Africa)*
12:30 – 14:00	Lunch
	SESSION 7 Venue: Mathematics Council Hall, Mathematics Building, University of Pretoria Chair: *John McGregor (CSIRO Atmospheric Research, Australia)* *Hannes Rautenbah (Meteorology, University of Pretoria, South Africa)*
14:00 – 15:00	Discussion session: A view of the future *Interactive discussion between institutions involved*
15:00	Closure and tea

REGIONAL ATMOSPHERIC MODELLING: PARAMETERIZATION- WORKSHOP #2

University of Pretoria, South Africa
25-29 November 2002

BACKGROUND

This workshop formed part of *Water Research Commission (WRC)* funded research projects that aim to promote, develop and improve the discipline of regional atmospheric modelling in southern Africa. This is the second workshop funded by the WRC and was collaboratively presented by:

- *University of Pretoria (Laboratory for Post Graduate Research in Atmospheric Modelling or LRAM)*
- *South African Weather Service (Prediction, Research and Development*)

Workshop #1 (13-16 August 2001) focussed on the introduction of numerical techniques and the basic parameterisation schemes. This workshop focussed on the physical parameterisation schemes of models, with specific emphasis on cumulus parameterisation schemes. The regional models that were tested are research models such as the DARLAM and MM5.

DELEGATES

Delegates from nine SADC countries attended. The countries are Namibia, Zambia, Tanzania, Botswana, Zimbabwe, Mauritius, Lesotho, Swaziland and South Africa. Details of delegates appear in the following table.

LIST OF DELEGATES

Adedoyin, A.	adedoyin@mopipi.ub.bw	University of Botswana, Botswana
Banitz, E.	estelle@weathersa.co.za	South African Weather Service, South Africa
Bartman, A	bartman@weathersa.co.za	South African Weather Service, South Africa
Bopape, M.J.	mbopape@yahoo.com	University of Pretoria, South Africa
Burger, R	roelof@metsys.weathersa.co.za	METSYS, South Africa
Drew, G	drew@egs.uct.ac.za	CSAG, University of Cape Town, South Africa
Engelbrecht, F.A.	fengelbr@postino.up.ac.za	University of Pretoria, South Africa
Green, G	gcgreen@wrc.org.za	Water Research Commission, South Africa
Kachiwanda, Y.E.	yobu_kachiwanda@hotmail.com	Malawi Meteorology Service, Malawi
Karunga, O.M.	om_karunga@yahoo.com	Namibia Meteorology Service

Klopper, E.	klopper@weathersa.co.za	South African Weather Service, South Africa
Landman, W. A.	willem@weathersa.co.za	South African Weather Service, South Africa
Makarau, A.	makarau@science.uz.ac.zw	University of Zimbabwe, Zimbabwe
Maletjane,M.	motsomim@yahoo.com	Lesotho Meteorology Service, Lesotho
Malherbe, J.	johan@iscw.agric.za	Institute: Soil, Climate and Water, South Africa
Marx, E.	estellep@weathersa.co.za	South African Weather Service, South Africa
Mdoka, M.L.	mdokam@weather.utande.co.zw	Zimbabwe Meteorological Services, Zimbabwe
Molongwane,C.M	masule@hotmail.com	Botswana Meteorology Service, Botswana
Mutasa, C	zimmeteo@weather.utande.co.zw	Zimbabwe Meteorological Services, Zimbabwe
Mwangase,A.O.	mmilk3@yahoo.co.uk	Zambian Meteorology Department, Zambia
Pathack, B.	meteo@intnet.mu	Mauritius Meteorological Services, Mauritius
Poolman, E.	poolman@weathersa.co.za	South African Weather Service, South Africa
Pyuzza, N.D.	met@meteo-tz.org	Tanzania Meteorological Agency, Tanzania
Rautenbach, C.J.	hrautenb@postino.up.ac.za	University of Pretoria, South Africa
Riphagen, H.	hilarie@weathersa.co.za	South African Weather Service, South Africa
Seth, A	seth@iri.columbia.edu	International Research Institute, USA
Sewel, R	rds@weathersa.co.za	South African Weather Service, South Africa
Seyama, E.	weather@africaonline.co.sz	Swaziland National Met. Service, Swaziland
Thachrah,A.	anneke@iscw.agric.za	Institute for Soil, Climate and Water, South Africa
Tennant, W	tenant@weathersa.co.za	South African Weather Service, South Africa
Thovhakale, B.	tbridget81@yahoo.co.uk	South African Weather Service, South Africa
Vevha, R.	rvevha@weather.utande.co.zw	Drought Monitoring Centre, Zimbabwe

PROGRAM

Participants and resource people of the workshop consisted of varied researchers and professionals. The invited guest was Dr Anji Seth from the International Research Institute for Climate Prediction in New York. The proceedings were opened by Prof Johan Malherbe from the University of Pretoria. Prof Malherbe is the head of the School of Physical Science. He welcomed all the delegates and expressed his department and the Universities interest in atmospheric sciences. The key note address was delivered by Dr George Green from the Water Research Commission. Dr Green stated the importance of atmospheric research to the South African water sector. Dr Nelson Pyuzza from Tanzania who talked about the experiences from the first workshop and linked it to this second workshop closed the first session. During the second session Dr Anji Seth gave a review on the regional modelling work being done at the IRI. Mr Eugene Poolman from the South African Weather Service then gave feed back on the African Strategy for Numerical Weather Prediction. Post processing and data were the two topics after lunch. Dr Willem Landman (South African Weather Service) explained how Model Output Statistics can be employed to downscale regional model output. Dr Warren Tennant (South African Weather Service) talked on downscaling of General Circulation Model forecasts. Ms Anneke Thackrah from the Institute of Soil, Water and Climate gave a description of available data sets to verify models. She highlighted the strong and weak points of these data sets. Ms Gillian Drew from the University of Cape Town closed the day by showing the interaction of between vegetation types and atmospheric processes. The second day of the workshop was devoted towards cumulus convective characteristics (presented by Mr Roelof Burger from the South African Weather Service) and cumulus parameterization schemes. The schemes discussed were: Convective adjustment in models, Kuo scheme, Arakawa scheme and the Bets-Miller scheme. These were presented by Dr Hannes Rautenbach and Mr Francois Engelbrecht from the University of Pretoria, and Ms Bridget Thovokale from the South African Wetaher Service. The day was closed by three talks on Tropical Cyclones and their representation in regional models. Dr Akintayo Adedoyin from the University of Botswana talked in general on parameterization of tropical cyclones. Dr Beenay Pathack from the Mauritius Meteorological Service delivered a talk on tropical cyclone simulation. Lastely Dr Willem Landman showed how domain choice can affect tropical cyclone prediction. The following two days were spent performing hands on exercises. These were lead by Mr Francois Engelbrecht who explained in great detail to the delegates how these parameterizations are applied in models. The delegates experienced how convection changes a sounding, how thunderstorm properties are simulated and the effect of different adjustment schemes. The effect of different cumulus parameterization schemes on the simulation were compared. A talk was given by Dr Landman on El Niño and its effects on our region. He also showed some pitfalls of statistical modeling. The lecturers delivered during this workshop will be put on CDROM and send to all participants.

3. Student Seminar & Launch of LRAM

Between 17 and 18 July 2003 a student seminar was presented at Pumulani Lodge where students had the opportunity to present their research and to exchange ideas during discussion sessions. At the same event the *"Laboratory for Research and Training in Atmospheric Modelling (LRAM)"* was launched. The seminar and LRAM form an integral part of this project. The establishment of LRAM created a basis for future research in atmospheric modelling.

Laboratory for Research and Training in
Atmospheric Modelling - LRAM

Activities at the 2003 Student Seminar. Apart from the students, high officials from the National Nuclear Regulator (NNR) showed interest in using fine resolution models to simulate wind patterns for trajectory analysis (bottom right).

CHAPTER 1

INTRODUCTION

1.1 BACKGROUND

Since the first attempt to utilise numerical methods for predicting weather was made by the British scientist Lewis Fry Richardson (1882-1953), many scientists undertook the challenge to produce improved methods for simulating atmospheric processes and flow. The motivation for these efforts is primarily manifested through the benefits the methods hold for short-term planning (daily Numerical Weather Prediction (NWP) and air pollution modelling), seasonal risk analysis (seasonal forecasting) and early warning of the need to adapt to possible variations in the climate system (future climate change projections).

Synoptic general circulation of the atmosphere is governed by a number of forces that collectively originate from factors such as imbalances in the energy budget between the equator and poles, the rotation of the Earth, vertical gravity and friction. Through planetary-scale atmospheric flow these forces modulate the exchange of energy between equatorial and polar regions. Prevailing horizontal atmospheric features arising from these circulation patterns vary from persistent zonal high-pressure regions over the sub-tropics and poles to complex low-pressure belts, accompanied by fast moving frontal systems, over the mid-latitudes. In the vertical, well-defined Hadley and Ferrel cells (Ferrel, 1859; Coffin, 1875) dominate the meridional atmospheric flow, while Walker cells contribute to the zonal shift and location of low and high-pressure systems. Differences in the day-night energy budget of the atmosphere and the seasonal north-south displacement of synoptic systems, result in a strong diurnal and seasonal variability in the weather over most regions of the Earth. Smaller-scale atmospheric phenomena driven by the combination of large-scale flow and local surface forcing emphasize the complexity of circulation processes in the atmosphere.

In an early effort to improve their understanding of the many factors that contribute to atmospheric processes, scientists indicated that atmospheric flow could be approximated in terms of a number of mathematical equations known as the primitive equations or the Eulerian hydrodynamic equations modified by the assumption of hydrostatic equilibrium. The primitive equations are non-linear meaning that they have no known analytical solutions. The only means of solving these equations is by numerical approximation. In numerical models, the future state of atmospheric flow may be estimated to a certain degree of accuracy by integrating the numerical formulation of the primitive equations forward with respect to time (Arakawa, 1966). A model integration of the atmosphere is started with defined atmospheric initial conditions (usually observed values at the initial state) and then kept on track by boundary forcing (usually energy forcing from Earth surface characteristics). An important requirement, which also applies to the formulation of numerical approximations, is that total momentum, mass and energy be conserved in the atmospheric system.

As mentioned before, the first attempt to utilise numerical methods for predicting weather was made by Richardson (1922). He indicated that the primitive equations could be approximated in numerical terms by using finite difference methods (Haltiner, 1971; Washington and Parkinson, 1992; Kalnay, 2003). By considering a discrete field of observed grid point values as initial input, he integrated the numerically computed tendencies of various meteorological variables ahead with small increments in time. All the computation was then performed by hand and formed the basis for today's sophisticated atmospheric models that run on the biggest super-computers in the world. Richardson proposed the so-called "forecast factory" that would function like a vast orchestral performance, where 64000 people, each with a mechanical calculator, would perform forecast calculations (Randall, 2000). With this Richardson would probably be able to calculate weather only about as fast as it happens. Unfortunately, Richardson's results were out by several orders of magnitude, which might be attributed to inadequate initial data or linear instability in numerical solutions caused by truncation errors. Despite this, Richardson established the first basis for modern numerical modelling. Only in the 1940s, when digital computers appeared on the market, did Richardson's technique become practical.

A consequence of using numerical methods to integrate the primitive equations is that extremely large numbers of calculations are required per model time step. With the arrival of the first digital computer during the late 1940s, computing power became available to assist in the numerical integration of the primitive equations. The development of the first NWP models soon followed. Through the advent of numerical modelling, as well as the rapidly improved capacity of super computers during the past six decades, weather and climate prediction models have collectively led to surprisingly realistic simulations of all the major observed features of the atmosphere.

Apart from predicting the day-to-day weather, modern computerised numerical models of the atmospheric circulation have been used for many other purposes. Today numerical atmospheric models are applied in:

- Assimilation of the present state of the atmosphere for estimating initial conditions in NWP models and routine air pollution research.

- Short-term NWP that involves day-to-day weather forecasting.

- Climate variability research and products that include sensitivity studies and techniques for longer-term forecasting such as seasonal forecasting.

- Possible future climate change estimations such as greenhouse enhanced future climate scenario simulations.

1.2 REGIONAL ATMOSPHERIC MODELING IN SOUTH AFRICA

Initially regional numerical modeling of the atmosphere was confined to efforts by the early South African Weather Bureau (SAWB) who obtained models from international institutions for use in NWP. At the same time training in numerical modeling also took place at the SAWB who, in collaboration with the University of Pretoria (UP), presented a BSc degree in Meteorology with a strong emphasis on dynamic meteorology. In the 1980s the Climatology Research Group at the University of the Witwatersrand (WITS) started to use models in climate change research, but since early models required large computer capacity, it was difficult for research groups to run models in-house without the aid of super computers. However, in the 1980s and 1990s WITS managed to produce simulations with the regional RAMS model to investigate the impact of Sea Surface Temperatures (SSTs) on tropical temperate troughs over South Africa (Crimp et al.

1998). Model simulations for South Africa were mainly performed at international institutions and the local SAWB. With the establishment of the CORDATA Chair in Meteorology during the late 1980s, a CONVEX supercomputer was donated to the University of Pretoria. With the rapid advance in computer technology the CONVEX soon became outdated, although valuable Atmospheric General Circulation Model (AGCM) simulations were performed in the form of climatology control runs (Jury et. al., 1996). These were probably the first atmospheric simulations performed at an institution outside the SAWB. During the early 1990s the University of Cape Town (UCT) put in a large effort to start running regional models and a 16-cluster workstation structure was installed for this purpose. The MM5 nested model was obtained and the first regional scale simulations were performed by an institution outside the SAWB. At the same time a CRAY EL94 was donated by the CORDATA Meteorology Educational Trust for model simulations by the University of Pretoria. This entry-level supercomputer significantly supported research on numerical seasonal forecasting performed by the University of Pretoria (Rautenbach, 2003). During the late 1990s the Universities of Pretoria and Cape Town established a good relationship in atmospheric modeling with particular emphasis in regional scale modeling, and many climate related simulations were since performed on local workstations (Engelbrecht, et.al., 2002). At the same time the new South African Weather Service (SAWS) continued with its own regional-scale modeling program for routine NWP purposes. As part of this project a research laboratory in atmospheric modeling was established at the University of Pretoria.

With the training in dynamic meteorology and numerical techniques at the University of Pretoria, and the capacity at South African research institutions to perform their own model simulations, the question was soon asked whether South African research institutions should become involved in model development (Engelbrecht and Rautenbach, 2000). The possibility of developing a unique atmospheric model on African soil by African researchers was also mentioned. Modern atmospheric models are in an advanced stage with sophisticated numerical formulation and parameterizations. These models were developed over years, and it would therefore not be easy to start developing a totally new model. South African scientists that are interested in numerical modeling may, however, benefit significantly from close collaboration with, and involvement in, international modeling efforts. These thoughts inspired the research initiatives and achievements discussed in this report.

1.3 AIMS OF THE PROJECT

Objectives of the research presented in this report may be summarized as follows:

- To modify the dynamic formulation and physical parameterization schemes of internationally competitive regional atmospheric circulation models in order to improve the simulation of water related atmospheric variables over South Africa.

- To equip scientists and prospective students from the South Africa and southern African community with the necessary knowledge and skills to develop, maintain and use the regional atmospheric models by means of innovative water research training.

1.4 RESEARCH APPROACH

Over the past few decades atmospheric modeling has advanced to a complex science. Not only have new numerical methods been developed to improve and solve the primitive equations, but sophisticated physical schemes have also been introduced (Randall, 2000; Kalnay, 2003). That includes the parameterization of the radiation budget, convection with cloud formation and rainfall as well as Earth surface processes, such as surface-atmosphere interaction. In addition, new ocean and soil models have been introduced to interact with atmospheric models. Another aspect of importance is the continued need to address local processes by producing finer resolution model simulations – a development primarily hampered by limited computer capacity. The process of modeling the Earth system has therefore become more demanding, which means that modern models are based upon years of experience and manpower.

To start developing a completely new atmospheric model would be a tremendous task, and the project team therefore decided to rather make use of existing models to achieve the project objectives. An international partner who is directly involved in model development therefore had to be found, and a good bilateral collaborative relationship with that partner had to be established. One must keep in mind that, as outlined in the project objectives, it was not the project's intention to import an existing model and to simply use results of simulations in verification studies, but rather to modify the dynamic formulation and physical parameterisation schemes of such a model in order to improve the simulation of water related atmospheric variables over South Africa. At the beginning of the project the project team decided that a suitable model had to be found according to the following criteria:

- *Excellence:*
  The model to be considered would be one of the leading models in the world, with particular emphasis on advanced numerical formulation of the atmospheric dynamics.

- *Accessibility:*
  In order to improve the model the WRC research team needed direct access to the model's source code and direct research collaboration with the model's developing team. It was the intention to not only collaborate and verify model results, but rather to participate in, and even contribute to, model development.

- *Applicability:*
  The model was to be capable of producing high-quality atmospheric simulations on the meso-scale and smaller, and its numerical formulation needed to be of such a nature as to enable operation on a standard workstation. The project team was therefore looking for a model that was most suitable for use in South Africa where access to supercomputers was limited.

It was decided to approach the CSIRO (Atmospheric Research) or CSIRO-AR in Australia, Melbourne. Reasons for this decision emanated from previous collaboration with this research organisation in the field of seasonal forecasting (Rautenbach, 2003). Here collaboration focused on results produced by an existing Atmospheric General Circulation Model (AGCM), and aspects related to model development were not addressed at all. However, there was no doubt that regional models developed at the CSIRO-AR, especially the new Conformal Cubic Atmospheric Model (C-CAM) with its numerical semi-Lagrangian advection scheme, complied with the criteria of excellence, accessibility and applicability. C-CAM, as well as the older Division of Atmospheric Research Limited Area Model (DARLAM), were accessible since the core-code of both models was made available to the WRC research team under licence agreement. Both models were designed to perform meso-scale simulations of high standard and the semi-Lagrangian scheme that allowed for larger time-steps made the models most suitable for simulations on standard workstations. It will be indicated later in the report that simulation times varied from around 6-hours for a one-month simulation (DARLAM) to 4-hours for a one-month simulation (C-CAM) both on a horizontal resolution of approximately 60km x 60km. The fact that simulations could be completed in such short time periods on a one-processor (1800 mHz – 2000 mHz) workstation was seen as a major advantage.

Nevertheless, at the beginning of the project it was a challenge to expand bilateral relationships with the CSIRO-AR to such an extent that the WRC research team could be seen as capable and worthy of a place in CSIRO-AR' model development program – certainly the core of any modelling effort. Through regular research visits and workshops the project team not only succeeded in establishing an excellent and sustainable research relationship with world leaders in atmospheric modelling at the CSIRO-AR, but also proved to the international community that South Africa has the capacity to contribute to model development. Both groups benefited from the research and the following have been achieved:

WRC research team based at the University of Pretoria

- The WRC research team received the source code of two of the most sophisticated regional models in the world (DARLAM and C-CAM). Many model simulations were performed on local workstations.

- The availability of regional models and the knowledge gained through the international collaboration enabled the WRC research team to contribute to training and knowledge transfer in South Africa. As outcome the project produced excellent local scientists that are already appointed in key positions in atmospheric modelling at the SAWS.

- The project encouraged local scientists to develop a non-hydrostatic dynamic kernel, which already forms the basis for current fine resolution wind field simulations in South Africa. Even though it employs a unique split explicit method developed by the WRC research team (in contrast to the semi-implicit method applied in C-CAM) the non-hydrostatic dynamic kernel approach has been used by CSIRO-AR scientists to transform C-CAM to a non-hydrostatic model. This is a major achievement by the WRC research team and one that contributed significantly to international model development.

- Annual workshops for the purpose of bringing atmospheric modellers from the SADC region together were a major success. These workshops, each presented over five days, contributed to collaboration, capacity building and knowledge transfer in the SADC region. The workshops formed part of this project and were well attended by the leading scientists involved in dynamic meteorology and atmospheric modelling in Africa (as far as Tanzania and Kenya). In 2003 a student seminar on numerical modelling was also presented to local students and scientists. More detail about the workshops and seminar is available in APPENDIX A.

- At the student seminar in 2003 the “Laboratory for Training and Research in Atmospheric Modelling” (LRAM) was launched. LRAM is a product of this research project, and the Laboratory will form the base from which future research and training initiatives in atmospheric modelling at the UP will be launched.

International atmospheric modellers at the CSIRO-AR

- Regional models from the CSIRO-AR received exposure in Africa. The many model simulations that were performed made both DARLAM and C-CAM known in Africa. Exposure and application are two important aspects since it makes modeling worth the effort. Scientists from the CSIRO-AR visited South Africa, as well as African countries, on an annual basis.

- The WRC research team developed a non-hydrostatic dynamic kernel that was used by CSIRO-AR scientists to transform C-CAM to a non-hydrostatic model. A local scientist visited the CSIRO-AR in January 2004 to collaborate in the implementation of the non-hydrostatic formulation of C-CAM.

1.5 RESEARCH ROUTES

Research in the project was first divided into two main routes as indicated in Figure 1.1.

1.5.1 Research route 1

Research route one aimed to improve model simulated rainfall patterns over South Africa. This is in line with the research objective to improve the simulation of water related atmospheric variables over South Africa. The WRC research team performed many simulations on local workstations in order to verify different model versions on a regular basis. Model rainfall biases were identified and CSIRO-AR researchers were notified. Researchers at the CSIRO-AR then adjusted / improved rainfall parameterization schemes in the model code, whereafter the improved code was sent back to the WRC research team for further verification. This process of code exchange took place for almost three years, meaning that a large number of model simulations were executed on local workstations.

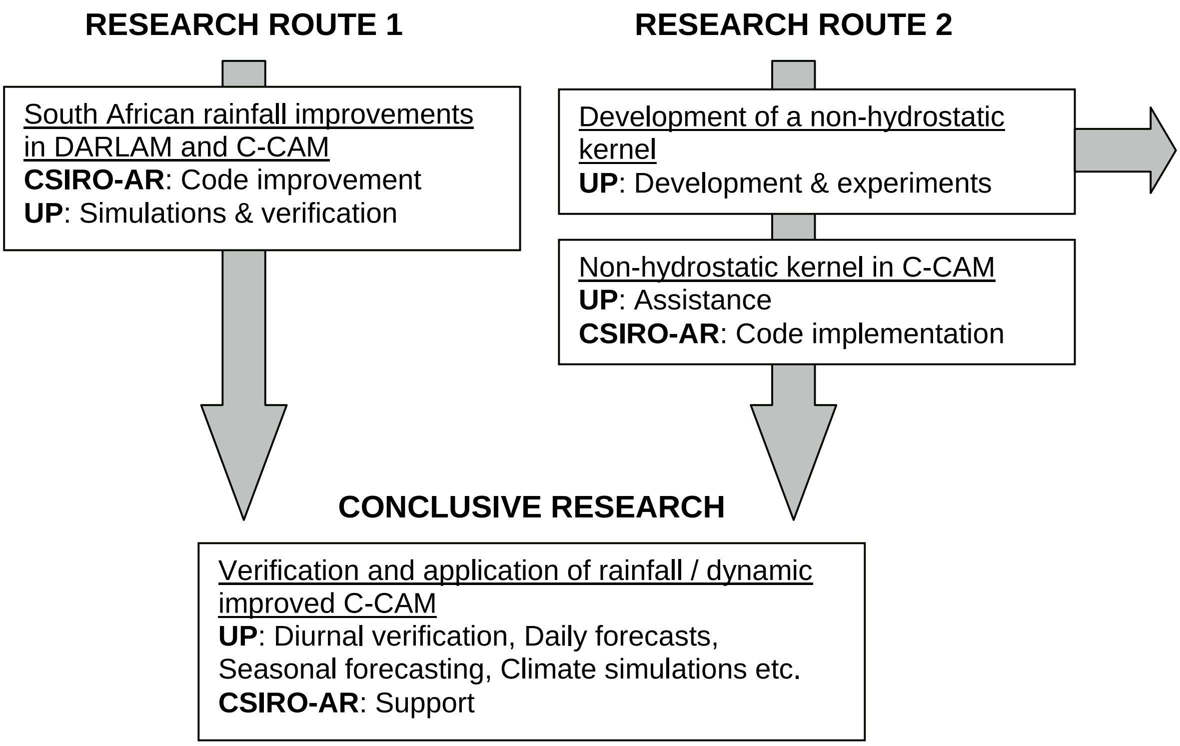

Figure 1.1 A diagram showing the major research routes taken in this project

1.5.2 Research route 2

Research route two consisted of two components. (1) In the first place an unique non-hydrostatic kernel was developed by the WRC research team in South Africa. Many tests were performed in the form of the release of thermal bubbles in the model atmosphere. In future other components (radiation budget, surface characteristics, moisture and rainfall etc.) may be added to the kernel to develop a more comprehensive model. (2) The dynamics developed were used as guideline for making C-CAM non-hydrostatic at the CSIRO-AR. This task was completed during a visit of a WRC researcher to the CSIRO-AR in February 2004.

These two research routes yielded model improvement in rainfall as well as general circulation (dynamics). It also established a sustainable basis for model development in South Africa, both institutional and human-related. In the conclusive research the latest version of C-CAM was used for final simulations, and these simulations were verified. Model development is an ongoing process. Since the WRC project is time-restricted, the WRC research team had to decide on a deadline point for the conclusive research. The conclusive research could not take place before the WRC research team was convinced that significant progress had been made with respect to deliverables from the two research routes.

The achievements, capacity building, knowledge transfer and sustainable bilateral collaboration established by this project, not only between South Africa and the CSIRO-AR but also among African countries, proves that the research approach and routes were greatly successful.

1.6 ORGANISATION OF THE REPORT

Existing international rainfall fields that are available for model verification are critically evaluated in Chapter 2. As a result of various shortcomings in these fields the research team decided to construct fine resolution rainfall fields from 1027 quality controlled data point over South Africa. These fields were used for model verification in the project. The grid configuration of C-CAM is discussed in Chapter 3 and various grid projections over South Africa is shown. C-CAM was obtained from the CSIRO-AR and a number of sensitivity studies were completed with the purpose to produced improved rainfall simulations. Different simulations where model parameters were altered were completed. The most important results from these sensitivity studies are outlined in Chapter 4. In Chapter 5 results from the latest rainfall simulations over South Africa are shown. The results are a significant improvement on the overestimated rainfall simulations that were produced at the beginning of the project. As part of the project the research team put in a large effort to produce code for a unique South African atmospheric flow model. A lot of progress has been made since the beginning of the project. The mathematical and numerical formulation of the dynamic kernel of the model is presented in Chapter 6. The ultimate purpose of a regional atmospheric model is certainly to use the model as a numerical weather prediction model. A licence for this purpose was obtained and a number of C-CAM forecasts are verified in Chapter 7.

CHAPTER 2

OBSERVED RAINFALL FOR MODEL VERIFICATION

2.1 INTRODUCTION

Model performance is evaluated by comparing model results with observations. Many global observational fields are currently available for model verification. These fields are normally in grid format, meaning that they are interpolated from unevenly distributed observations towards a regular grid. The value at a grid point usually represents the non-weighted spatial average of observational points located within the boundaries of the associated grid box. The value of a grid point is therefore a function of the spatial coverage of observations in the grid box domain. As modern model simulations are performed at increasingly finer grid resolutions, the demand for denser observational networks becomes greater. Coarse resolution observational fields (here regarded as coarser than 1^o x 1^o) might be useful to verify general large-scale atmospheric patterns as well as averaged climate fields, but they are not suitable for verification use in fine resolution model development studies where the sensitivity of the atmosphere to fine resolution initial and boundary fields are evaluated. Global fine resolution observational fields are not commonly available, most probably because it is not yet possible to allocate observed data values to all sub-grid scale Earth surface / atmosphere locations.

Rainfall, in particular, is highly variable in space and time, and although point rain gauge measurements are recorded at many locations, ocean and remote land regions are not yet well covered. Even areas that are well covered might not reflect a complete spatial representation of rainfall totals, since there is still the possibility that rain clouds might cross over an area between rain gauges – as indicated by radar studies. To compensate for these shortcomings, estimated satellite derived rainfall data (normally associated with thermal properties of convective clouds) and model assimilated rainfall data were recently introduced and merged with rain gauge measurement fields to produce estimated global rainfall fields (Xie and Arkin, 1996; 1997).

When verifying finer resolution model results against observations, one must always keep in mind that the so-called observational rainfall fields are subject to errors, and that weak comparisons between model and observational fields do not necessarily imply poor model performance.

In the following Sections results of monthly rainfall totals for January and July from some of the world's best-known observational data sets are displayed and compared. It will become evident that some of these data sets are unsuitable for fine resolution model verification purposes since, although at a relatively high resolution, observed rainfall over southern Africa is significantly under or overestimated. Smoothed coarser resolution observational fields with smoothed topography do not capture the impact of steep topography on rainfall distribution, a feature regarded as extremely important in fine resolution modeling. These smoothed fields are also regarded as unsuitable. This Chapter aims to identify or produce a rainfall observational field that is suitable for use in fine resolution model verification over South Africa, especially with model development in mind.

Since the contribution of steep topography on rainfall is an important feature in fine resolution modeling research, we focused on summer (January) rainfall over the smaller domains of the Lesotho Drakensberg and winter (July) rainfall over the Western Cape. Maps for these regions are provided in addition to larger scale observational rainfall maps of South and southern Africa.

2.2 CRU OBSERVATIONAL DATA FOR RAINFALL

The CRU Global climate dataset is available through the Inter-Governmental Panel for Climate Change (IPCC) Data Distribution Center (DDC)[1]. The data set is commonly used to verify model results in climate, climate change and other related studies. The data consists of monthly climatology for land areas, excluding Antarctica, for the period 1961-1990 (30-years). Time series of more recent years are also available. Data fields have a 0.5º x 0.5º resolution. The CRU climate data set is decribed in New et. al. (2000). For comparison with other fields, CRU maps of average monthly total rainfall for January and July are shown in Figures 2.1 and 2.2. The first impression is that the general

[1] http://ipcc-ddc.cptec.inpe.br/ipccddc/html/cru_data/examine/cru_climate.html

summer and winter rainfall patterns are well presented over South Africa. Figure 2.2 indicates that the influence of high topography on rainfall is captured in the CRU observations, since increased rainfall appears along the slopes of both mountain ranges.

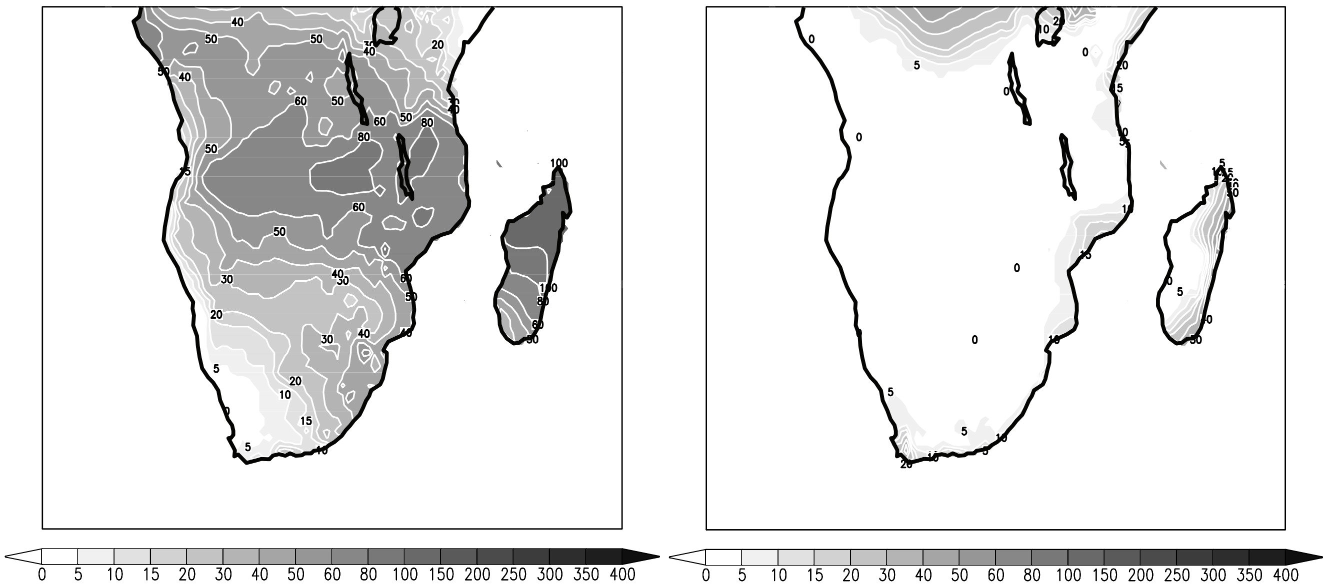

Fig 2.1 Average month total observational rainfall (1961-1990) for the African domain in mm for January (left) and July (right) as presented by the CRU climate data set.

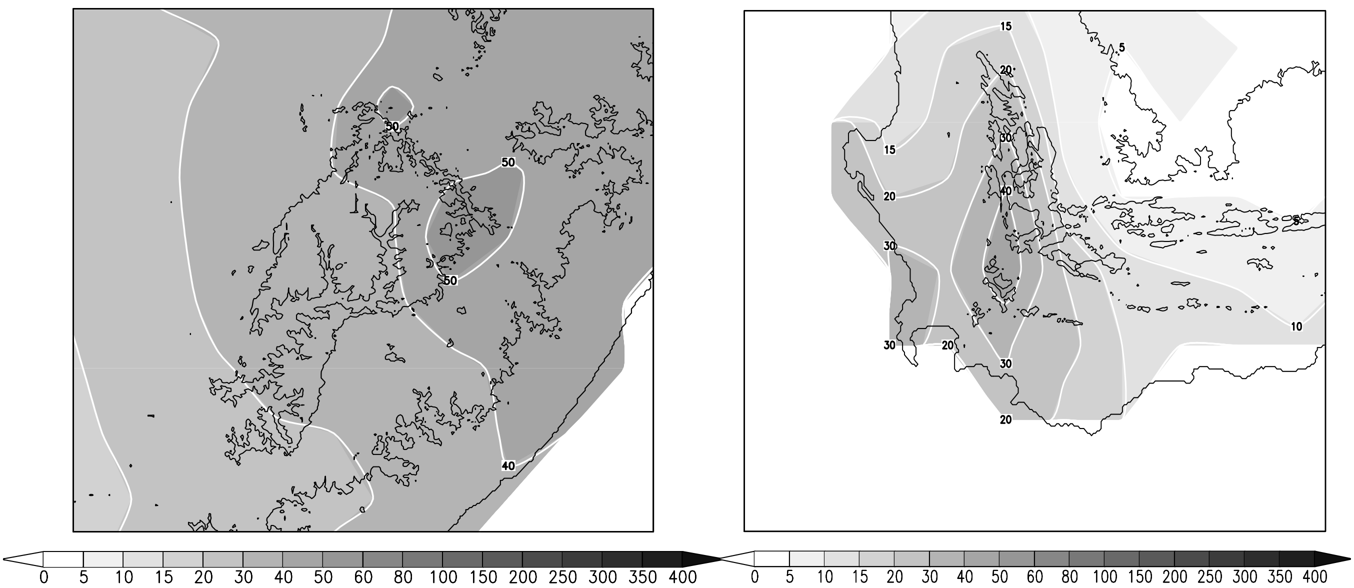

Fig 2.2 Average monthly observed rainfall (1961-1990) for the Drakensberg domain in January (left), and for the Western Cape domain in July (right) as represented by the CRU climate data set. Rainfall values are in mm. Topography with 1000m intervals is drawn as black contours.

2.3 GLOBAL CPC CMAP OBSERVATIONAL DATA FOR RAINFALL

The Climate Prediction Center (CPC) Merged Analysis of Precipitation (CMAP)[2] is a monthly data set of precipitation constructed by merging gauge, five kinds of satellite estimates and numerical model simulations. The data set is commonly used as observational reference to verify model results. The latest version of the data consists of global monthly total precipitation for the period January 1979 to September 2003, (25 years of January and July data) and is updated on a routine basis. In this study, long-term averages for January and July were calculated. The data has a 2.5º x 2.5º resolution. Details about the CPC CMAP climate data set are presented in Xie and Arkin (1996; 1997). For model verification purposes CPC CMAP maps of average monthly total rainfall for January and July are shown in Figures 2.3 and 2.4.

The CPC CMAP rainfall data covers ocean and land areas. Again the general summer and winter rainfall patterns are well presented over South Africa, although smoothed significantly. This particularly applies for the smaller mountainous domains (Figure 2.4) where the impact of high topography on observed rainfall cannot be seen at all.

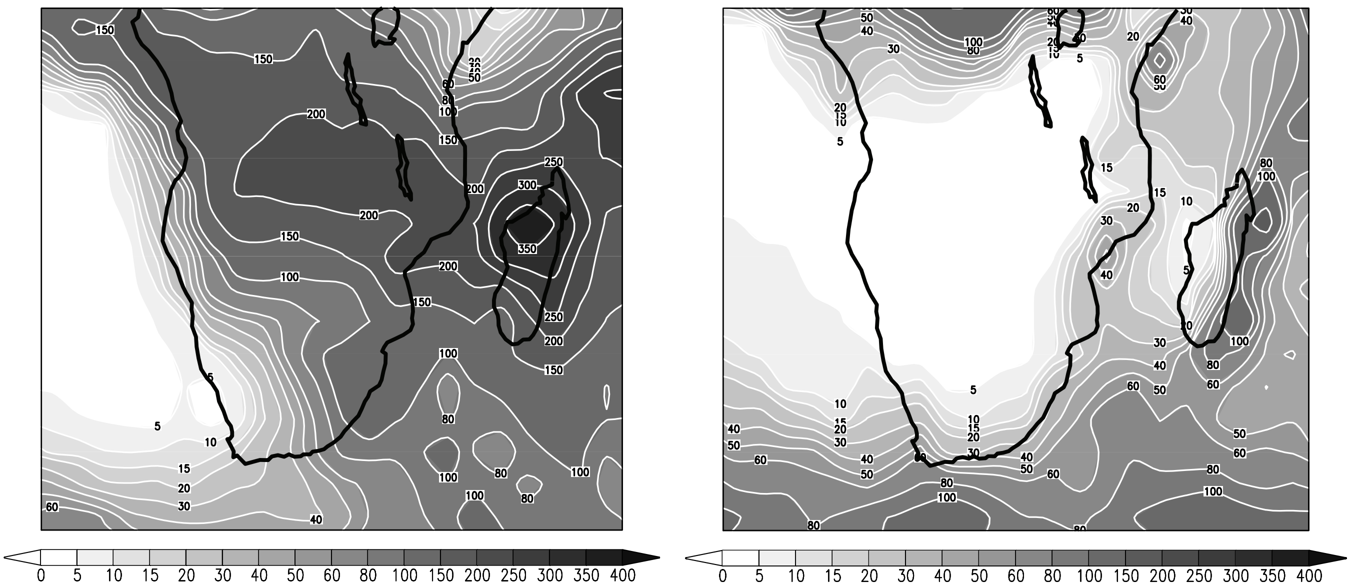

Fig 2.3 Average monthly observed rainfall (1961-1990) for the African domain in mm for January (left) and July (right) as represented by the CPC Merged Analysis of Precipitation climate data set.

[2] http://iridl.ldeo.columbia.edu/SOURCES/.NOAA/.NCEP/.CPC/.Merged_Analysis/.monthly/

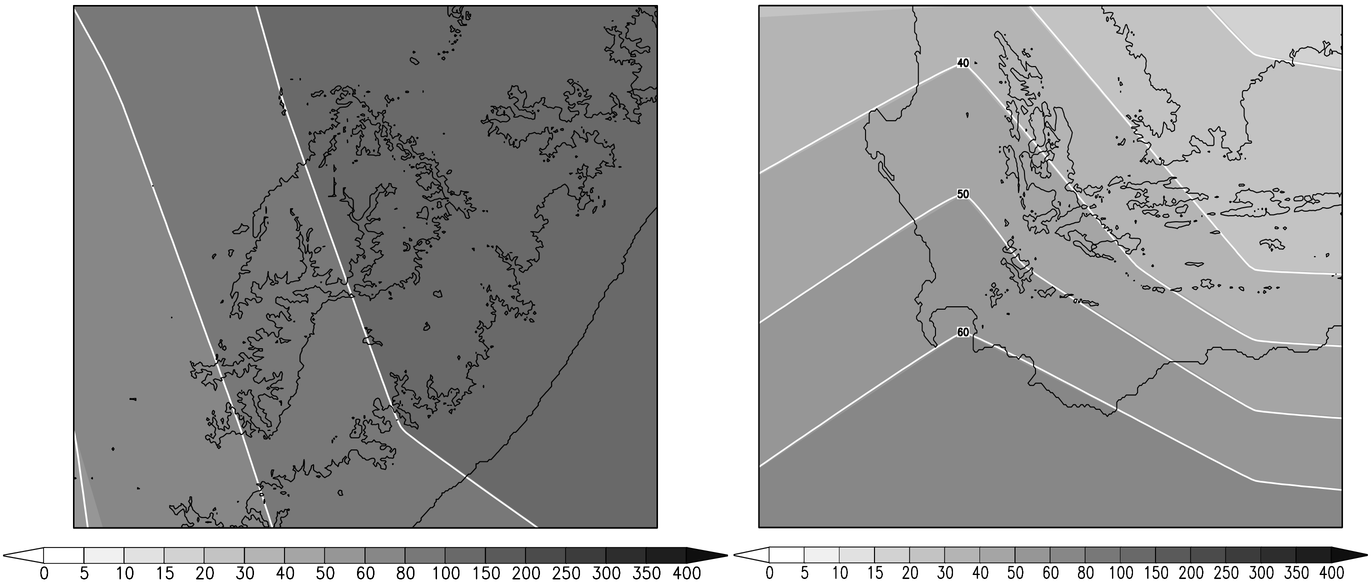

Fig 2.4 Average monthly observed rainfall (1961-1990) for the Drakensberg domain and January (left), and for the Western Cape domain and July (right) as represented by the CPC Merged Analysis of Precipitation climate data set. Rainfall values are in mm. Topography with 1000m intervals is drawn as black contours.

2.4 SAWS RAIN GAUGE OBSERVATIONS

In an effort to produce a finer resolution observational rainfall field suitable for fine resolution model verification over South Africa, a data point concentration-dependant weight function was used to construct a rainfall grid field of resolution 0.1717^o x 0.1313^o (19023.65 m x 14599.06 m) from the records of 1027 rain gauges distributed over South Africa. Averages of monthly total rainfall for January and July (1960-2002) were considered. The spatial coverage of rainfall gauges is shown in Figure 2.3. The quality-controlled data were obtained from the South African Weather Service (SAWS). This was done because the resolution of both the CRU and CPC CMAP data sets appeared to be too low for detailed regional model verification. Models used in this study have a resolution of approximately 60 km x 60 km.

2.4.1 Interpolation technique

Several interpolation algorithms have been developed to create homogeneous grid fields from heterogeneously distributed data. A shortcoming in most of these algorithms is the assumption that observed data field concentrations are fairly homogeneous over the grid field area. The method for constructing the weight functions as discussed here (Rautenbach, 1996) overcomes this problem by including a variable dependant on the concentration of observed data points in the weight function. This implies that the sphere of influence of an observed rainfall data value becomes less localized as data point concentrations decline. The weight function is particularly applicable to South Africa where the concentration of rainfall stations varies significantly.

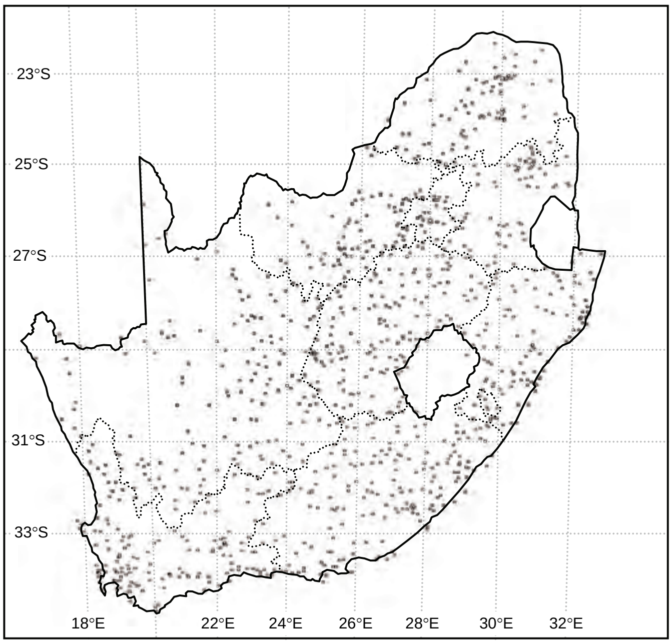

Fig 2.5 Spatial coverage of 1027 observational rainfall data points used to construct a finer resolution grid field that appeared to be more suitable for regional model verification. The quality-controlled data set was obtained from the South African Weather Service (SAWS)

The proposed data point concentration dependant weight function is an extension of a Gaussian weighting scheme, i.e.,

$$\mathbf{W(r_{kij}) = e^{-a.(r_{kij})^2}} \qquad (2.1)$$

Where $W(r_{kij})$ is the weight function of the k^{th} data value C_k for $k=1,\ldots,n$ at grid point (i,j). The distance between the position of any data observed point value C_k and a grid point value C_{ij} is denoted by r_{kij}. The subscript (i,j) refers to the i^{th} and j^{th} grid point in the x and y directions, located at a point with coordinates $((i-1)\ .\ \Delta x\ ,\ (j-1)\ .\ \Delta y)$ where Δx and Δy are the grid point inter-space values in the x and y directions respectively. The value of parameter a is chosen arbitrarily.

The grid point value for each grid point can be determined by a method of weighted interpolation defined by

$$\mathbf{C_{ij}} = \frac{\sum_{k=1}^{n} \mathbf{W(r_{kij}).C_k}}{\sum_{k=1}^{n} \mathbf{W(r_{kij})}} \tag{2.2}$$

The influence of an observed data point value becomes more localised as the value of a in equation 2.1 increases. Seeing that the square $(r_{kij})^2$ in equation 2.1 only contributes to the radius of influence of an observed data point value, it can be replaced by r_{kij}. This results in the following modified weight function.

$$\mathbf{W(r_{kij}) = e^{-a.r_{kij}}} \tag{2.3}$$

A disadvantage of weight functions (2.3) is that the computed grid point value C_{ij} at position (i,j) can become unrealistically small if a, as well as the smallest value of r_{kij} become relatively large (widely distributed observed data points). It is therefore appropriate to enlarge the radius of influence at an observed data point value C_k at any grid point (i,j) as the distance from the grid point to the nearest observed data point increases. Define

$$\mathbf{r_{(min)ij} = \frac{min}{k}(r_{kij})} \tag{2.4}$$

The value of a strongly contributes to the radius of influence of any observed data point value C_k. Replace a by the function $a(r_{(min)ij}) = a_{ij}$. Let the maximum weight ($W(r_{kij})=1$ for this case) be allocated to an observed data point at distance $r_{(min)ij}$ from a grid point. Thus

$$\mathbf{W(r_{kij}) = e^{-a_{ij}.(r_{kij}-r_{(min)ij})}} \tag{2.5}$$

Define the parameter b by letting $W(r_{kij})=b$ for $b > 0$ at any observed data point at distance $2x(r_{(min)ij})$ from the position of grid point C_{ij}. Applying this to equation (2.5) results in the following function.

$$\mathbf{W(r_{kij}) = b^{\frac{r_{kij}-r_{(min)ij}}{r_{(min)ij}}}} \quad ; \quad \mathbf{r_{(min)ij} \neq 0} \qquad (2.6)$$

The data point dependant weight function (2.6) is of such a nature that the radius of influence of an observed data value decreases with an increase in the value of the parameter b, and increases with an increase in the distance $r_{(min)ij}$. Weight function (2.6) is quite applicable for rainfall grid field interpolation in a country like South Africa where observed data point concentrations are higher over the eastern parts, and lower over the western parts of the country.

2.4.2 A fine resolution climatology

Figure 2.6 presents maps of interpolated average rainfall total data (1960-2002) over South Africa for the months January and July. In comparison to the rainfall maps in Figures 2.1 (CRU data) and 2.3 (CPC CMAP data), Figure 2.6 contains much more detail.

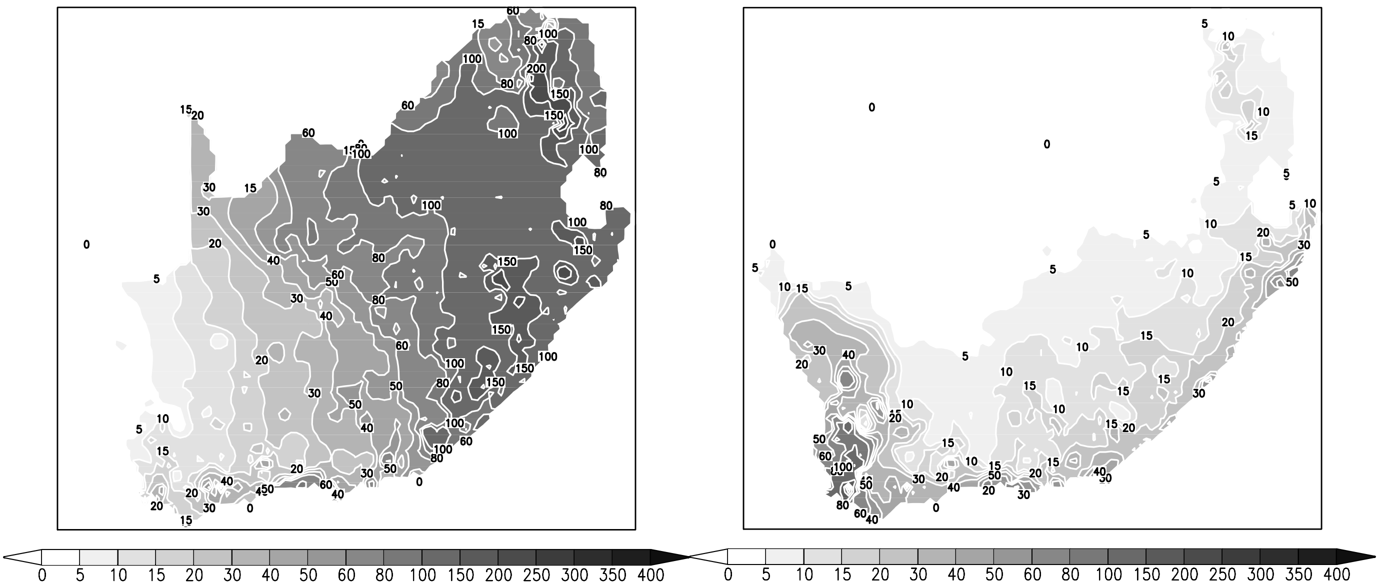

Fig 2.6 Average monthly observed rainfall (1960-2002) for the South-African domain in mm for January (left) and July (right) as represented by the SAWS climate data set.

The grid dimension of the data is summarized at the beginning of Section 2.4. Model development in this research focuses on water related atmospheric variables such as rainfall, and in particular rainfall over high topography. In agreement with the CRU and CPC CMAP data the east-west gradient in summer rainfall (Figure 2.6 left) and the Western Cape and coastal winter rainfall (Figure 2.6 right) are well represented. As previously we will here, in addition to the South African maps, also focus on smaller domains with high topography. Figure 2.7 shows average rainfall maps for the Drakensberg domain (January), and for the Western Cape domain (July).

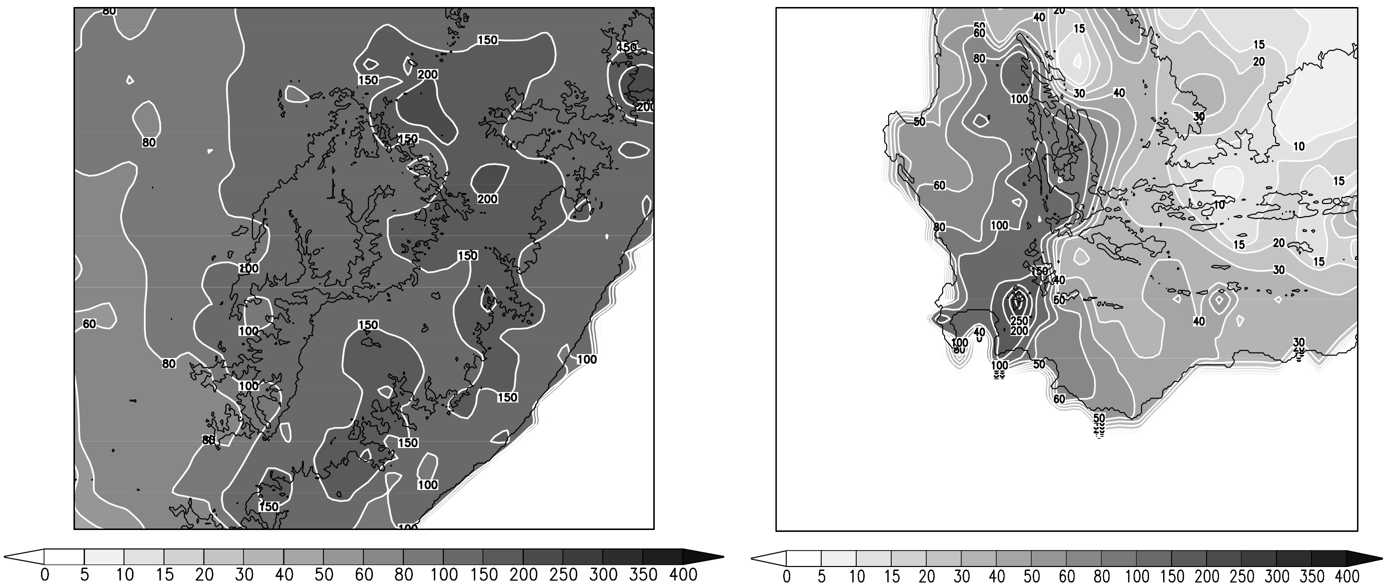

Fig 2.7 Average monthly observed rainfall (1960-2002) for the Drakensberg domain and January (left), and for the Western Cape domain and July (right) as represented by the SAWS climate data set. Rainfall values are in mm. Topography with 1000m intervals is drawn as black contours.

2.5 CONCLUSIONS

The CRU and CPC CMAP observational data sets have a relatively coarse grid resolution and important fine resolution features such as the influence of high topography on observed rainfall is smoothed out significantly. Apart from this, observed summer rainfall is significantly underestimated by the CRU data (almost 100mm difference between Figures 2.1, 2.2 and 2.6, 2.7), and the project team would be surprised if scientists even consider using this data for any model verification studies over South Africa. The coarse resolution CPC CMAP observational data is also regarded as unsuitable for model verification purposes, especially with model development in mind. Important to note is that this Chapter points out that international rainfall observational fields are not always suitable for use in South African research.

In contrast, fine resolution features are well captured in the interpolated gauge measurement rainfall grid fields (Figures 2.6 and 2.7). These fields may obviously improve if more rain gauge values are added or even if satellite and radar estimates are incorporated. Nevertheless, the project team decided to use the maps in Figures 2.6 and 2.7 for model verification in this study.

CHAPTER 3

A CONFORMAL CUBIC ATMOSPHERIC MODEL

3.1 INTRODUCTION

The regional model DARLAM was obtained from the CSIRO-AR and many simulations were completed at UP (Figure 3.1). Results are discussed in detail in the scientific paper Engelbrecht et.al. (2002), and will not be duplicated in this report.

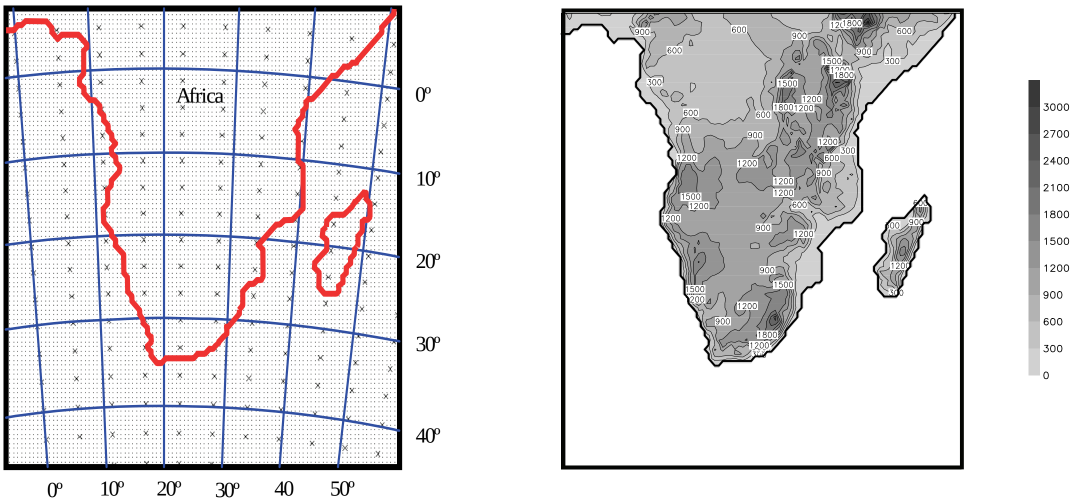

Figure 3.1 The DARLAM domain used for simulations over the SADC region (left). The 60 km x 60 km spaced model grid points on a Lambert conformal projection are indicated by dots. Gaussian grid points of the R21 CSIRO-9 GCM are indicated by crosses. DARLAM representation of topography over the SADC region are shown on the right. The contour interval is 300m.

After a significant number of model simulations were completed with DARLAM, the project team decided to start focusing on C-CAM. In principle, C-CAM contains the same dynamic and physical configuration as DARLAM. The benefit of C-CAM is that it is a global stretched grid model and problems related to nested modeling are therefore avoided. The change of models followed from a decision by the CSIRO-AR to stop all future development on DARLAM.

In this Chapter the grid configuration of C-CAM is introduced. The primitive equations in the new coordinate are provided, and a number of model simulations are performed to address issues related to possible disadvantages of using a stretched grid model for regional simulations.

Sadourny (1972) discovered that the spherical grid is subjected to instabilities since clustering of grid points appear at the poles. As a consequence, a significant reduction in the size of the time step is required according to the CFL stability requirement:

$$\left| \frac{c\Delta t}{\Delta x} \leq 1 \right| \tag{3.1}$$

where c is the phase velocity of waves propagated in the x direction and Δt the time step (Haltiner and Williams, 1980; McGregor, 1996a)

Sadourny (1972) introduced the mapping of a regular polyhedron (in the form of a cube) onto a sphere by central projections. This was later known as gnomonic projection. Rancic *et al* (1995) defined the gnomonic projection of a cube onto a sphere as a radial projection from the center of the cube inscribed into the sphere, noting that the centres of the cube and sphere coincide. The coordinates of the mapping domain were represented by the angles of the projection rather than the distances on the cube. Each point on the cube was connected to the corresponding point on the spherical surface by a ray projecting from the center of the sphere. The ray then defined the mathematical transformation, a one-to-one function, which connects these points. Adjacent grid lines subtended equal angles (angles of the projection) at the center of the sphere. The result was a more regular distribution of grid boxes on the sphere on which the cube was projected (Rancic, *et al,* 1995).

If the sphere represents the Earth, its axis of rotation will enter through the centre of one panel of the cube and exit through the centre of the opposite panel. The north and south poles are therefore represented at the centres of opposite panels (McGregor, 1996a).

A problem with the gnomonic projection, as observed by Sadourny (1972), was the generation of noise on singular edges *i.e.* the corners of the spherical cube. According to Rancic' *et al* (1995) this was caused by angular discontinuity leading to non-orthogonal grid lines on the sphere. Instead of smooth transition across the edges, there was an angle between the incoming coordinates that became 120° at the corners of the spherical cube. To resolve this problem, a conformal mapping between the cube and the sphere was introduced (McGregor, 1996a). By definition a conformal mapping from one surface to another preserves the angles between intersecting smooth curves. Since the angles between the grid lines on the cube now had right angles, grid lines on the spherical cube were orthogonal. Conformal coordinates were generated numerically on each of the panels of the cube. The coordinate lines passed continuously and smoothly between the adjacent panels, except for corner points. Although grid boxes near the corners were reduced in size as a result of this process, linear stability was maintained (Rancic, *et al,* 1995).

An observer at a fixed geographical point on the Earth watching flow from that fixed point is located in an Eulerian coordinate system. Advection schemes in Eulerian coordinates perform well on regular Cartesian meshes. The problem is that time steps are restricted by grid resolution in order to maintain stability. In addition, an observer is not stationary in a Lagrangian advection scheme, but follows the flow. Larger time steps can be achieved in Lagrangian advection schemes. A disadvantage, however, is that Lagrangian schemes normally have an initially regularly spaced set of particles that generally evolves to a highly irregularly spaced set at later time intervals (Staniforth and Cote, 1991). A solution would be to bring the regular resolution of the Eulerian schemes and the enhanced stability of their Lagrangian counterparts together – a process that results in semi-Lagrangian schemes (Tanguay, *et al*, 1991).

3.2 A CONFORMAL CUBIC ATMOSPHERIC MODEL

C-CAM employs a conformal cubic projection over a sphere instead of a traditional longitudinal-latitudinal projection. An important feature of the conformal-cubic projection is that it avoids the stability problems previously experienced at the poles. In the conformal cubic projection the model grids are expressed on six panels of a cube, which is then radially projected onto a sphere (Figure 3.2). Each panel has a user prescribed number of grid points. The grid may then be stretched with a stretch factor ranging from 0 to 1 (Schmidt factors) for full-stretch and non-stretch modes, respectively. The model used in this study uses a staggered Arakawa C-grid.

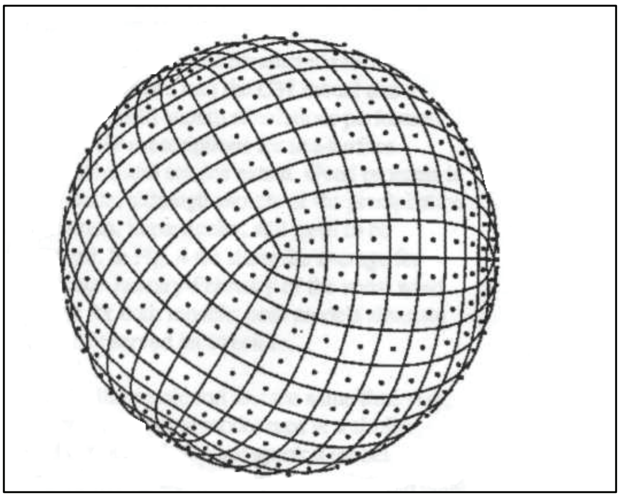

Figure 3.2 A conformal-cubic grid, each panel having 9x9 grid points. Grid points are shown as dots at the center of the grid boxes (Adopted from: McGregor and Dix, 2001).

An important feature is that C-CAM employs the semi-Lagrangian advection technique. A benefit of the semi-Lagrangian approach is that longer time steps can be achieved in model simulations, which makes C-CAM much faster than traditional models where time steps are restricted by grid resolution (Courant-Friedrichs-Levy or CFL criteria). Here the departure points are determined using, not only the velocity along a straight line trajectory as usual but also the acceleration, and when necessary, higher order curvature terms derived kinematically. This higher order scheme is more efficient and has a higher order of accuracy. In addition to the semi- Lagrangian technique, semi-implicit methods are used to solve the primitive equations of the model. Material derivatives are written in terms of a map factor that depends upon the stretch factor. The primitive equations are therefore functions of the stretch factor. Terrain-following sigma coordinates are employed in the vertical.

The physical parameterisations in C-CAM involve the Arakawa mass-flux cumulus convection scheme, the Tiedkte shallow convection scheme, downdrafts and detrainment, a stability dependent boundary layer, long-wave and short-wave radiation, interactive diagnosed cloud distributions, evaporation of rainfall, deformation based horizontal diffusion and a vegetation/canopy scheme with six layers for soil temperature and soil moisture.

3.3 CUBIC CONFORMAL PROJECTIONS OVER SOUTH AFRICA

Figures 3.3, 3.4 and 3.5 depict the global topography as captured on the six panels of the conformal cubic projection of C-CAM on the different resolutions used in this project. Note that the maximum stretch appears over panel two that contains the topography of South Africa. The resolutions considered were a C42 resolution (42 x 42 grid boxes per panel) and a Schmidt stretch factor of 0.3, a C42 resolution (42 x 42 grid boxes per panel) and a Schmidt stretch factor of 1.0 (non-stretched) and a C64 resolution (64 x 64 grid boxes per panel) and a Schmidt stretch factor of 0.3. In the stretched resolutions panel five (back panel) covers a much larger area than panel two (front panel). This allow for a finer resolution over the front panel that makes the model suitable for regional scale studies.

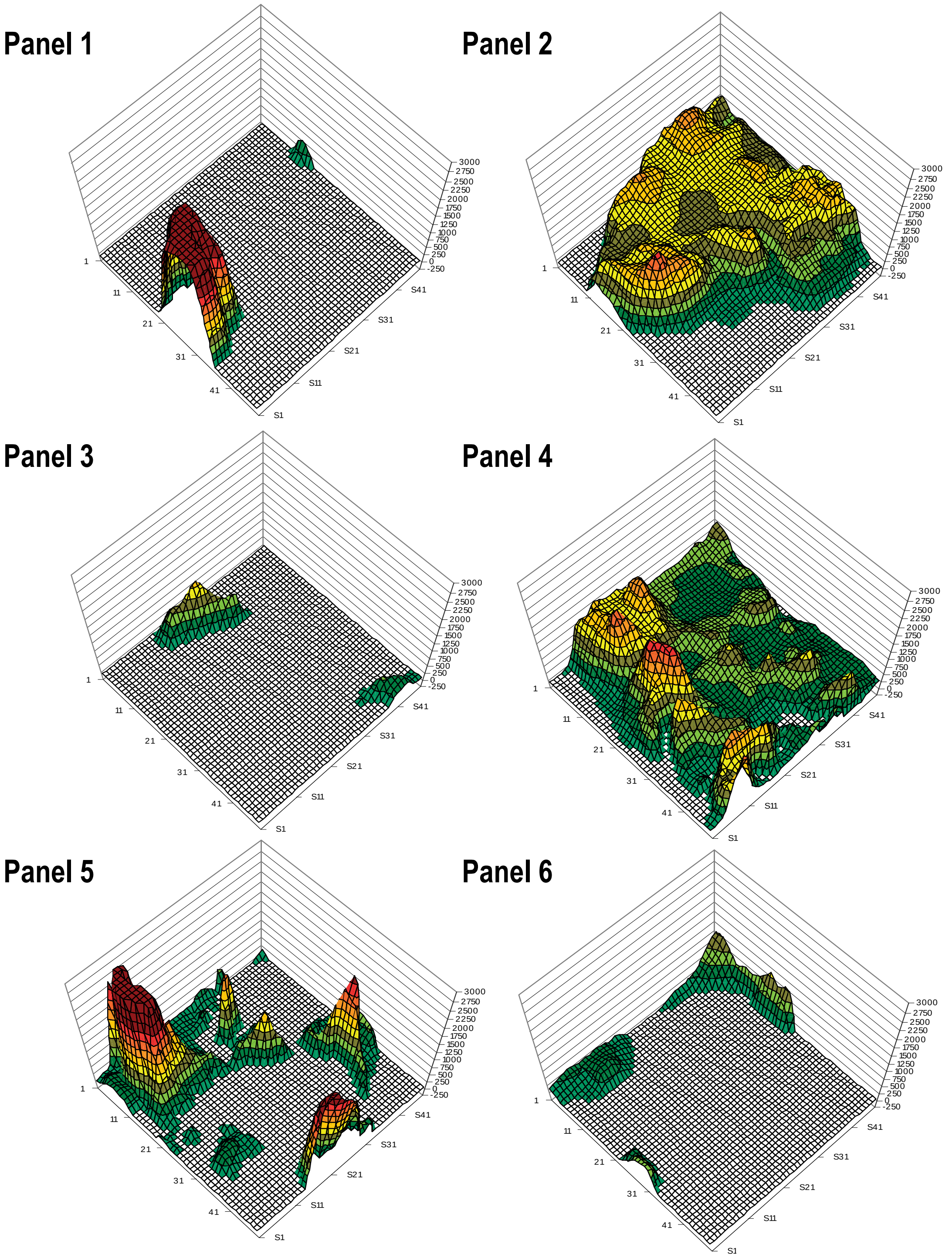

Figure 3.3 Six panels of the Conformal Cubic Model (C-CAM) with a C42 resolution (42 x 42 grid boxes per panel) and a Schmidt stretch factor of 0.3. Maximum stretch occurs over Panel 2 (front panel that contains South Africa). Note that Panel 5 (back panel) covers a much larger area than panel 2 (front panel).

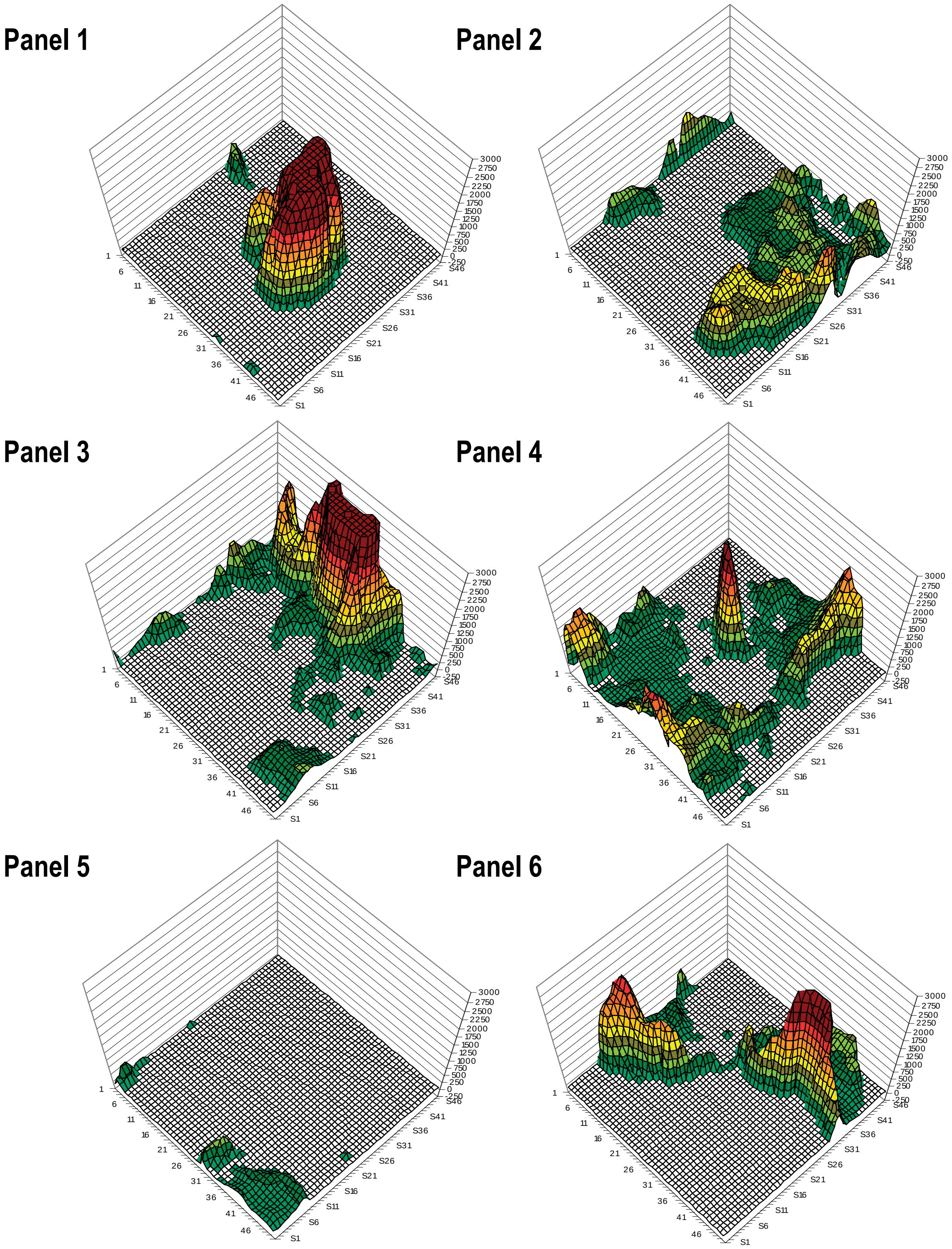

Figure 3.4 Six panels of the Conformal Cubic Model (C-CAM) with a C42 resolution (42 x 42 grid boxes per panel) and a Schmidt stretch factor of 1.0 (**non-stretched**). Note that all panels cover equal areas on the surface of the Earth.

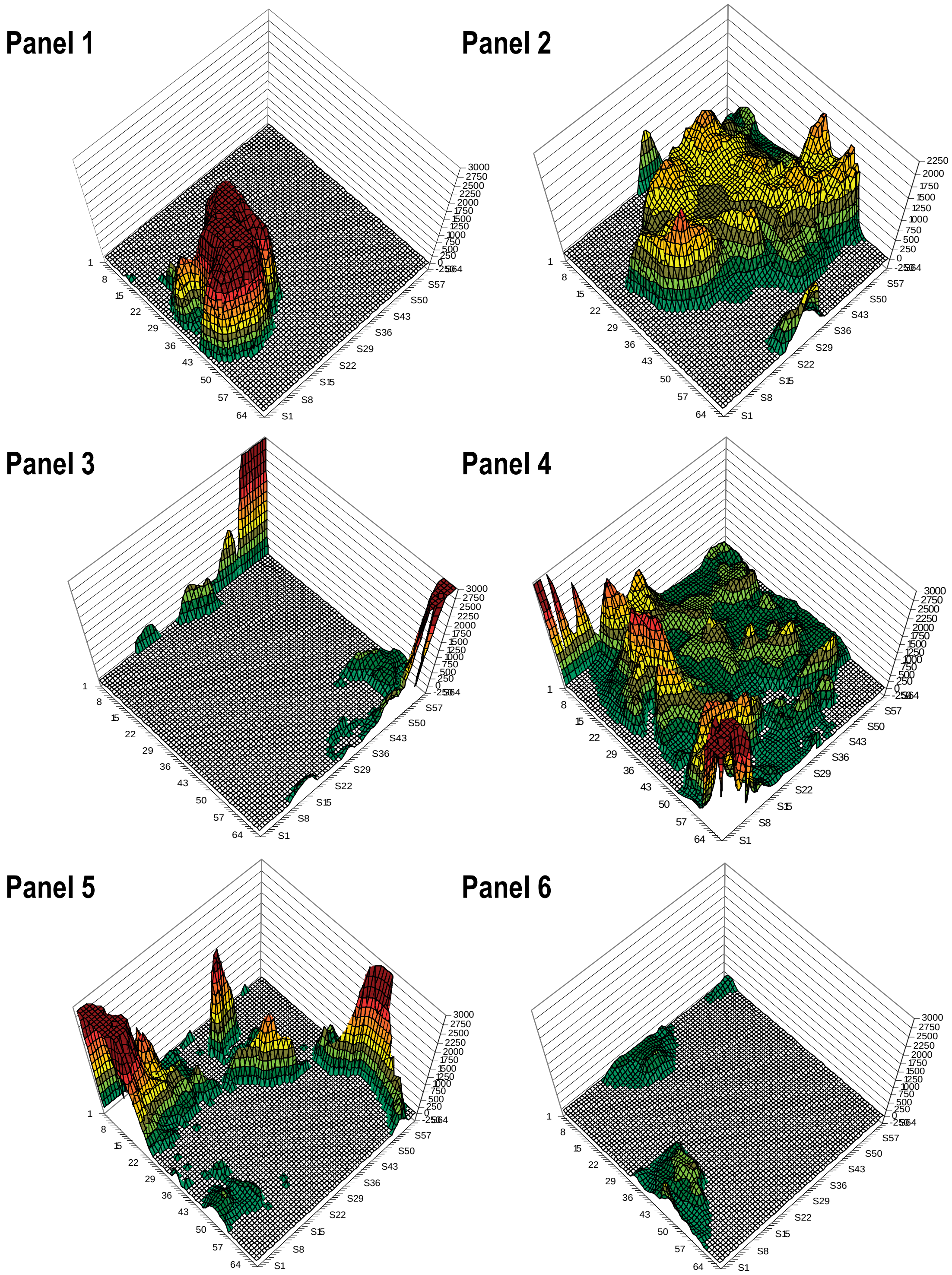

Figure 3.5 Six panels of the Conformal Cubic Model (C-CAM) with a C64 resolution (64 x 64 grid boxes per panel) and a Schmidt stretch factor of 0.3. Maximum stretch occurs over Panel 2 (front panel that contains South Africa). Note that Panel 5 (back panel) covers a much larger area than panel 2 (front panel).

CHAPTER 4

SENSITIVITY EXPERIMENTS WITH C-CAM

4.1 SENSITIVITY TO GRID RESOLUTION

C-CAM is a global variable-resolution model where the horizontal grid is defined over six panels of a cube that are projected onto a sphere (Figures 3.4 to 3.6). An important feature of the model is that the horizontal grid over one of the panels can be stretched to a finer resolution over the area of interest to produce fine resolution simulations. This will obviously lead to a coarser grid resolution over the opposite panel, which might result in errors filtering through to the front panel during model simulations. In this Section we investigate the degree of error generated by different horizontal grid resolutions over the period of one month. For this purpose simulations for 31 days ahead in time were initiated from the beginning of January 1975. These model simulations were performed with the following grid resolutions:

- ***Base line simulation***: A C48 (48x48 grid points per panel) simulation stretched with a Schmidt factor of 0.3 and nudged by twice per day far field winds from observed SST/sea-ice forced CSIRO T63 AGCM simulations.
- ***Stretched simulation***: A C48 (48x48 grid points per panel) simulation stretched with a Schmidt factor of 0.3 and forced by observed SST/sea-ice fields (same as for the base line simulation).
- ***Non-stretched simulation***: A C48 (48x48 grid points per panel) simulation with a Schmidt factor of 1.0 (non-stretched) and forced by observed SST/sea-ice fields (same as for the base line simulation).

“Far field winds” means winds over panel six, which is at the opposite side of the cube and that has the coarsest resolution.

All these simulations were Atmospheric Model Inter-Comparison (AMIP) type simulations (simulations where the model is forced by monthly observed SSTs), except for the fact that C-CAM was “kept on track” in the base line simulation by nudging the model with CSIRO T63 AGCM wind output. The baseline simulation was the simulation against which the other two simulations were compared. The base line simulation consisted of a fine resolution grid (approximately 60kmx60km) over South Africa while values on the coarse resolution of the opposite panel were “kept on track” by nudging from an intermediate resolution (approximately 1.9^o x 1.9^o).

First a stretched simulation was completed. This simulation consisted of a fine resolution grid over South Africa with a coarse resolution grid over the back panel. We hypothesized that the coarse resolution over the back panel should generate errors that would result in growing differences between the stretched and base line simulation as simulation time progresses. The second simulation was a completely non-stretched simulation, implying equal grid resolutions on all six panels. Since the grid resolution over the back panel is now finer than in the stretched simulation, we hypothesized that the propagation of errors should be limited.

Although C-CAM had a time step of 30 minutes, results were written out every 12 hours of simulation time. A total of 62 output times were therefore produced for January 1975. For the purpose of the sensitivity test we decided to investigate output time number 2 (almost at model initialisation), output time number 31 (middle of the month) and output time number 62 (last field simulated). Simulation results of rainfall (mm/day) and Mean Sea Level Pressure (MSLP) over South Africa are shown in Figures 4.1 to 4.3.

C-CAM simulations over the three different grid configurations do not differ significantly in output file number 2 (Figure 4.1), since the model was initialised with the same data. A well-established tropical temperate trough occurs in this simulation where tropical clouds link with a frontal low in the south-eastern corner of the Figures. There are however some small differences in the simulations with the largest differences in the coarser resolution non-stretched simulation (Figure 4.1 – right).

Figure 4.2 shows model results 15 days into the simulation. At this point 720 time-steps have been completed (30 minute time-step). In general, circulations patterns still look similar with the Atlantic High ridging to the south of South Africa, and a dominant low-pressure system further south of the country. Surprisingly, the smallest differences occur between the base line and stretched simulation, which means that the coarse resolution of the back panel still has little effect on fine resolution simulations over the front panel. The non-stretch simulation differed the most from the others since less rain is simulated over the African continent and pressure systems are formed and located differently.

Thirty-one days later (1488 time-steps later) model results from the three different resolution simulations still do not diverge greatly (Figure 4.3), although some larger differences appear in the non-stretched simulation. A consistent strong high-pressure system of 1020 hPa – 1024 hPa developed to the south-east of the continent. This implies that the non-stretch simulation performed broadly as well as the base line and stretched simulations.

The same conclusion may be drawn from latitude-time diagrams of rainfall and mean sea-level pressure (Figures 4.4 and 4.5). Although slightly different, the same basic patterns were simulated throughout the month. These graphs confirm that the stretched simulation did not diverge significantly from the other two simulations.

One might therefore conclude that the coarse resolution created over the back panel as a result of grid stretching does not have a noticeable influence on simulations over the front panel – at least on the scale of one month. These results gave the WRC research team much confidence in the application of a stretched grid approach.

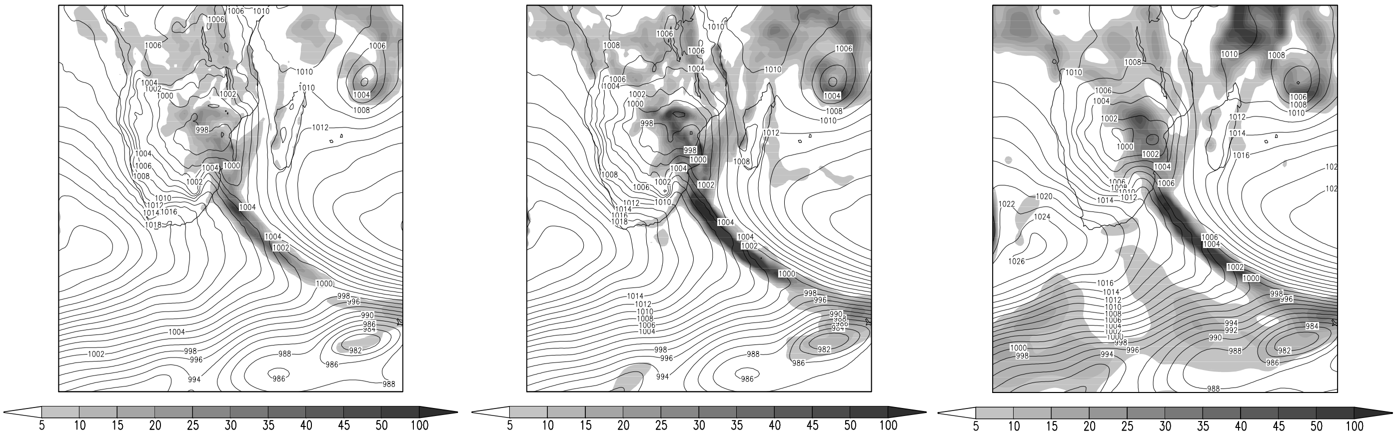

Fig 4.1 C-CAM simulations of rainfall (shaded) in mm/day and mean sea level pressure (MSLP) patterns in hPa for January 1975. Results are for the base line simulation (left), stretched simulation (middle) and non-stretched simulation (right) and for **output time number 2** (almost at model initialisation).

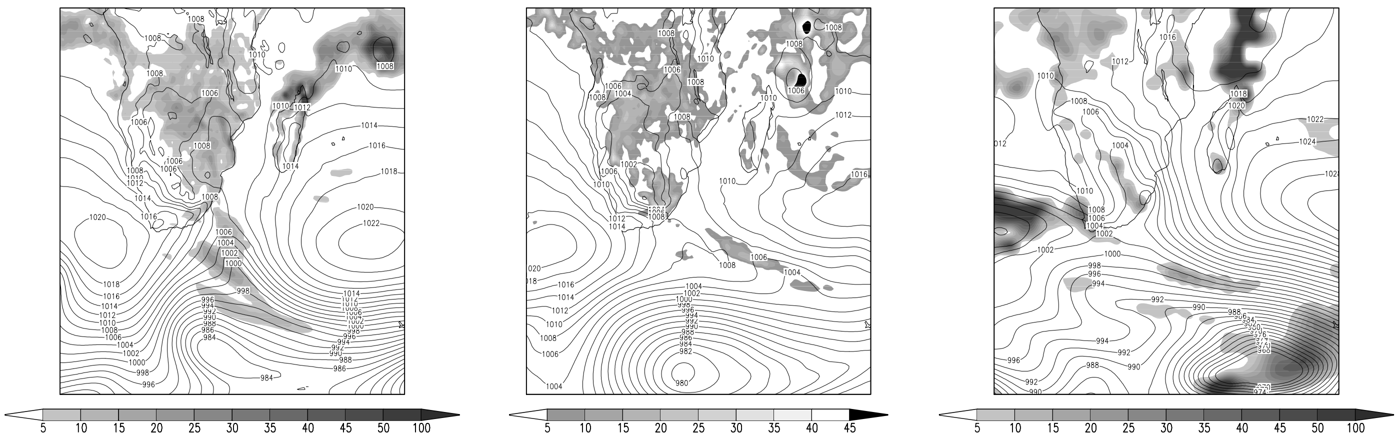

Fig 4.2 C-CAM simulations of rainfall (shaded) in mm/day and mean sea level pressure (MSLP) patterns in hPa for January 1975. Results are for the base line simulation (left), stretched simulation (middle) and non-stretched simulation (right) and for **output time number 31** (middle of the month).

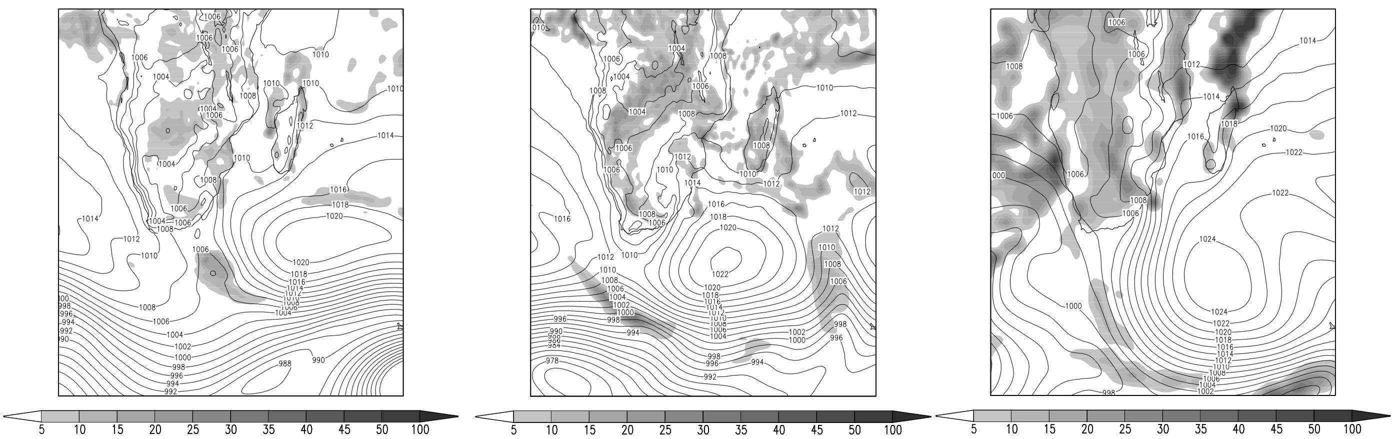

Fig 4.3 C-CAM simulations of rainfall (shaded) in mm/day and mean sea level pressure (MSLP) patterns in hPa for January 1975. Results are for the base line simulation (left), stretched simulation (middle) and non-stretched simulation (right) and for **output time number 62** (last field simulated).

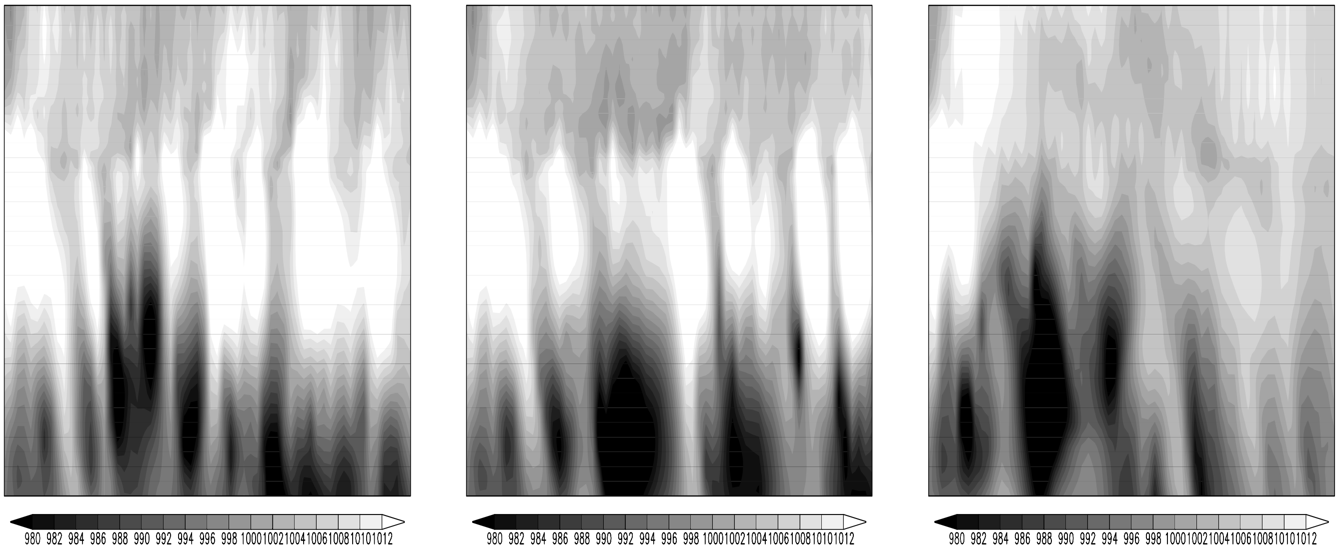

Fig 4.4 Time-latitude (x-axis: time ; y-axis: latitude) C-CAM simulations of mean sea-level pressure (MSLP) patterns in hPa for 31 days of January 1975 and longitude 0^o S to 60^o S. Darker / lighter shading denotes lower / higher pressures, respectively. Results are for the base line simulation (left), stretched simulation (middle) and non-stretched simulation (right).

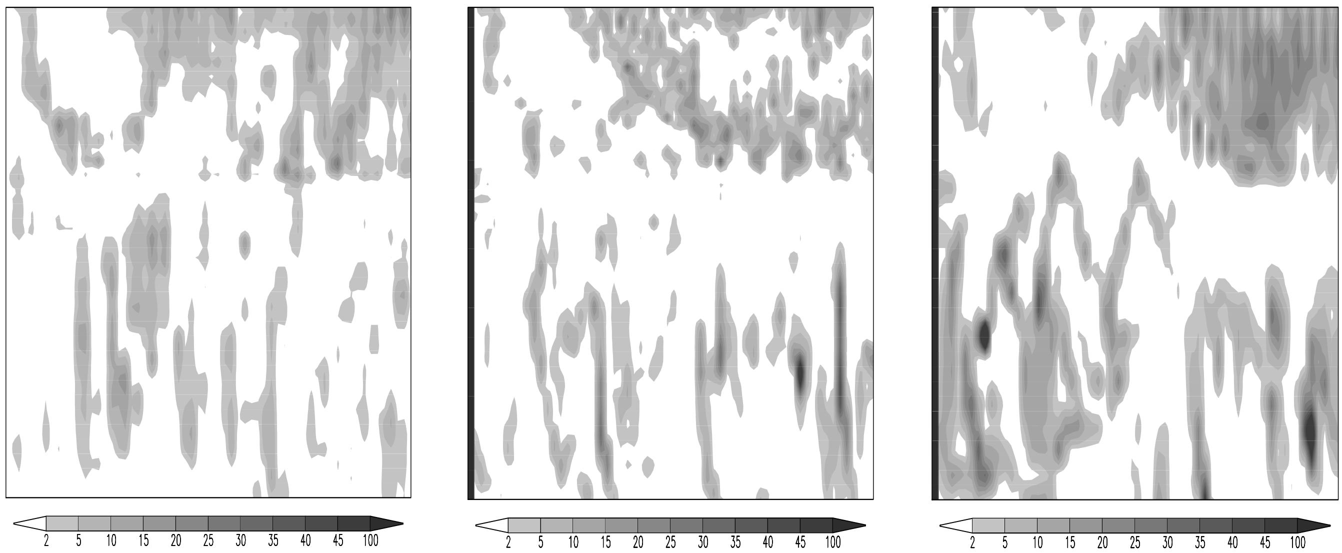

Fig 4.5 Time-latitude (x-axis: time ; y axis : latitude) C-CAM simulations of rainfall patterns in mm/day for 31 days of January 1975 and longitude 0^o S to 60^o S. Darker / lighter shading denotes higher / lower rainfall totals, respectively. Results are for the base line simulation (left), stretched simulation (middle) and non-stretched simulation (right).

4.2 JANUARY 1979 RAINFALL TOTALS AND SENSITIVITY TESTS

Observed rainfall totals over the Drakensberg domain for January 1979 are shown in Figure 4.6. The grid field was obtained by interpolating SAWS quality-controlled station data (see Chapter 2). The rainfall pattern for this month displays the usual high totals east of the escarpment (Figure 2.7), but an interesting maximum also appears to the west of the Lesotho-Drakensberg mountains. As pointed out earlier, this maximum is not present in the long-term average rainfall (Figure 2.7). Figure 4.7 shows January 1979 rainfall totals simulated by the first version of C-CAM (hereafter referred to as the F_2-simulation). The model was forced with AMIP sea-surface temperatures (SSTs) and sea-ice fields, and was initialized from NCEP-reanalysis data. Note that the F_2-simulation is just the first month of the 15-year F_1-simulation that is shown in the first part of Chapter 5. Compared to observations (Figure 4.6) the model performed exceptionally well in simulating a rainfall distribution with high totals to the west, north-east and south-east of the Lesotho-Drakensberg montains.

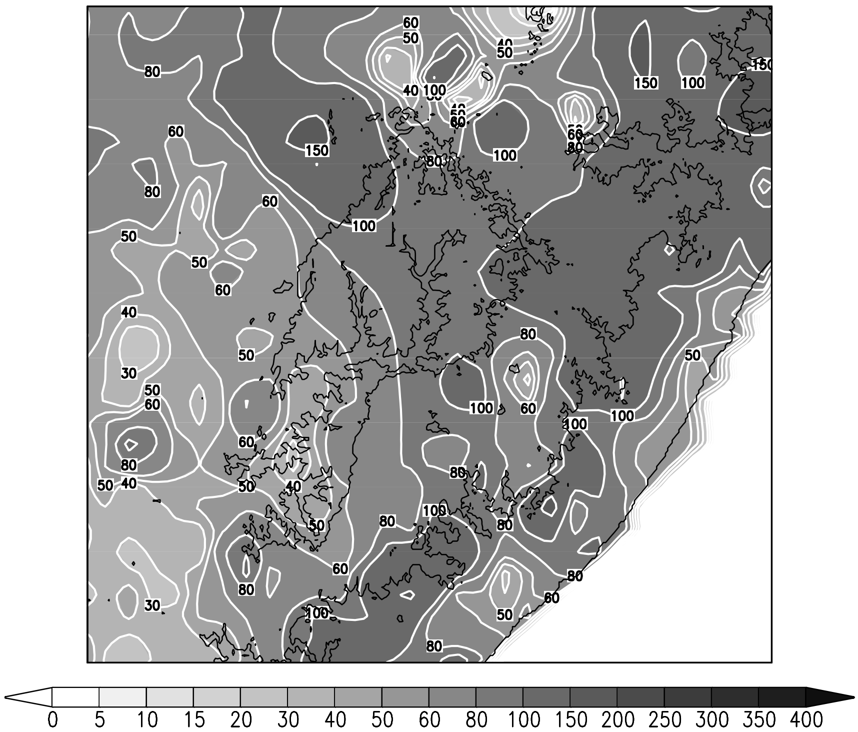

Figure 4.6 Observed rainfall totals (mm) over the Drakensberg domain for January 1979 (obtained from SAWS station data).

However, important to note is the excessively high rainfall totals simulated (more than 300 mm over certain regions).

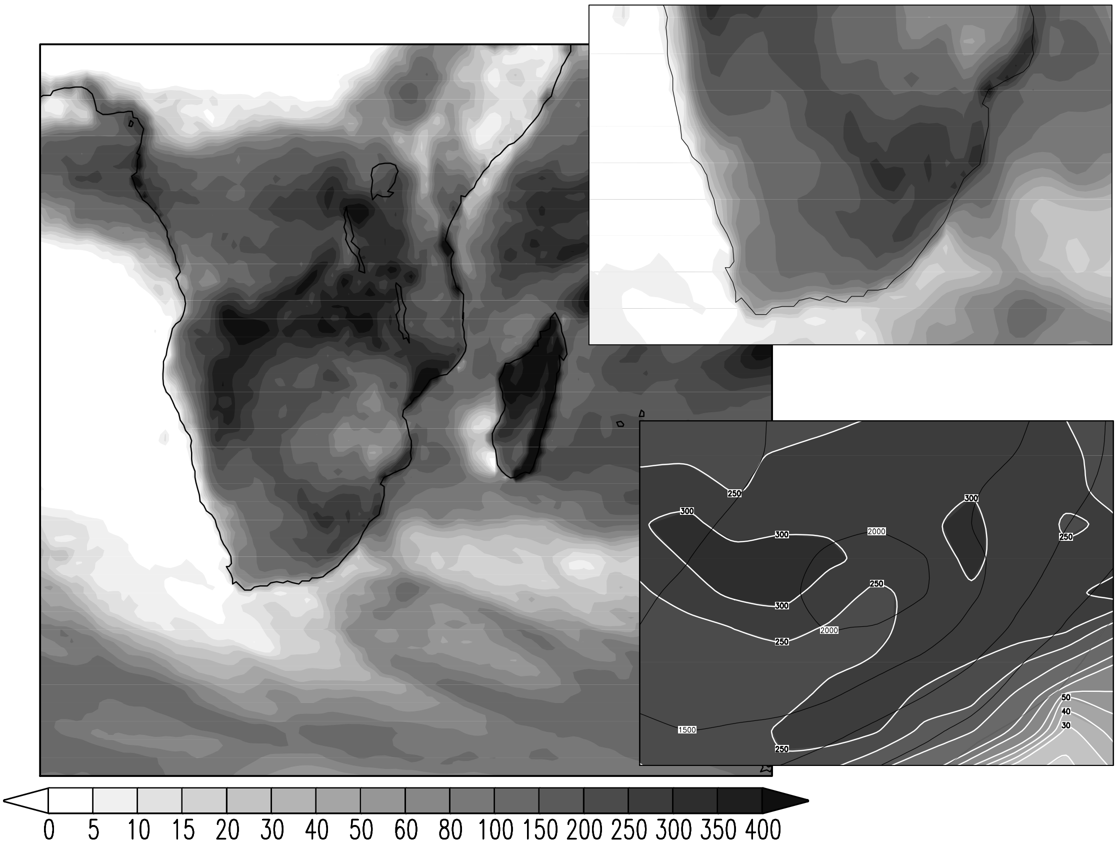

Figure 4.7 The F_2-simulation of rainfall totals (mm) for January 1979 forced with AMIP SSTs and sea-ice. Black contours indicate height above mean sea-level and the white contours are isohyets.

4.3 C-CAM RAINFALL IMPROVEMENT

Sensitivity tests performed to investigate the rainfall bias to the west of Lesotho in the long-term rainfall climatology as found in earlier simulations were largely based on changing the fraction of detrained air during the model integration (parameter “detrain” in the model’s convection scheme) and the duration of convection (parameter “convtime”). More detail is available in the following Sections. In a set of related sensitivity experiments, the importance of the magnitude of the time step used during the model integration was investigated. Details of the different sensitivity tests performed are shown in Table 4.1, with the associated acronyms used to refer to the different runs also included.

Table 4.1 C-CAM simulation acronyms and details about settings in the different model parameters					
Simulation acronym	Convtime	Detrain	Time-step (min)	Cloud scheme	Integration length
F1	0.3	0.05	20	Interactive	1979-01 – 1993-12
F2	0.3	0.05	20	Interactive	Jan 1979
A1	0.3	0.05	20	RH-based	Jan 1979
A2	0.3	0.02	20	RH-based	Jan 1979
A3	0.3	0.01	20	RH-based	Jan 1979
B1	1.0	0.05	20	RH-based	Jan 1979
B2=T3	1.0	0.02	20	RH-based	Jan 1979
B3	1.0	0.01	20	RH-based	Jan 1979
C1	1.5	0.05	20	RH-based	Jan 1979
C2	1.5	0.02	20	RH-based	Jan 1979
C3	1.5	0.01	20	RH-based	Jan 1979
T1	1.0	0.02	40	RH-based	Jan 1979
T2	1.0	0.02	30	RH-based	Jan 1979
T4	1.0	0.02	15	RH-based	Jan 1979
T5	1.0	0.02	10	RH-based	Jan 1979
T6	1.0	0.02	5	RH-based	Jan 1979

4.4 ALTERING THE DURATION OF CONVECTION

When unstable environmental lapse rates are present in the atmosphere, convection may be initiated. Convection is responsible for the transfer of huge quantities of heat, moisture and momentum in the atmosphere. When sufficient heat has been transferred to the environment via buoyant air parcels, the environmental lapse rate is stabilised and convection ceases to occur.

When integrating an atmospheric model, unstable environmental lapse rates are initiated in a similar way as in the true atmosphere. However, if the model is running at horizontal resolutions where convection can't be resolved (coarser than about 10-15 km), a convection-parameterisation scheme is needed for simulating convective processes so that the unstable lapse rates can be realistically stabilised. At horizontal resolutions finer than 10-15 km, convective circulation systems such as thunderstorms can be partially resolved by models. If a model is non-hydrostatic, it might be able to dynamically simulate some of the convection, but a parameterisation scheme may also be required to represent unresolved circulations. Only when the model runs at horizontal resolutions of a few 100 meters (in both the horizontal and vertical) the individual updrafts and downdrafts in a storm can be fully resolved and the use of a parameterisation scheme becomes unnecessary.

By increasing the value of the parameter "convtime" in C-CAM to be larger than the model time step (in hours), one delays part of the parameterised convective rainfall. As the potential instability is not fully removed, a greater proportion of resolved rainfall can be expected, and probably larger associated vertical velocities. The sensitivity tests performed confirm these ideas. The larger the value of "convtime" the more pronounced is the typical "orographic" rainfall pattern over eastern South Africa (compare the A-simulations to the B-simulations and C-simulations in Figures 4.9 to 4.17). Each of the "convtime" simulations are subdivided into three groups depending on the magnitude of detrainment as discussed in Section 4.5.

4.5 CHANGING THE FRACTION OF DETRAINED AIR

In C-CAM the fraction of convective rain used at each time step to moisten the environment can be altered. Increasing the parameter "detrain" to a value higher than 0.2 (these simulations are not shown in this report) did not work out well. It tends to moisten the environment to such an extent that excessive large-scale rain occurs. The preferred value seems to be closer to 0.05, 0.1 or 0.2. A series of experiments were performed in which the effects of smaller values of "detrain" (0.02 and 0.01) compared to "detrain"=0.05 were investigated as a function of "convtime" (see details in Table 4.1). Interesting to note is that changing "detrain" to 0.02 or 0.01 results in higher rainfall totals (Figure 4.8) over the analysis domain for any given value of "convtime". This may be the result of steeper environmental lapse rates that develop when less moisture (and therefore latent heat) is transferred to the environment because of smaller values of detrain. Steeper lapse rates will eventually trigger stronger convection.

For "convtime" = 1.5 the rainfall pattern over the Drakensberg Domain is not strongly dependent on the value of "detrain" (compare the C_1 to C_3 runs in Figures 4.15 to

4.17). This is to be expected over this region, where topographic (resolved) rain is dominant for convtime=1.5. In the A_1 to A_3 (Figures 4.9 to 4.11) and B_1 to B_3 simulations (Figures 4.12 to 4.15), where “convtime” yields the convective contribution to rainfall more important, the effects of “”detrain” are similar: Smaller values cause the rainfall pattern to assume a more “orographic” pattern, although the rainfall peak west of Lesotho remains well defined for the case of “convtime” =0.3 (the A_1 to A_3 simulations).

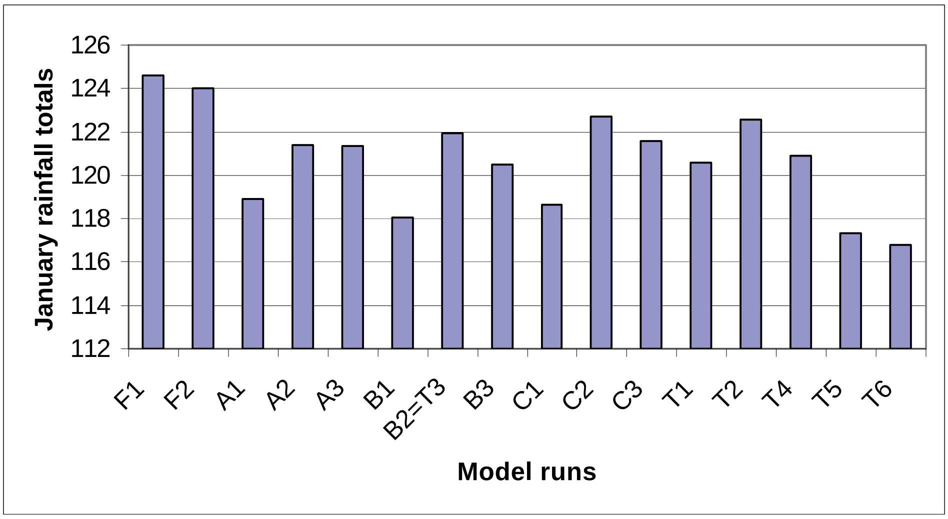

Figure 4.8 Average January/ January 1979 rainfall totals over the analysis domain (50º S to 10 º N) and (0ºE to 70ºE) as a function of model parameters.

Longer model simulations are required to determine the most appropriate values for “convtime”. The tests discussed here suggests that “detrain”=0.02 for “convtime”=0.3 (A_2 simulation) are the optimum values. However, longer simulations might prove that “convtime”=1 and “detrain”=0.05 or 0.02 are better options. Rainfall totals over the Drakensberg domain are overestimated with the “convtime”=1.5 options.

4.6 CHANGING THE MODEL TIME STEP

An important feature of the semi-implicit semi-Lagrangian formulation of the numerical solution procedure in C-CAM is that unconditionally stable integrations are possible. This means that the time-step in the model is not limited by the common CFL criterion, which states that $c\frac{\Delta t}{\Delta x} \le 1$ must hold for the integration to remain stable. Here c denotes the speed of the advecting wind, or alternatively the speed at which gravity or sound waves are travelling in the model atmosphere (if they are present). The implication is that with the numerical formulation of C-CAM the choice of the model time step is based on accuracy in matching the physical processes and not on stability considerations. To illustrate this, a series of sensitivity simulations were performed which employed different time steps (40, 30, 20, 15, 10 and 5 minutes). For these simulations “convtime”=1 and “detrain” =0.02 were used. The selected settings are summarised in Table 4.1.

In the T_1-simulation (Figure 4.18) the model used a time step of 40 min. Over the highest-resolution panel of the model the horizontal resolution is approximately 60 km x 60 km, which implies that the CFL-criterion is violated with a factor of about 2 for winds of 100 kts (50 ms^{-1}), which commonly occur in the real and model upper atmospheres. For gravity and sound waves (the latter is also present in hydrostatic σ-coordinate models in the form of Lamb waves) the CFL-criterion is violated with a factor of 12. Figure 4.18 reveals that the semi-implicit semi-Lagrangian scheme indeed ensured stability during the model integration. The synoptic-scale rainfall pattern does not differ significantly from other simulations shown in this Chapter, and generally rainfall totals over the model domain correspond well to that of the other simulations (Figure 4.8). However, rainfall totals simulated over the Drakensberg domain look rather unrealistic. Too much rain is simulated over the interior to the north-west of Lesotho, and the east-west rainfall gradient is not well captured. With large model time steps it is likely that larger instabilities will build up during the model integration before they are removed by the convection parameterisation scheme. The relative contribution of orographic rain in the model over the escarpment areas of the Drakensberg Domain is therefore likely to decrease compared to the proportion of convective rain, resulting in a less well-defined rainfall gradient over the area.

The T_2-simulation (30 min time-step, Figure 5.20) shows a similar pattern when compared to the T_1-simulation, but the T_3=B_2 - simulation (20 min time-step) is significantly different (Figure 4.13). A well-defined east-west rainfall gradient is now present in the model simulation, which corresponds better to the general characteristics of rainfall over the Drakensberg Domain (Figure 2.7), and also to the observed January 1979 rainfall (Figure 4.6). This improvement in accuracy is probably also related to a better balance achieved between the relative contributions of large-scale and convective rainfall when using a 20 minute time-step.

In the T_4 –simulation (15 min time step) the simulated rainfall pattern is different again (Figure 4.20). The east-west rainfall gradient is preserved, but high rainfall totals are present to the west of the Drakensberg. This is not a typical pattern for the region (Figure 2.7), but it shows some correspondence to the observed rainfall for January 1979 (Figure 4.6). Interesting to note are two simulated rainfall peaks to the east of Lesotho (Figure 4.20), where rainfall totals exceeds 200 mm. The pattern present in Figure 4.20 is also to be found in Figure 4.21 (T_5-simulation, 10 min time-step) and Figure 4.22 (T6-simulation, 5 min time-step). However, in the latter two runs the overestimation of rainfall totals east of the Drakensberg is more severe, with totals exceeding 400 mm in the T_6 - simulation. Interesting to note is that the T_5 and T_6-simulations give the lowest rainfall totals over the full analysis domain (Figure 4.8). For small time steps, but with "convtime" = 1, the convection scheme has a small effect on the simulations, so that moist instabilities will be removed by the large-scale moisture scheme as they develop – hence the large rainfall totals near mountains. It is likely that simulations with small time steps will yield more realistic simulations for smaller values of "convtime". Such experiments are intended for the near future, and should confirm the present idea of convtime=0.3 to be the best choice for parameter "convtime".

Experiments indicate that a time-step of 20 min offers the best compromise between efficiency and accuracy at the described resolutions and with the present settings of the convection scheme. More tests are required (trying different settings of convtime and performing longer simulations) to confirm this preliminary conclusion.

The new interactive cloud scheme developed at CSIRO-AR has been improved considerably since the initial experiments described in this Section were performed (F_1 and F_2–simulations) and a new set of sensitivity simulations are envisaged in the near future. An entrainment option is also available in the latest version of C-CAM and this should provide additional opportunity to improve the simulation of rainfall patterns and totals over southern Africa. It should be noted that model development is an ongoing process. The research team at UP is having the opportunity to collaborate with an active international modelling group, and valuable experience has been gained.

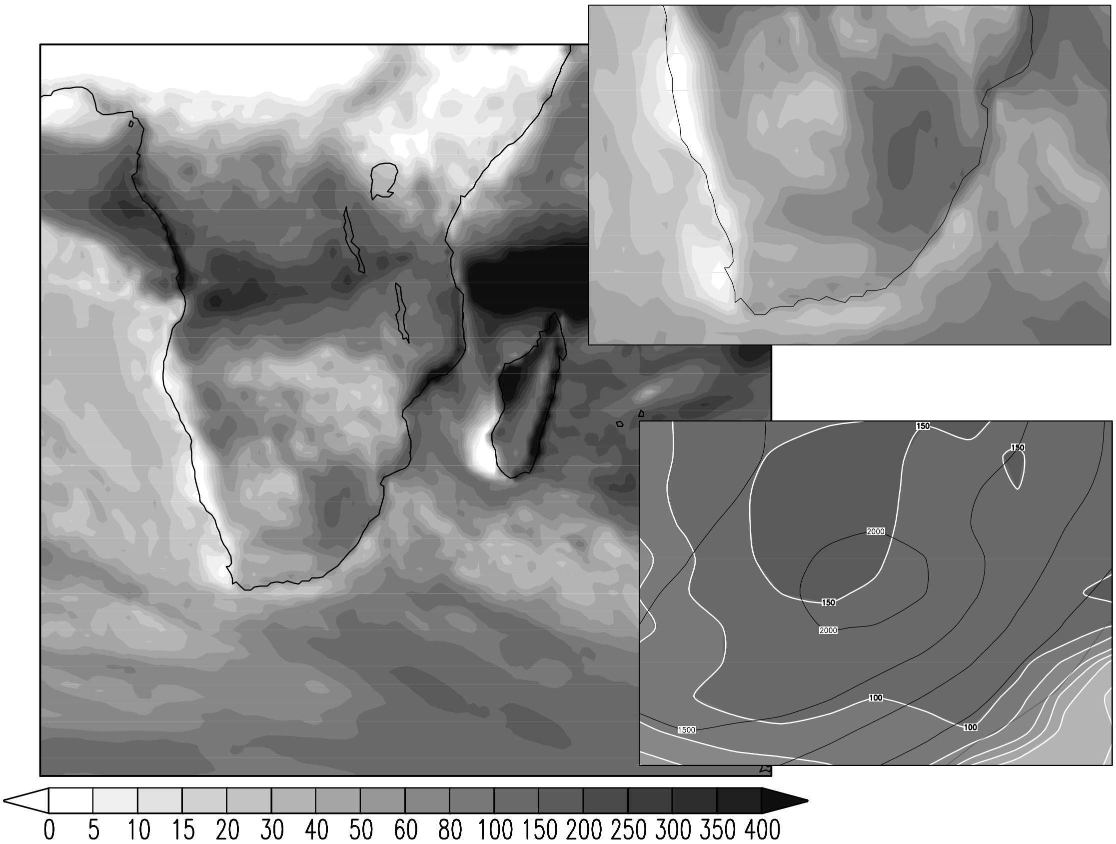

Figure 4.9 Same as Figure 4.7, but for the A_1-simulation

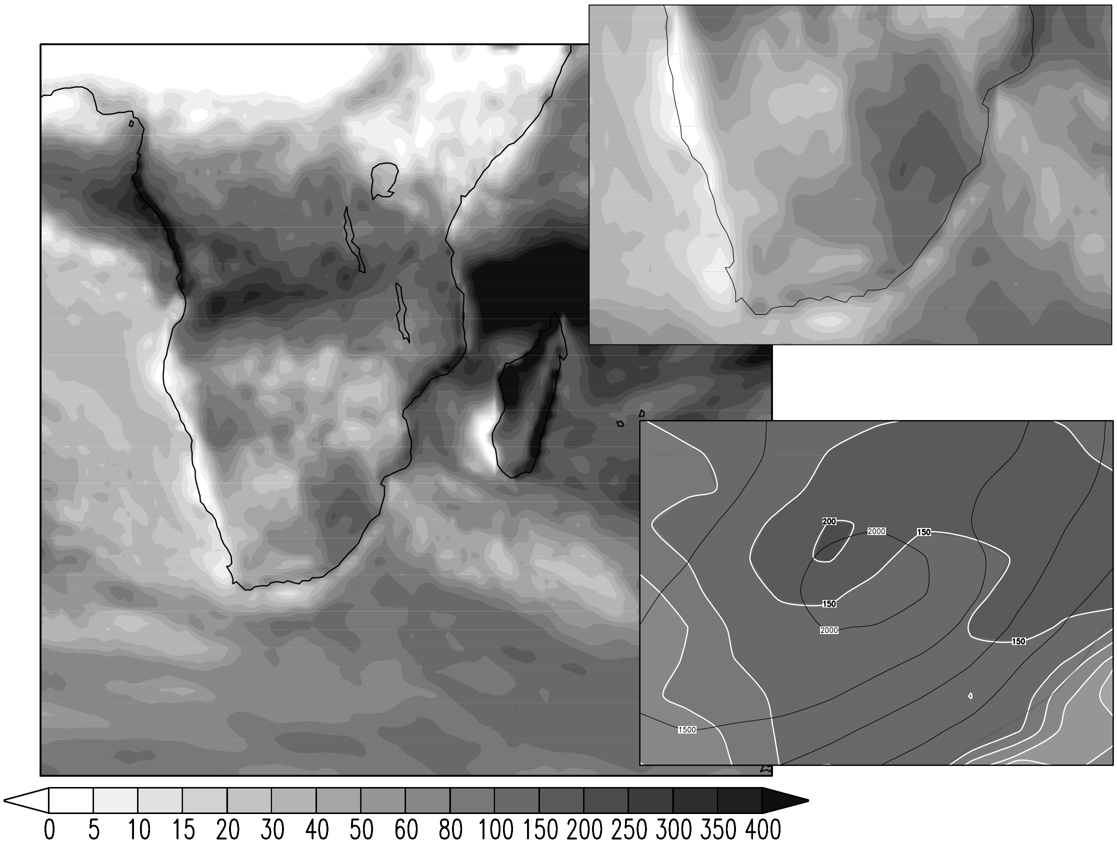

Figure 4.10 Same as Figure 4.7, but for the A_2-simulation

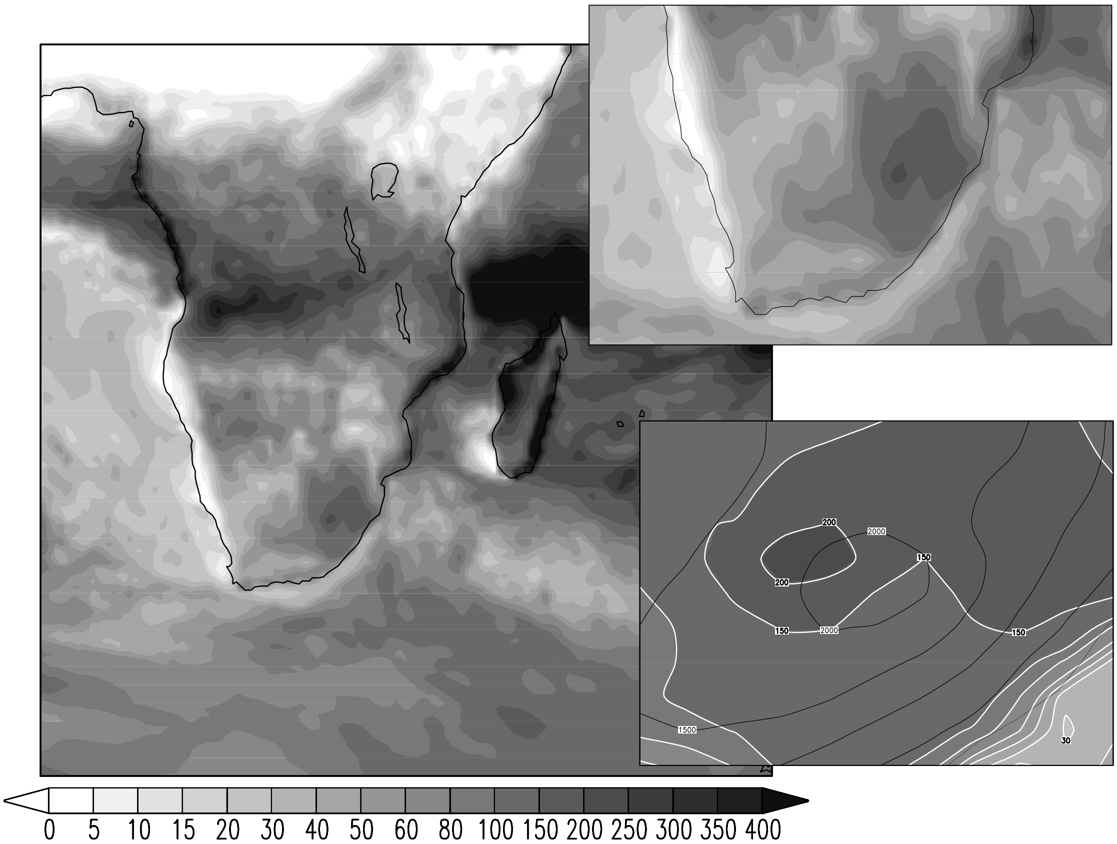

Figure 4.11 Same as Figure 4.7, but for the A_3-simulation

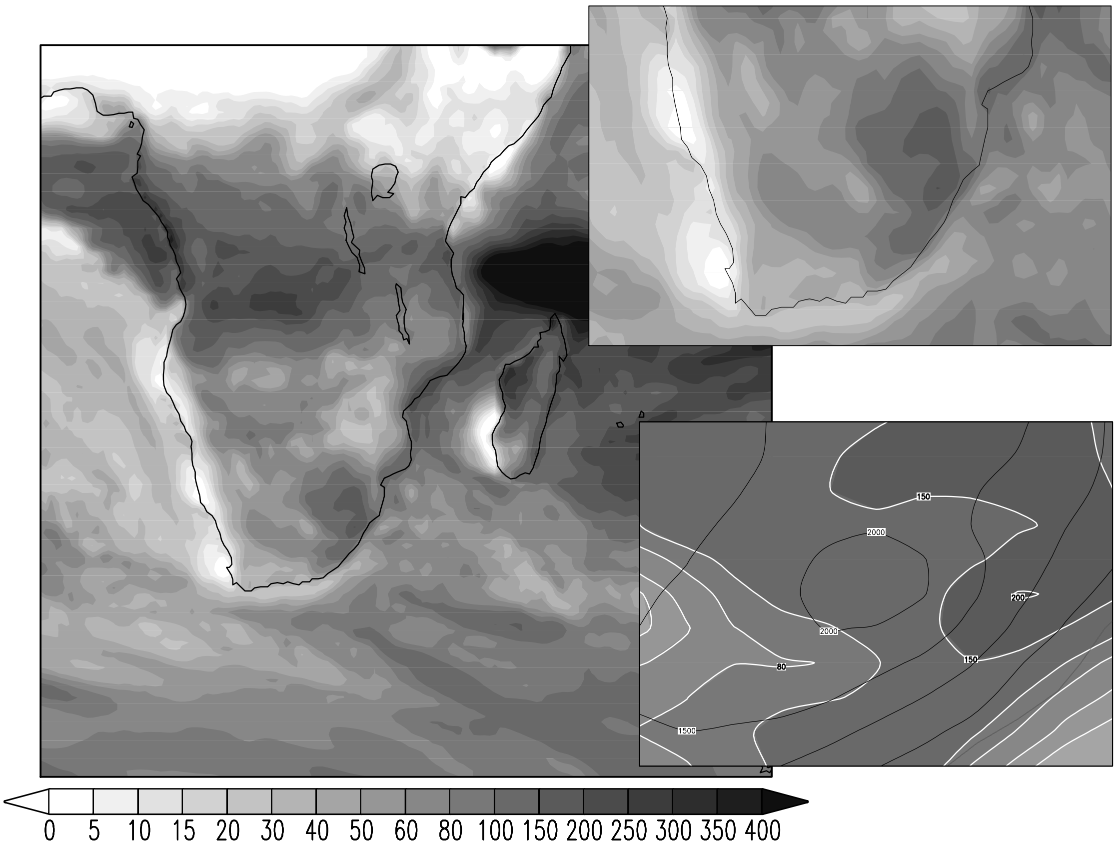

Figure 4.12 Same as Figure 4.7, but for the B_1-simulation

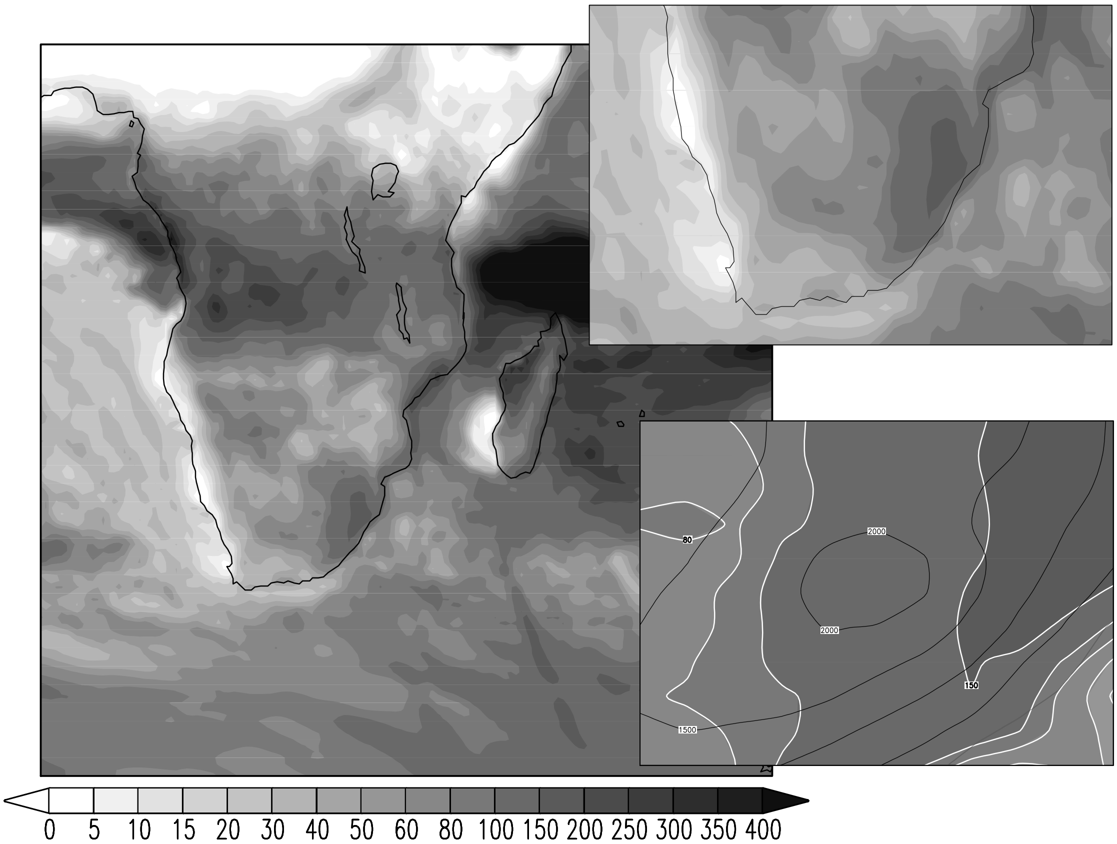

Figure 4.13 Same as Figure 4.7, but for the B_2-simulation

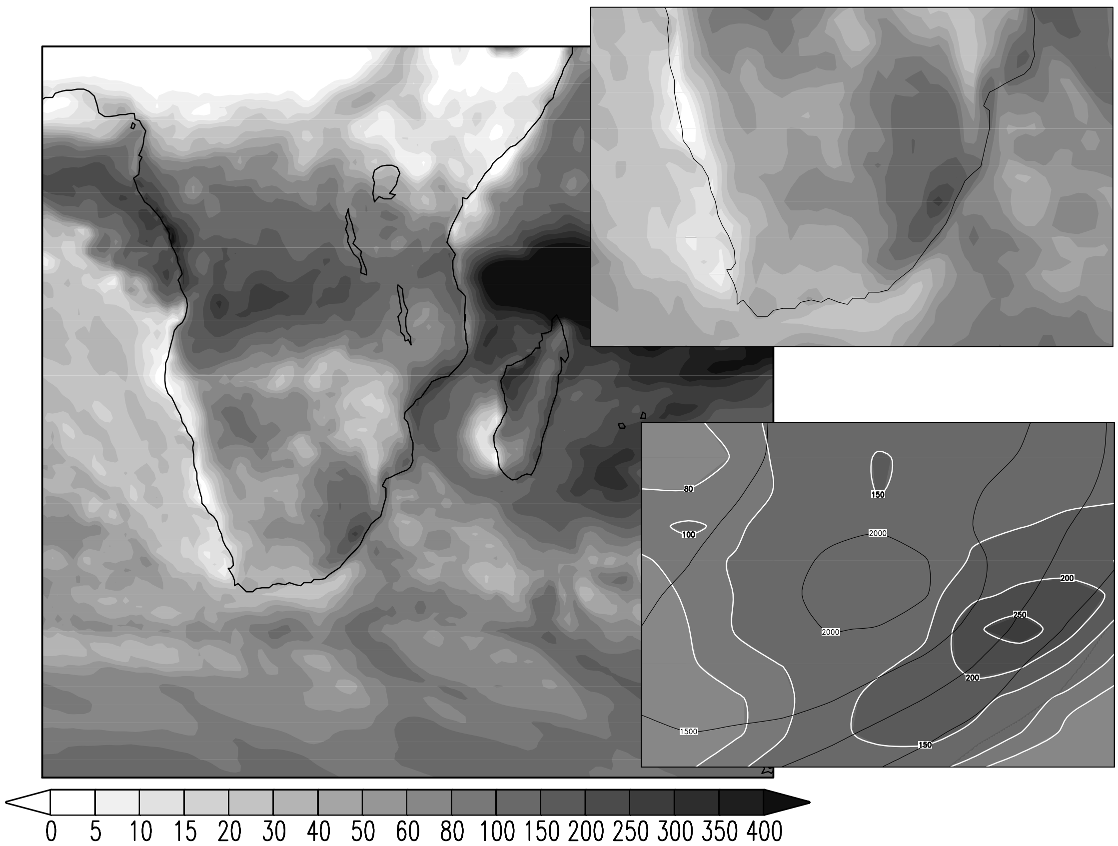

Figure 4.14 Same as Figure 4.7, but for the B_3-simulation

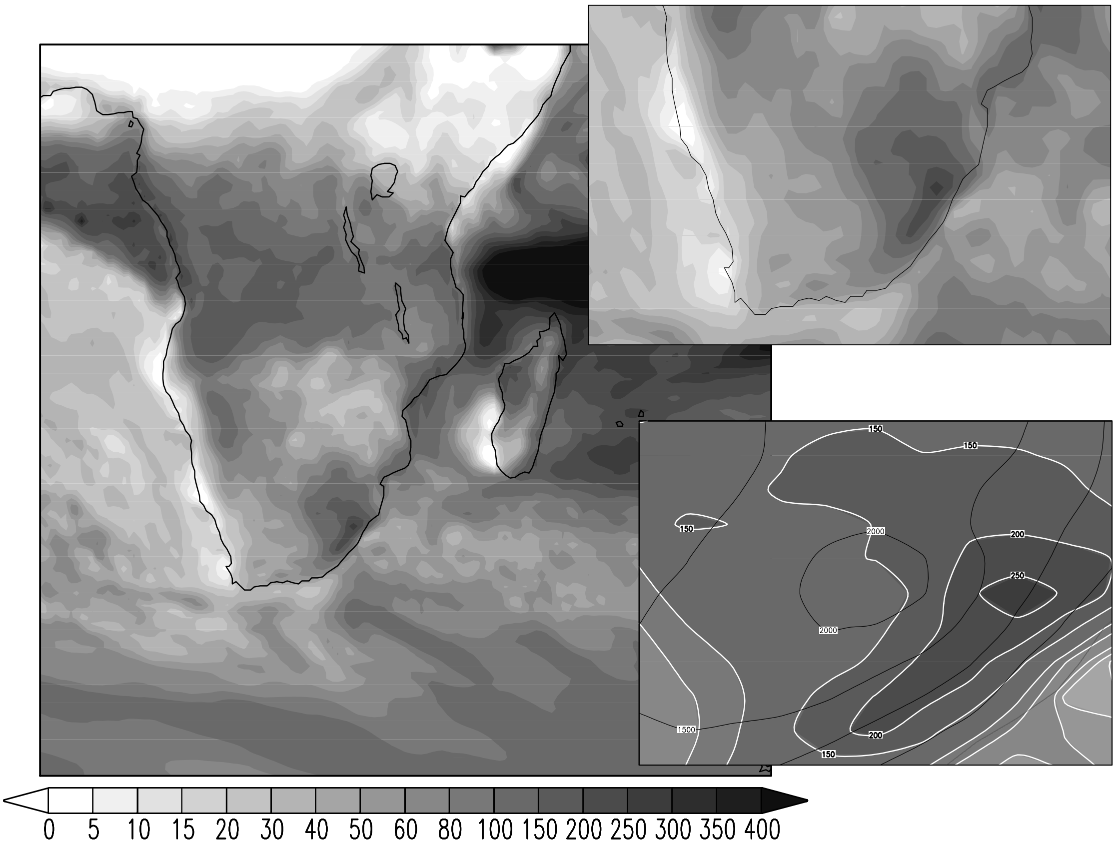

Figure 4.15 Same as Figure 4.7, but for the C_1-simulation

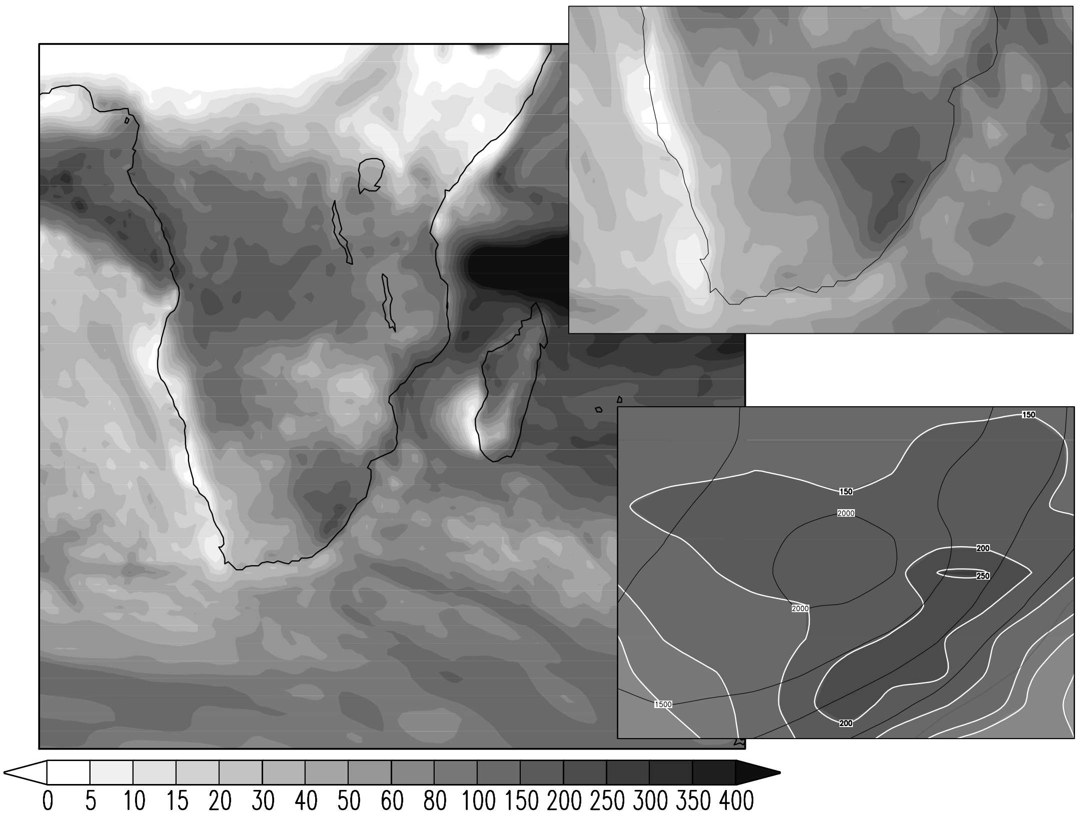

Figure 4.16 Same as Figure 4.7, but for the C_2-simulation

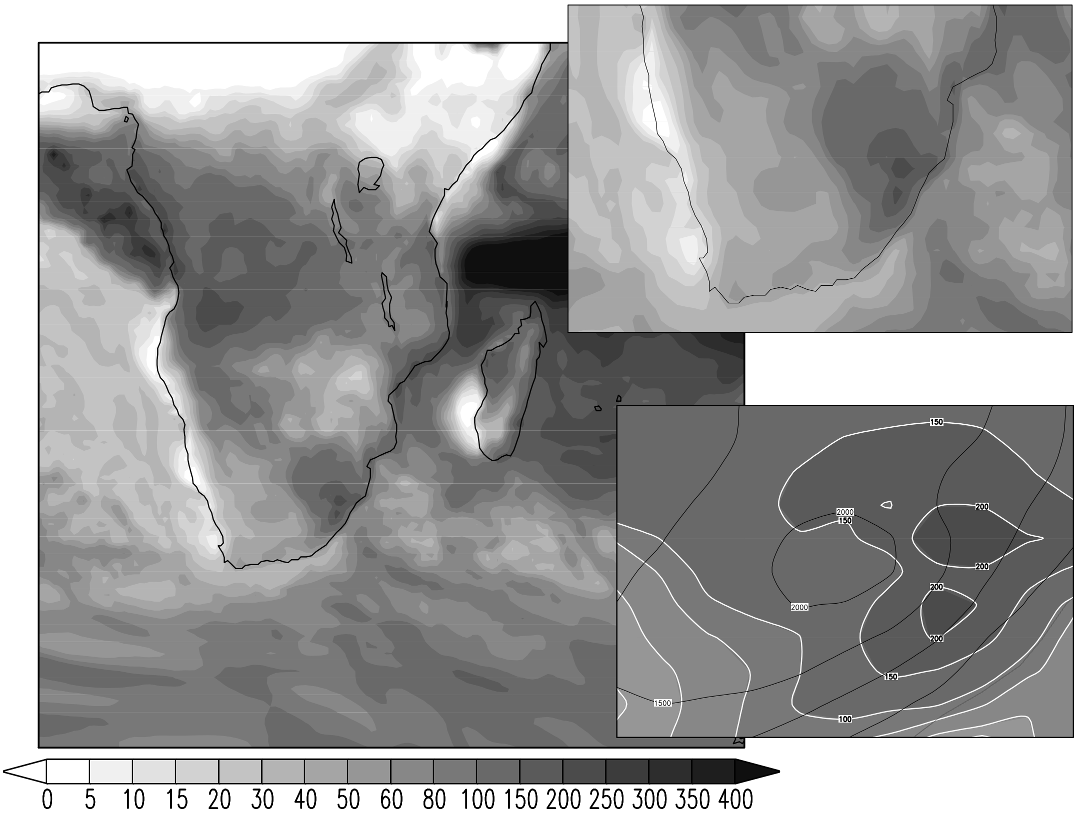

Figure 4.17 Same as Figure 4.7, but for the C_3-simulation

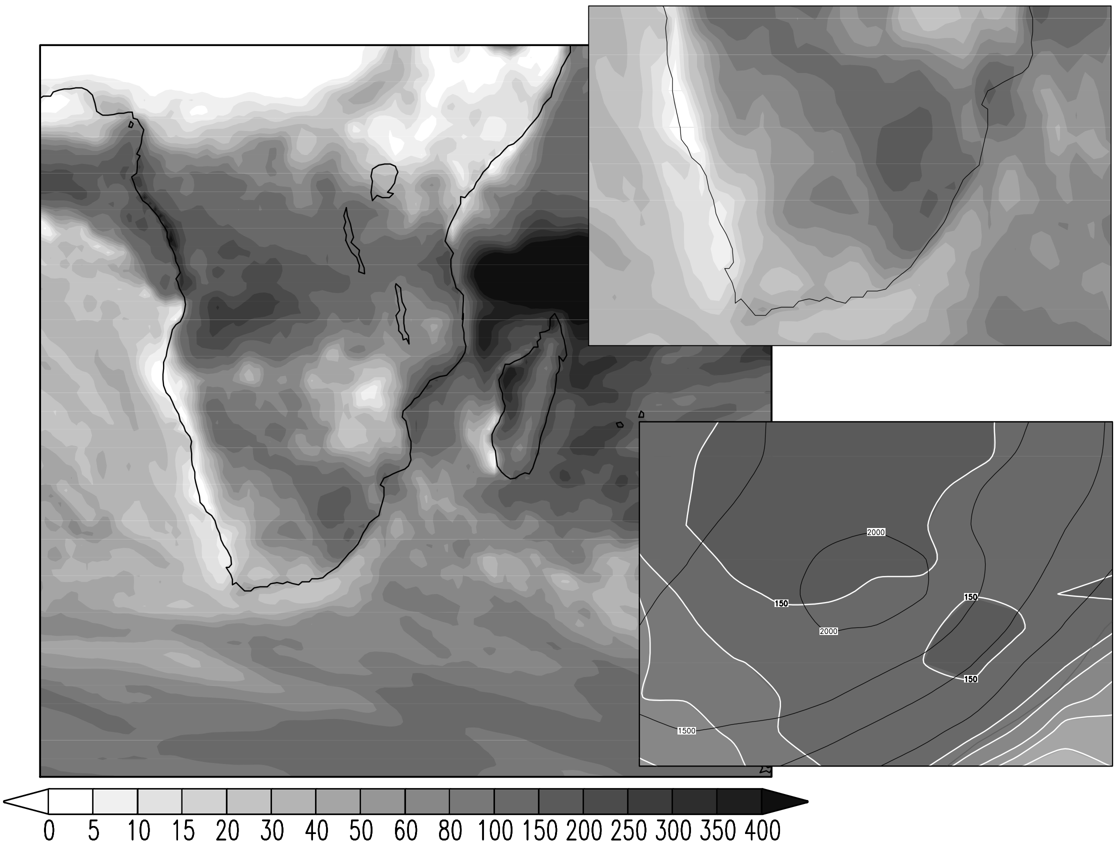

Figure 4.18 Same as Figure 4.7, but for the T_1-simulation

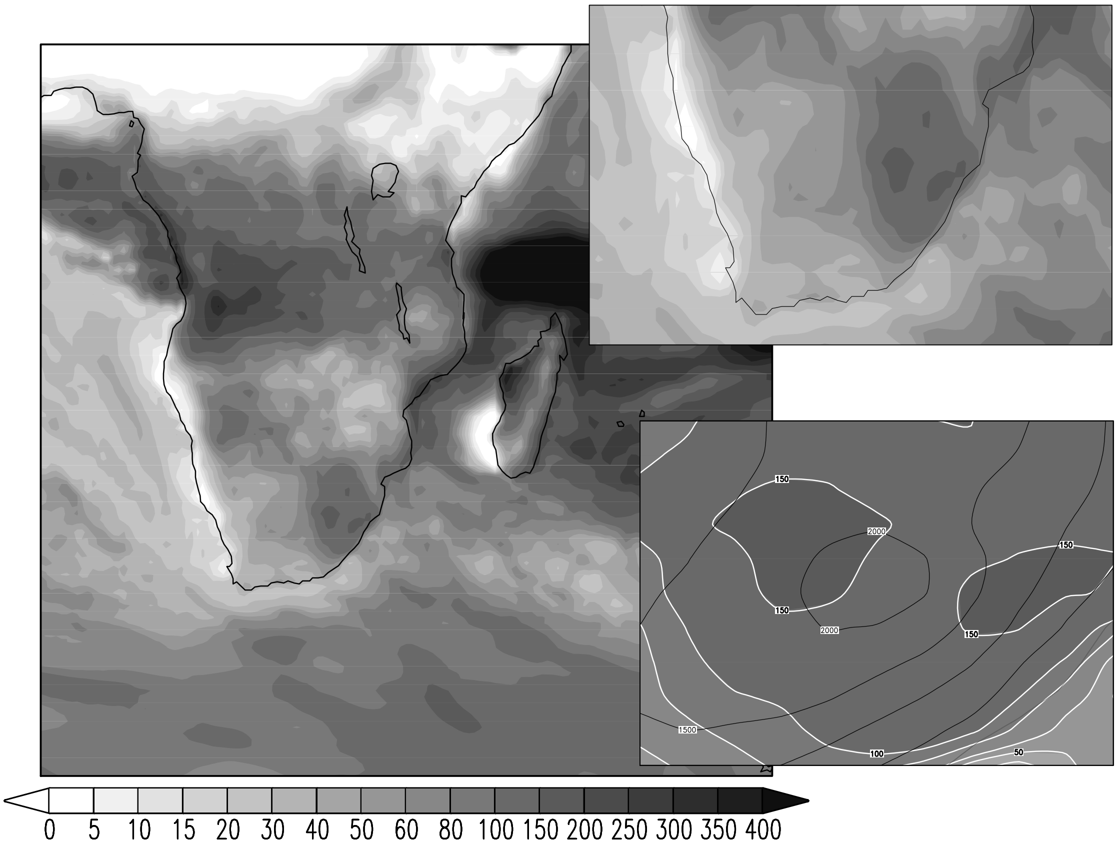

Figure 4.19 Same as Figure 4.7, but for the T_2-simulation

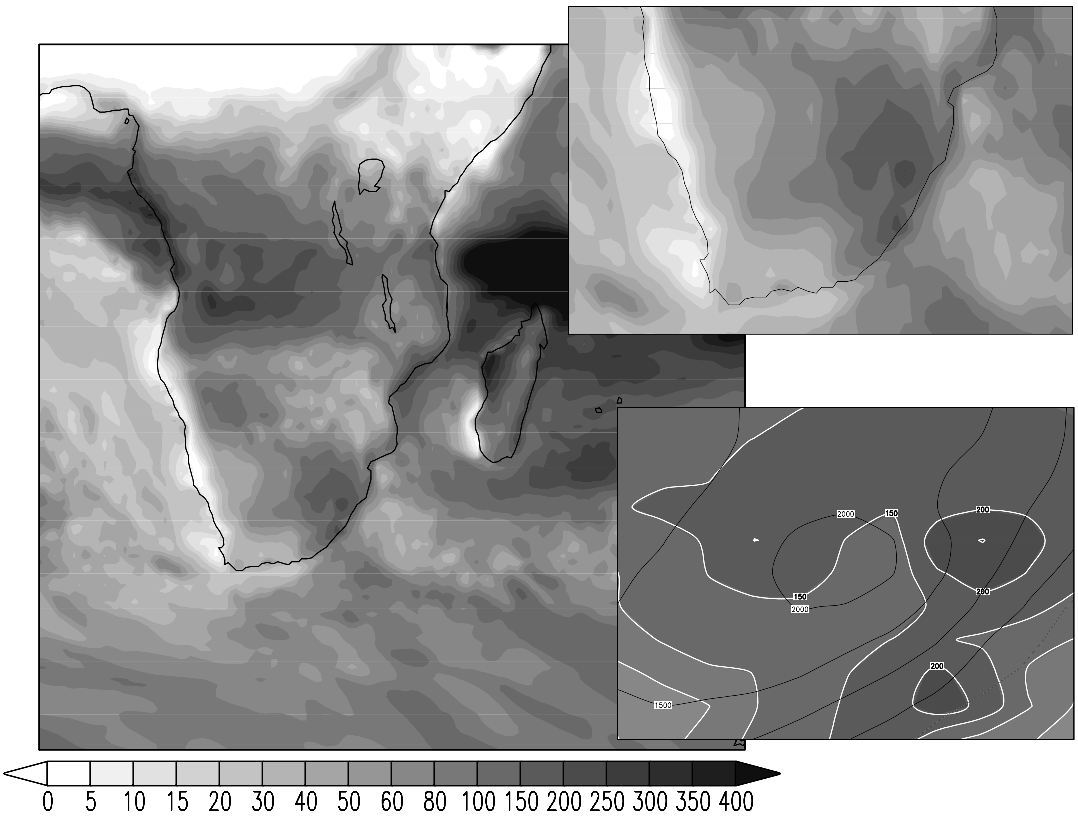

Figure 4.20 Same as Figure 4.7, but for the T_4-simulation

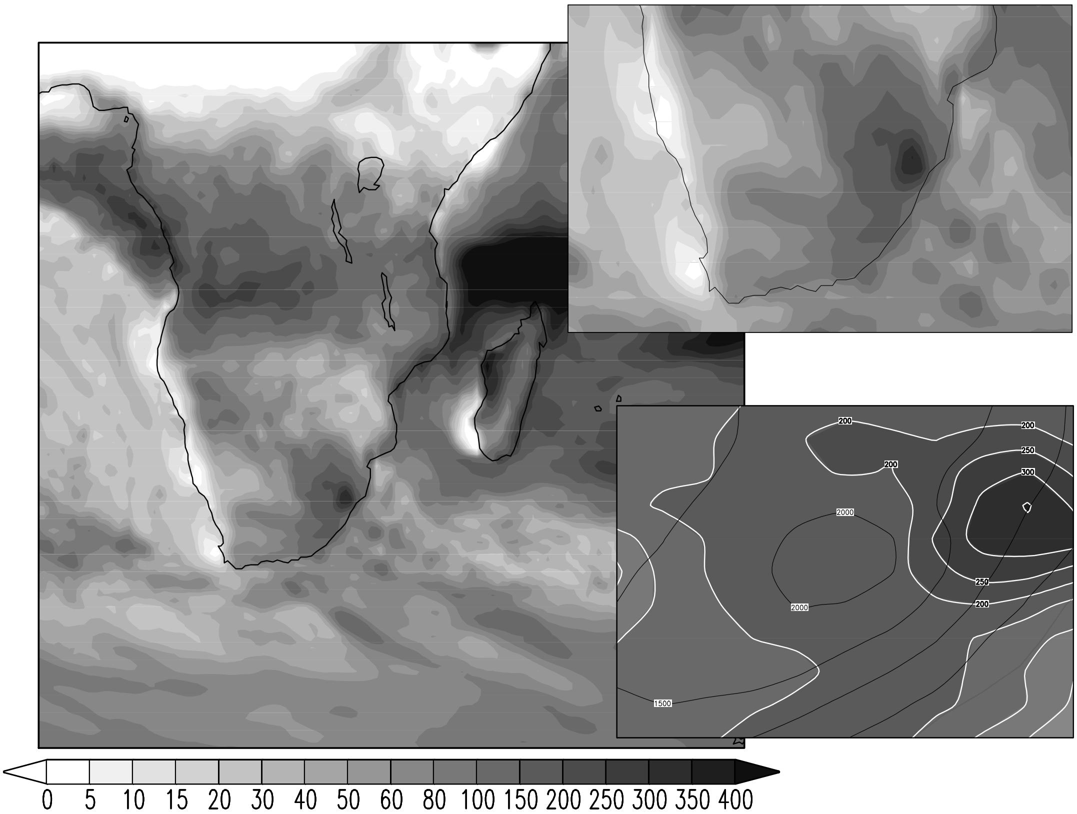

Figure 4.21 Same as Figure 4.7, but for the T_5-simulation

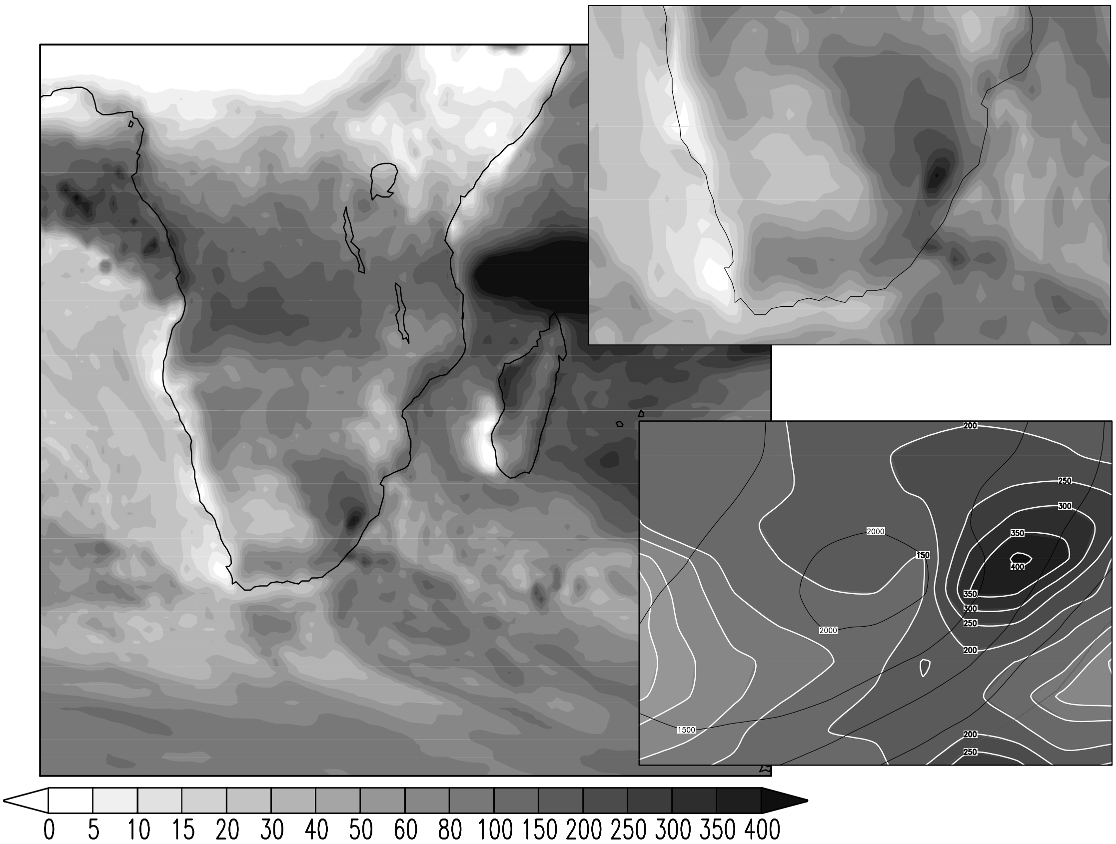

Figure 4.22 Same as Figure 4.7, but for the T_6-simulation

CHAPTER 5

C-CAM CLIMATE SIMULATIONS

5.1 FIRST 15-YEAR SEASONAL CYCLE SIMULATION

A 15-year full seasonal-cycle simulation was performed with the first version of C-CAM obtained at the beginning of 2003 from CSIRO-AR. This was a non-nudged stretched simulation (Schmidt factor of 0.3) at C64 horizontal resolution (64 x 64 grid points per panel) with 18 σ-levels in the vertical. The model was forced at its lower boundary with observed SSTs and sea-ice fields, for the period January 1979 till December 1993. Figure 5.1 shows the simulated average January rainfall totals over southern Africa for the 15-year period. The rainfall climatology for January as shown in Figures 2.6 and 2.7 is used for model verification. The analyses of the simulation lead to the identification of two important biases in the model's rainfall fields, namely:

- Rainfall was generally overestimated compared to observations in Figure 2.7.
- The rainfall maximum over South Africa was simulated to the west of Lesotho – in reality the January rainfall maximum over South Africa occurs to the east and north-east of the Lesotho Drakensberg (Figure 2.7).

Despite the mentioned biases in the simulation, the model successfully managed to capture important characteristics of the general summer rainfall distribution over southern Africa. The prominent banded nature of southern African summer rainfall (Engelbrecht et al., 2002) is well simulated, namely the band of relatively high rainfall between 15ºS and 10ºS, the band of relatively low rainfall between 25ºS and 20ºS, and the region of higher rainfall over eastern South Africa. The model simulation of relatively drier conditions over western South Africa, Namibia and Angola is satisfactory (Figure 5.1). The observed rainfall maximum over north-west Madagascar and rainfall minimum over south-west Madagascar were both simulated. Synoptic-scale rainfall patterns as simulated by C-CAM for the other months (not shown here) also agree well with observations (at least qualitatively).

The rather severe overestimation of rainfall totals by the first version of C-CAM used at LRAM turned out to be caused by a new interactive diagnostic cloud scheme used in the model, in combination with the moisture conservation scheme used at that time. When these were replaced by the older cloud scheme based on relative humidity (RH) values (the scheme used in DARLAM) and the correct options for moisture conservation, the simulated rainfall totals turned out to be much more realistic. The rainfall bias to the west of Lesotho remained however, and the model clearly needed some fine-tuning for application over southern Africa. A large number of sensitivity tests were performed with the aim of removing the bias. Some of these results were discussed in Chapter 4.

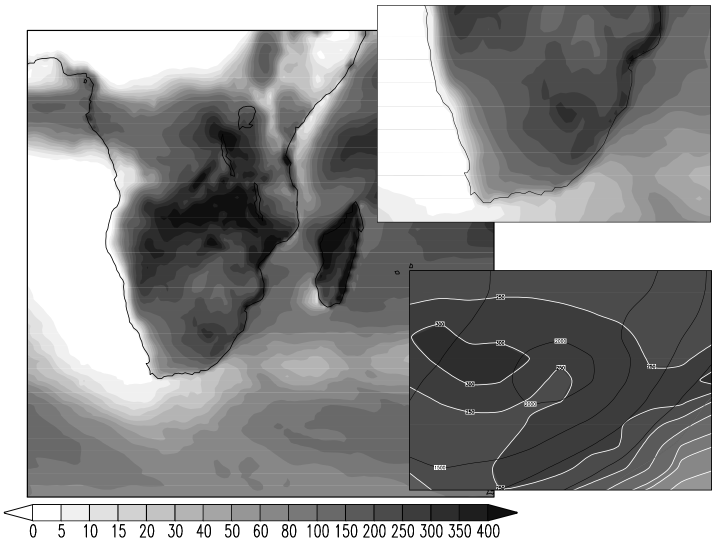

Figure 5.1 F_1-simulation of average rainfall totals (mm) for January over the period (1979-1993) (15 years) forced with AMIP SSTs and sea-ice. Black contours indicate altitude above mean sea-level (MSL) and white contours are isohyets.

5.2 LATEST IMPROVED C-CAM SIMULATIONS

Final results that reflect the best rainfall model simulations from the project are shown in Figures 5.2 to 5.13. These Figures represent observed and C-CAM simulated rainfall averages over a period of 10-years (1980 to 1989). The year 1979 was used as a model spin-up year and was not considered in the simulations. Maps of observed rainfall were produced by using 1027 rainfall stations from the SAWS.

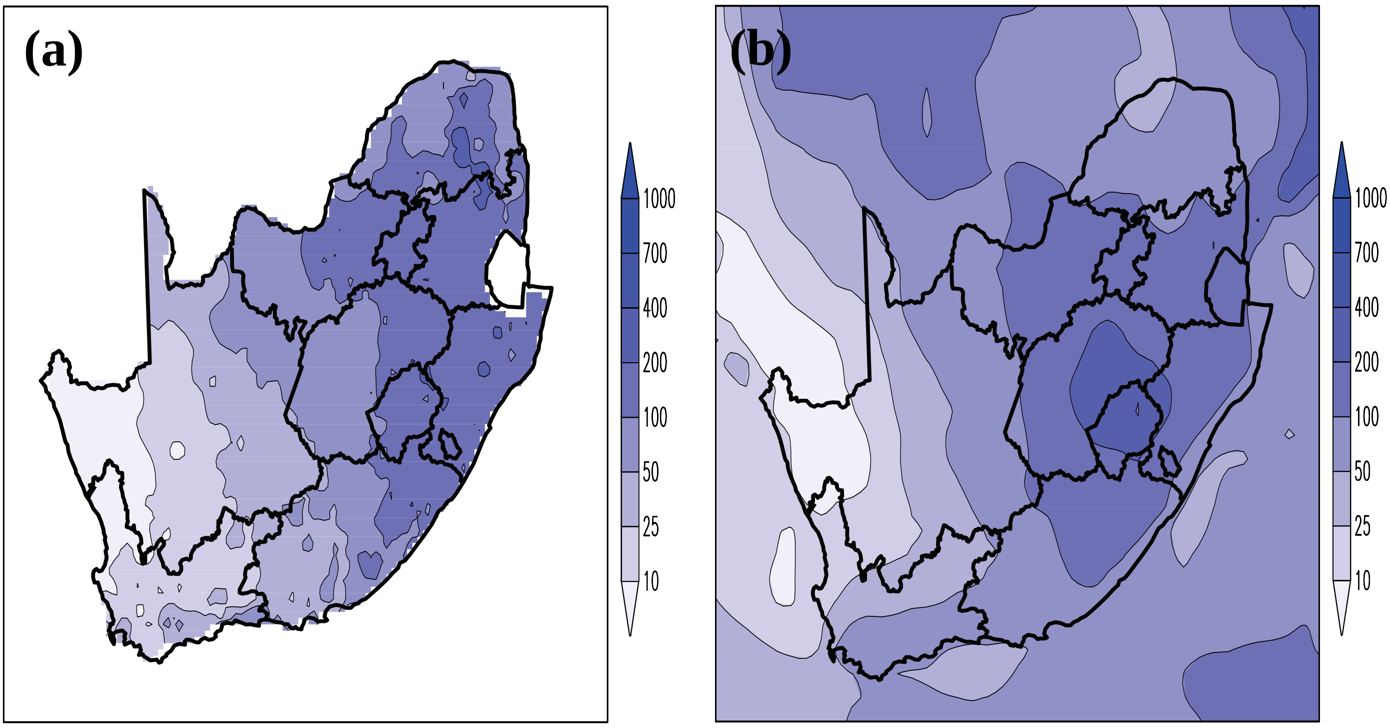

Figure 5.2 Observed (a) and C-CAM simulated (b) rainfall average (1980-1989) for January

Figure 5.3 Observed (a) and C-CAM simulated (b) rainfall average (1980-1989) for February

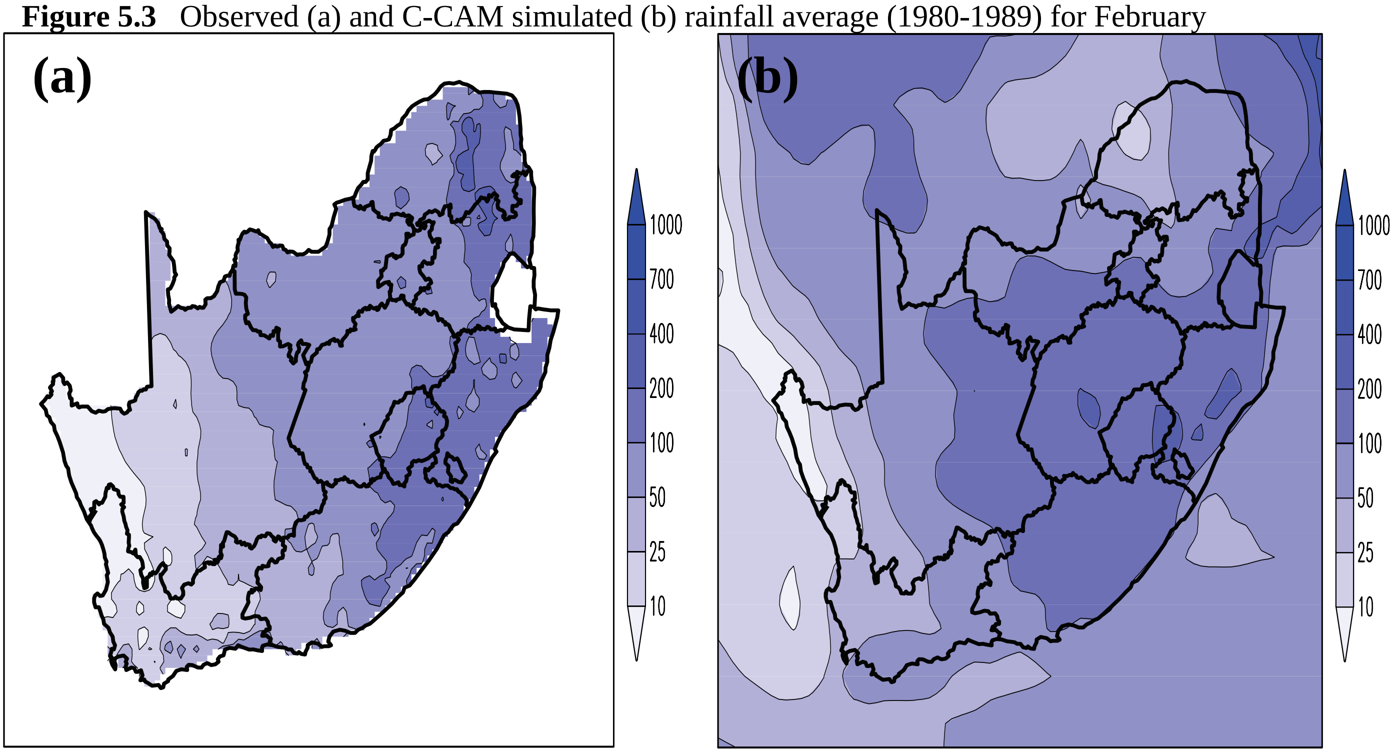

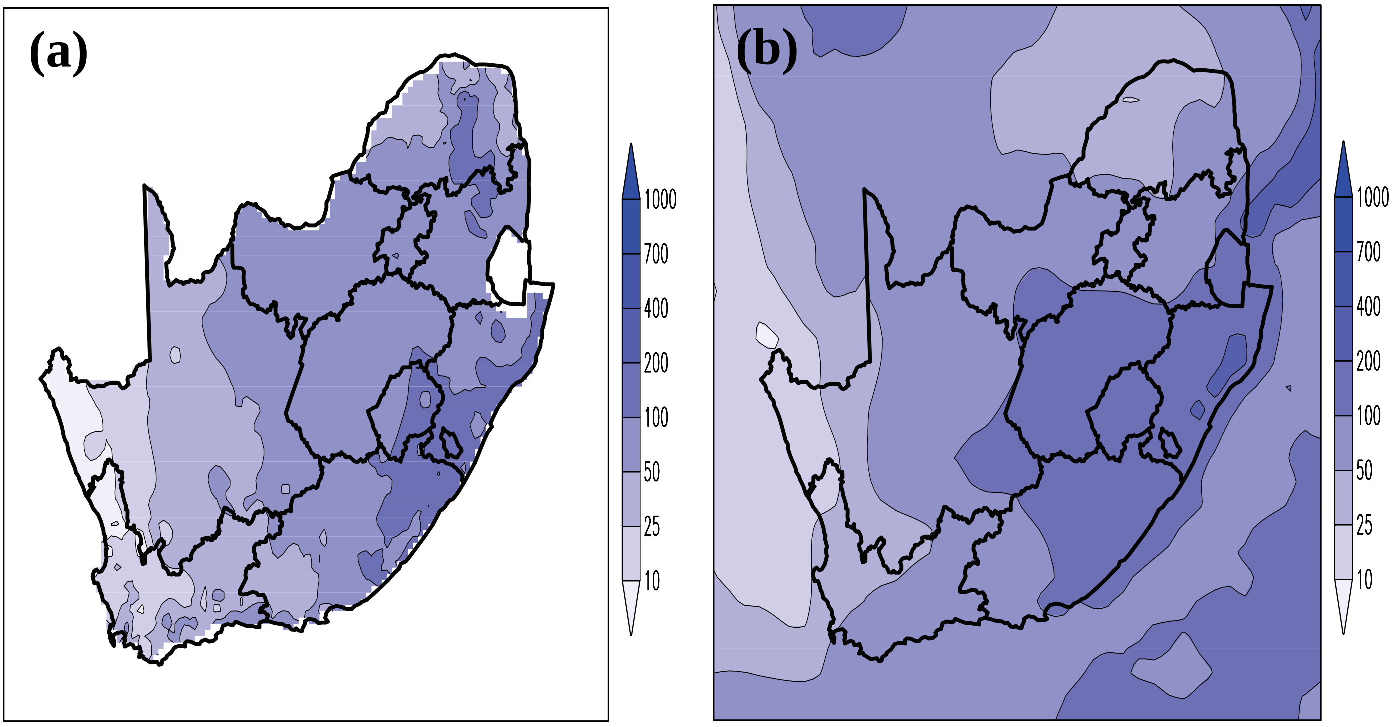

Figure 5.4 Observed (a) and C-CAM simulated (b) rainfall average (1980-1989) for March

Figure 5.5 Observed (a) and C-CAM simulated (b) rainfall average (1980-1989) for April

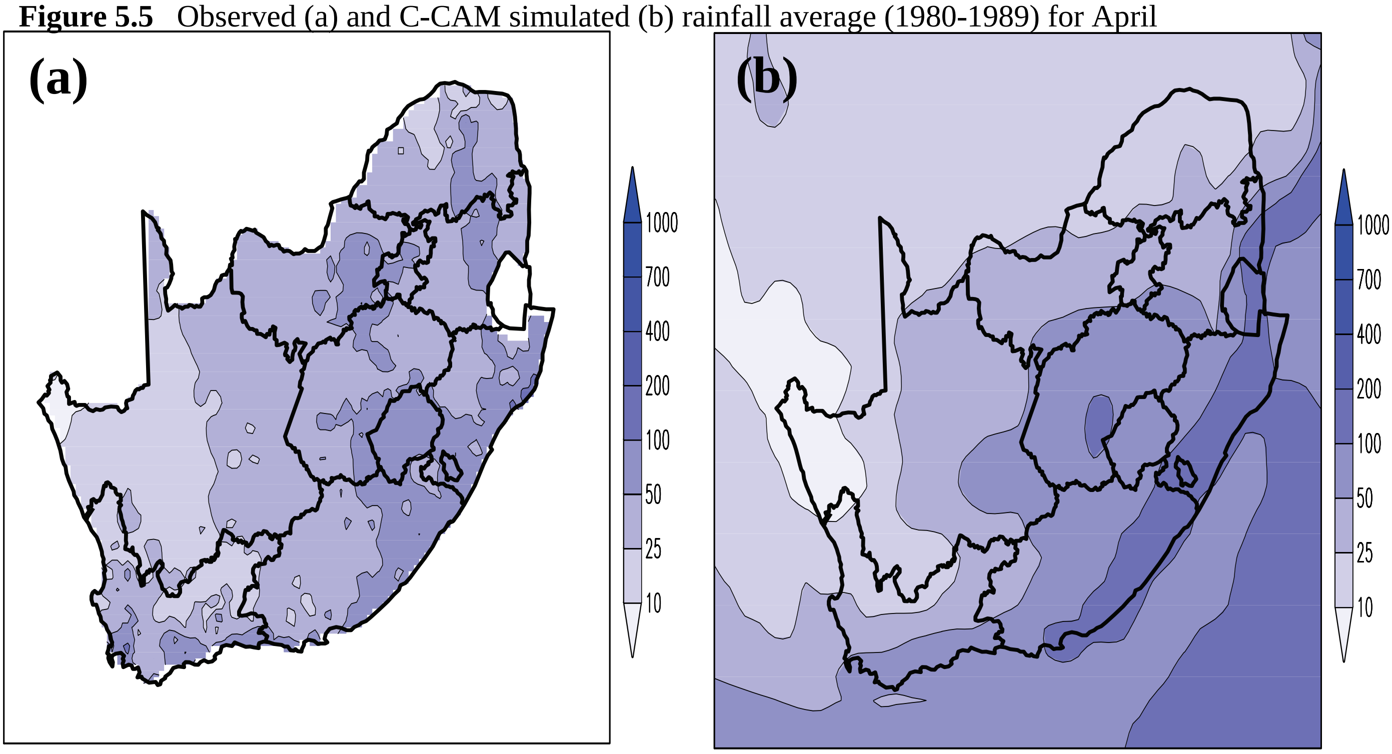

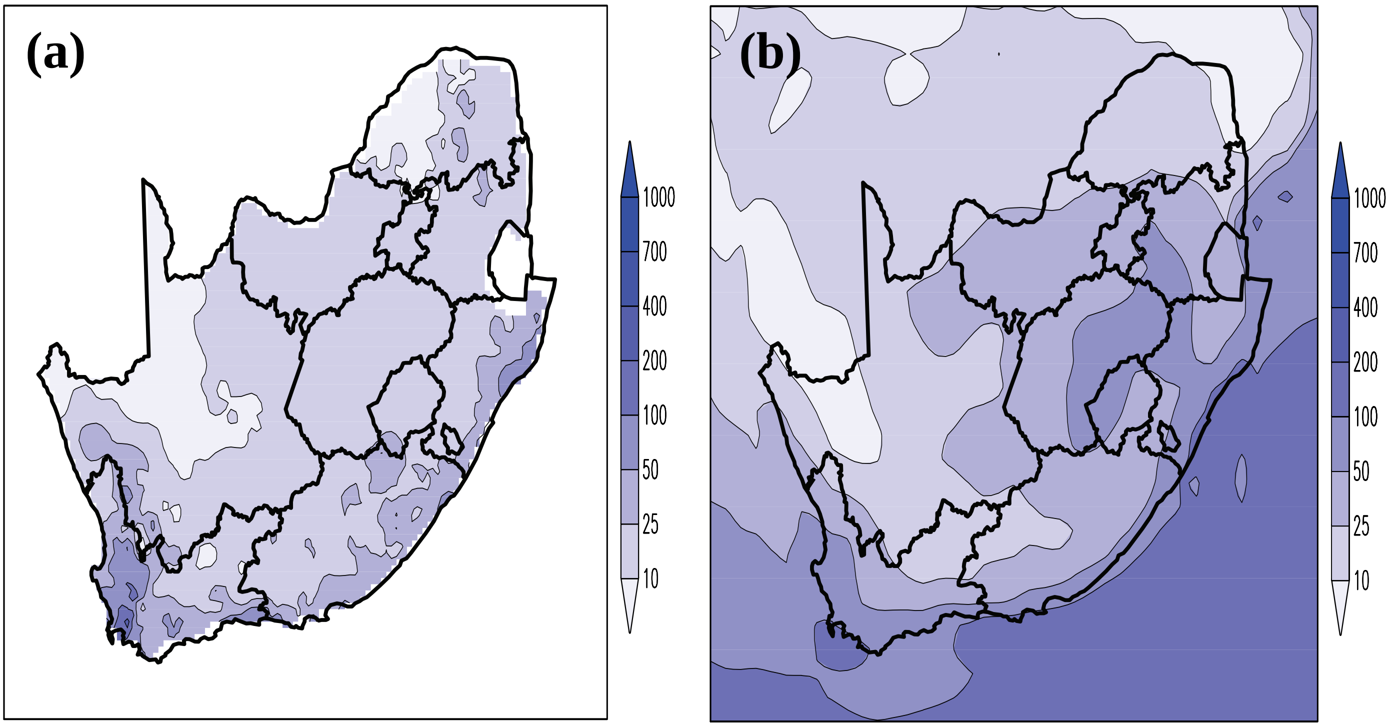

Figure 5.6 Observed (a) and C-CAM simulated (b) rainfall average (1980-1989) for May

Figure 5.7 Observed (a) and C-CAM simulated (b) rainfall average (1980-1989) for June

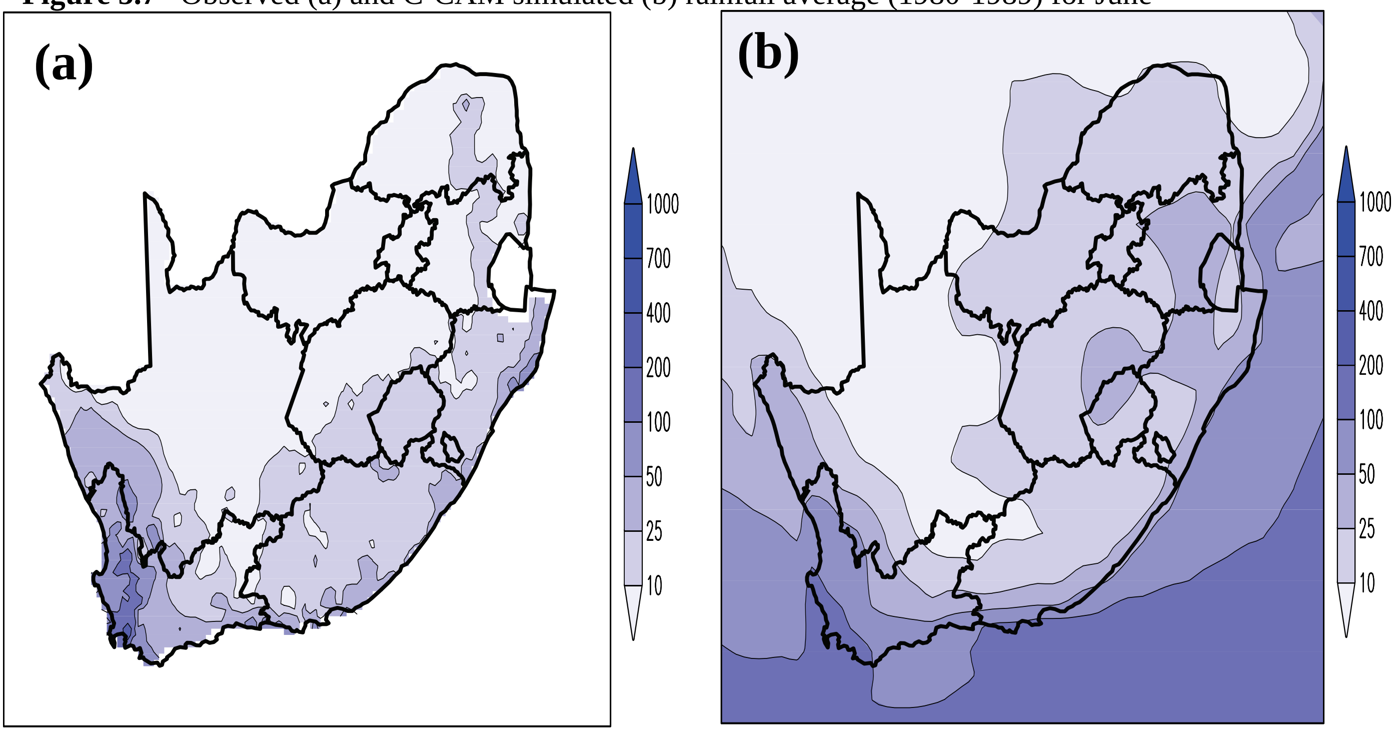

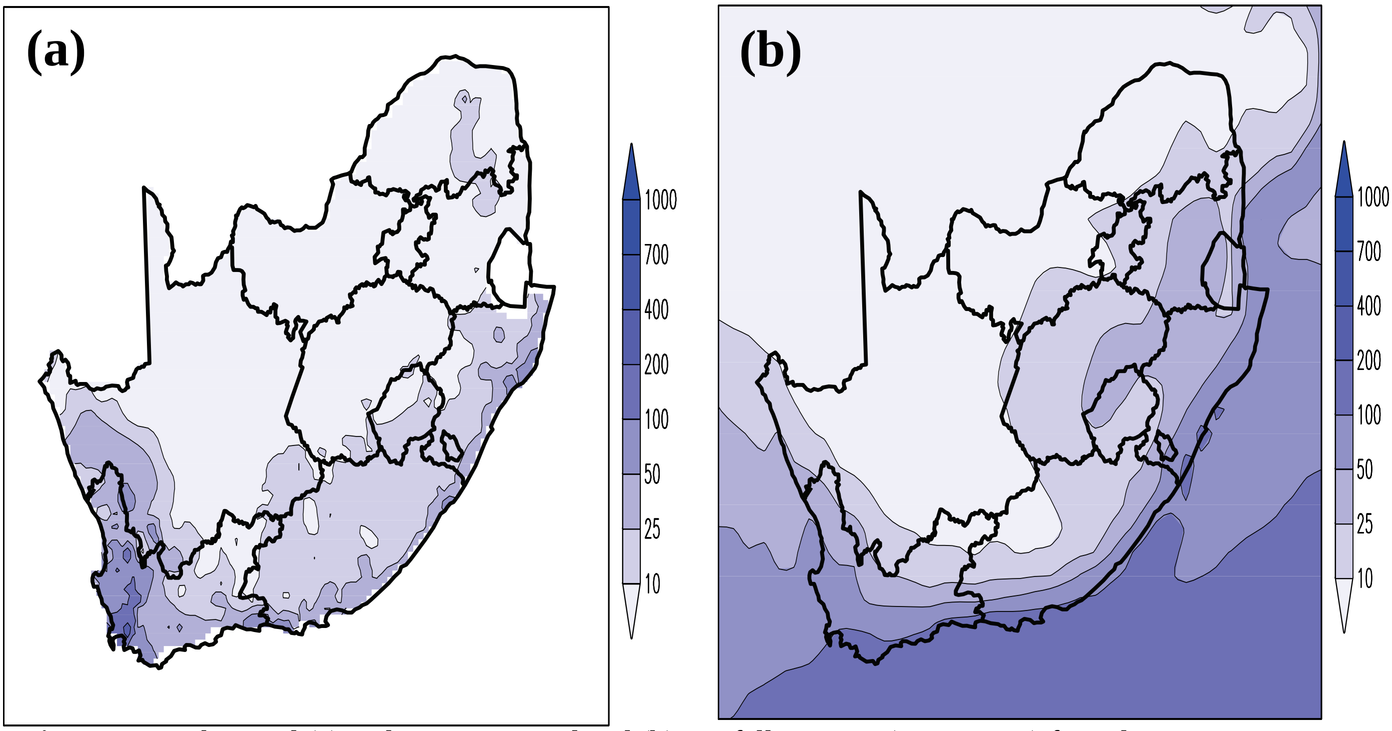

Figure 5.8 Observed (a) and C-CAM simulated (b) rainfall average (1980-1989) for July

Figure 5.9 Observed (a) and C-CAM simulated (b) rainfall average (1980-1989) for August

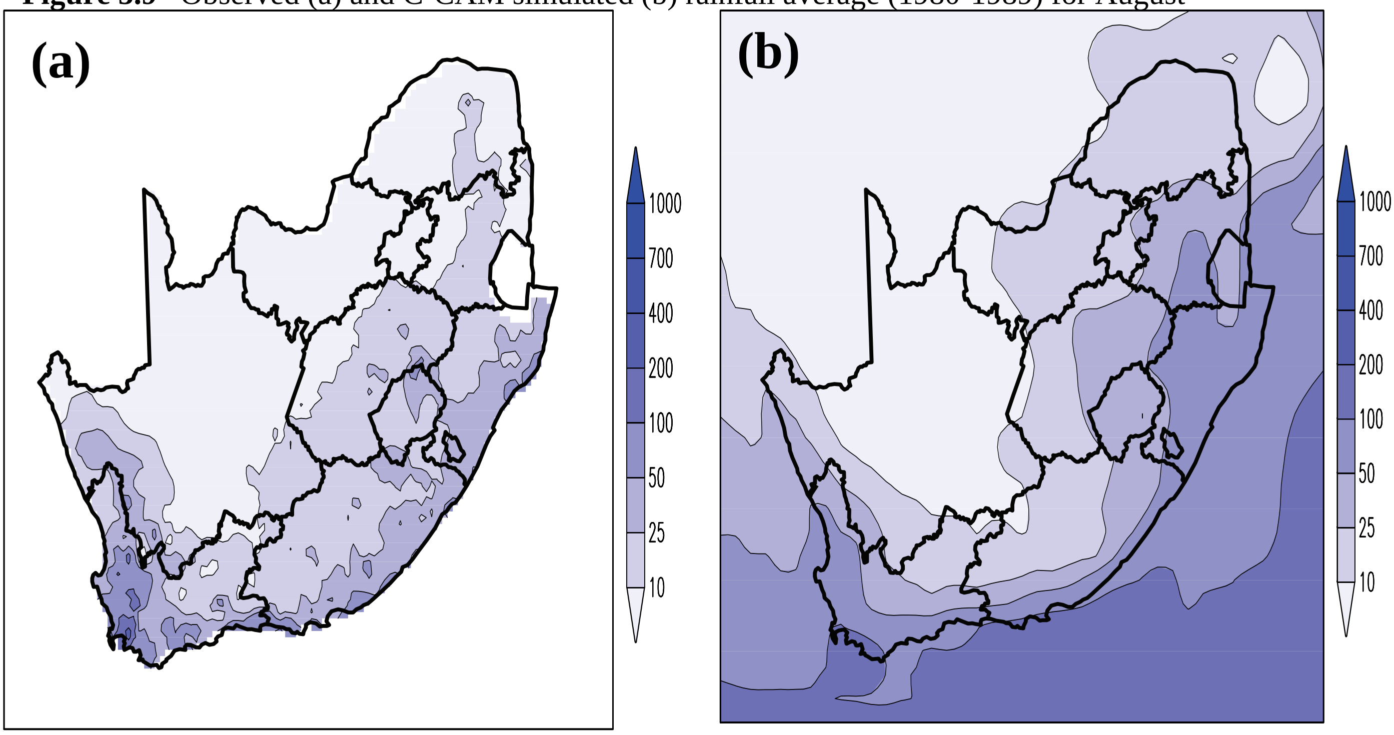

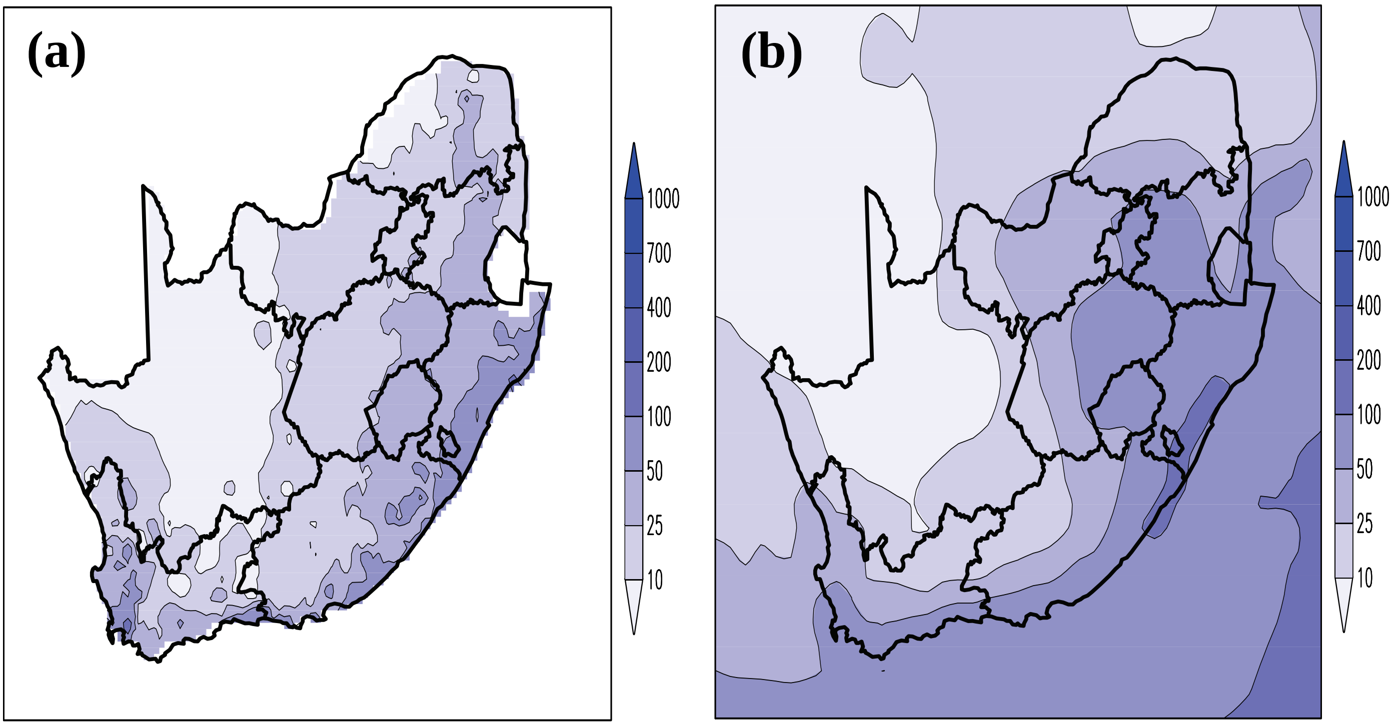

Figure 5.10 Observed (a) and C-CAM simulated (b) rainfall average (1980-1989) for September

Figure 5.11 Observed (a) and C-CAM simulated (b) rainfall average (1980-1989) for October

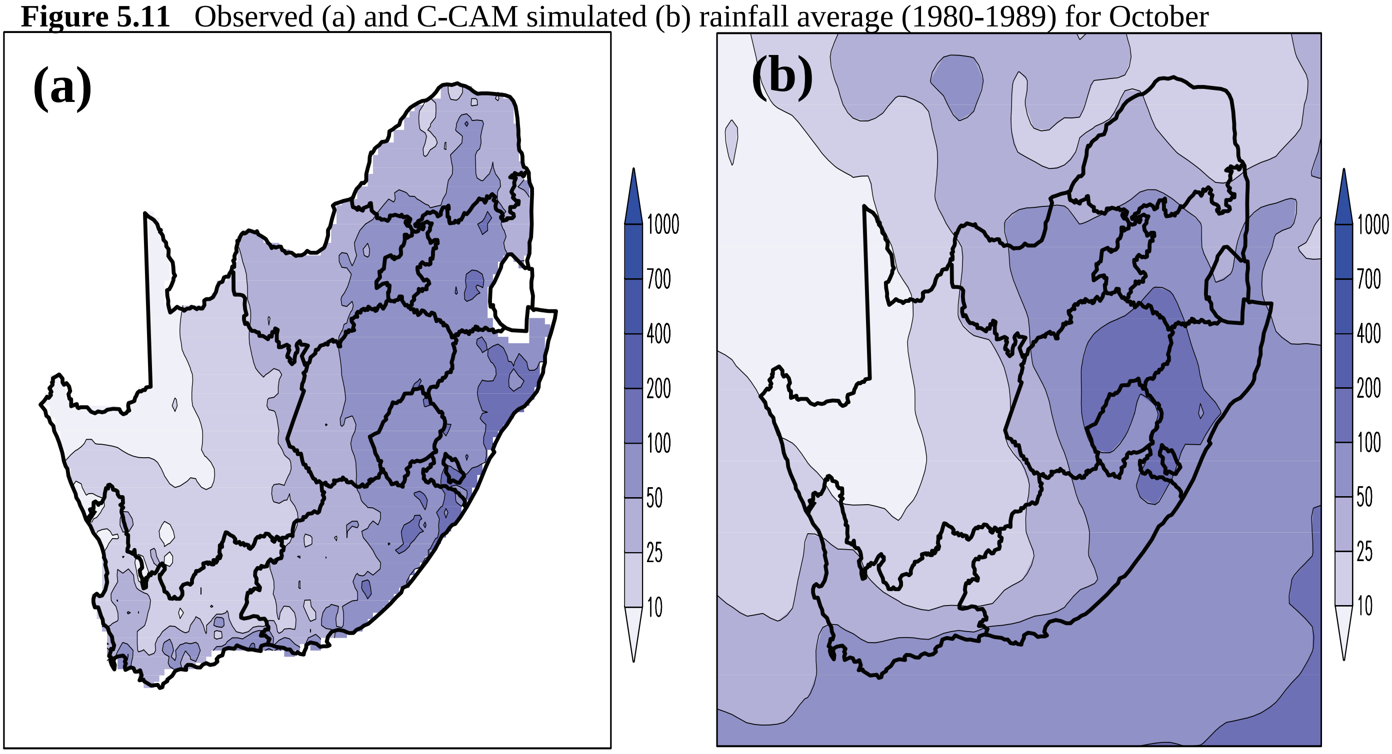

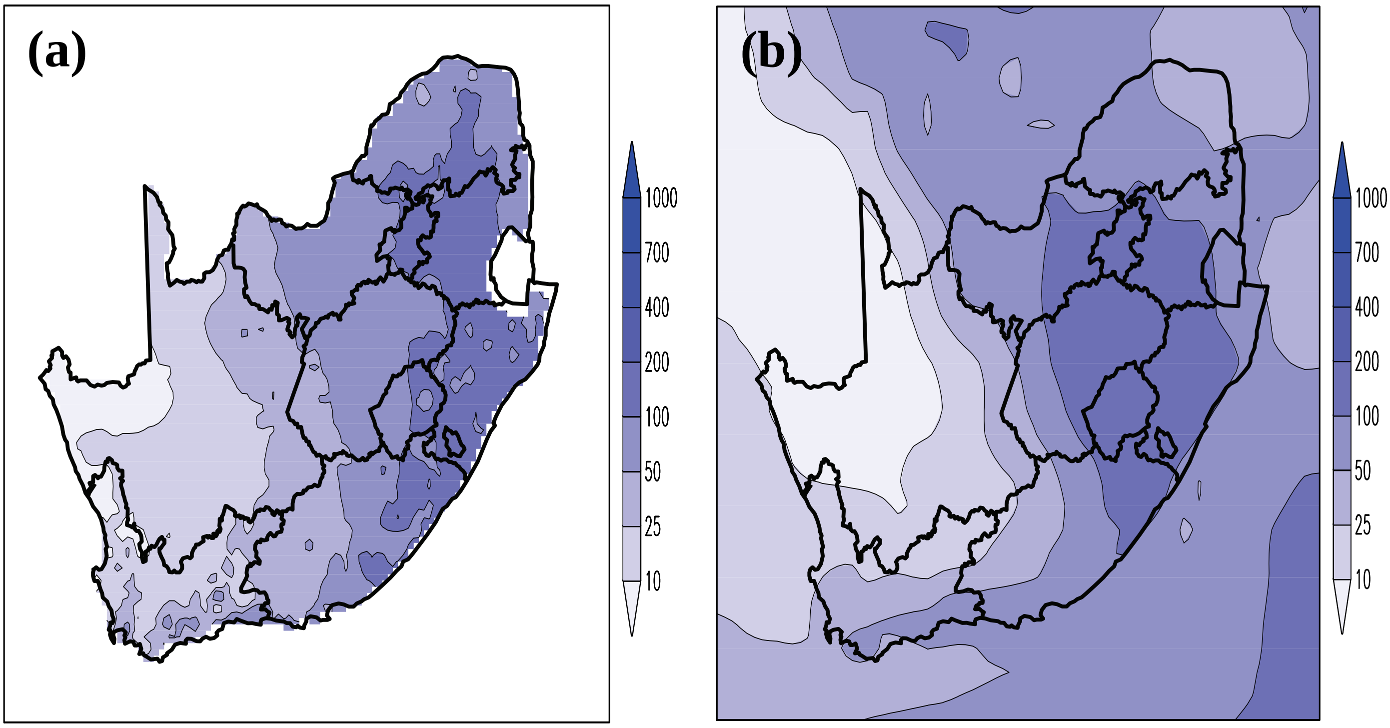

Figure 5.12 Observed (a) and C-CAM simulated (b) rainfall average (1980-1989) for November

Figure 5.13 Observed (a) and C-CAM simulated (b) rainfall average (1980-1989) for December

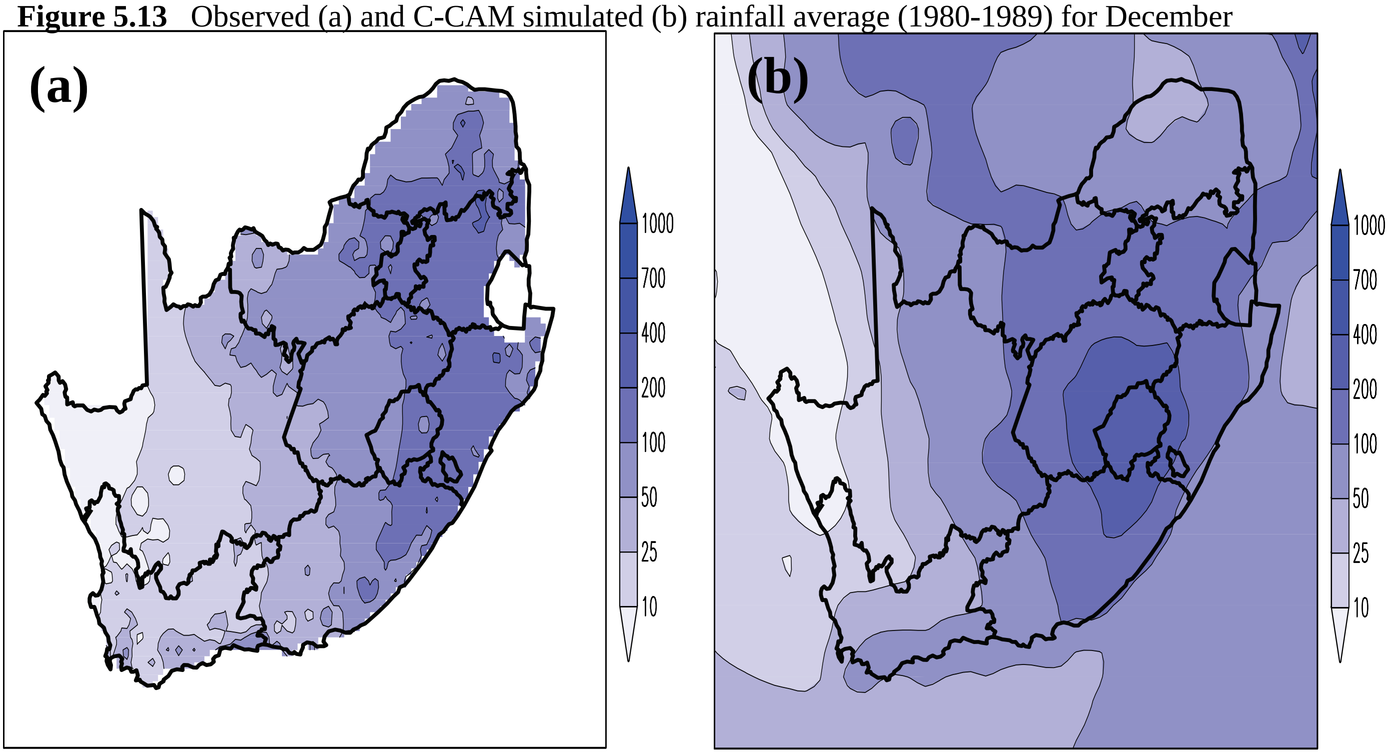

CHAPTER 6

DEVELOPMENT OF A NONHYDROSTATIC KERNEL

6.1 INTRODUCTION

Numerical modelling research at LRAM focuses on the development of a non-hydrostatic equation set and associated numerical solution procedures, suitable for application in terrain-following pressure-based (σ) coordinate models. The set of equations should be constructed in such a way that its application requires minimal modification to an existing hydrostatic σ-coordinate model. Still, it should be able to handle the meteorologically significant aspects of non-hydrostatic dynamics. The research at LRAM is carried out in close collaboration with CSIRO Atmospheric Research. Here the aim is to develop a non-hydrostatic kernel for the hydrostatic C-CAM, which employs a semi-implicit semi-Lagrangian solution procedure. A second branch of the research focuses on developing a nonhydrostatic dynamic kernel for a new split semi-Lagrangian atmospheric model presently under development at LRAM. In this Chapter of the report we motivate the choice of the set of equations used for the development process. Two different numerical solution procedures (split semi-Lagrangian for the new kernel and semi-implicit semi-Lagrangian for C-CAM) are presented, and the results from numerical tests are shown.

6.2 NONHYDROSTATIC EQUATIONS

Only a few atmospheric models use the fully-compressible (unapproximated) set of meteorological equations (e.g. Tanguay et al., 1990; Laprise, 1992; Robert, 1993; Janjic and Gerrity, 2001). The reason for this is that high-frequency sound waves, which are valid solutions of these equations, impose a severe restriction on the size of the time step that can be used to obtain stable numerical integrations of the equations. The most common approach to overcome this problem is to use approximated equations from which the sound waves are eliminated as possible solutions (Rõõm, 1998; Robert, 1993). Large-scale models use the hydrostatic approximation (relating the geopotential to the vertical thermal profile) (Eliassen, 1949). Convection (nonhydrostatic) models often use the anelastic assumption (assuming that the local time tendency of density vanishes) (Ogura and Charney, 1962; Robert, 1993). Hydrostatic models are not capable of simulating atmospheric processes on the convective scale (because vertical acceleration and buoyancy can't be explicitly resolved). The anelastic assumption suppresses the air's compressibility, which makes it non-trivial to apply the resulting equations at larger scales. Quite often the slow dynamics are distorted by the anelastic assumption (Rõõm, 1998). The advantage of using the fully-compressible equations is that both the hydrostatic approximation and the anelastic assumption are avoided, which means that these equations can potentially be applied at any scale. In order to partially avoid problems with sound waves, these models use specialised integration schemes designed to produce stable integrations with fewer calculations than the number required with classical integration algorithms (Robert, 1993). Still these models remain time-consuming to integrate, even on present-day supercomputers.

There exists another family of nonhydrostatic equations that may provide a computationally feasible alternative to the fully compressible equations while remaining suitable for universal application. They have been termed the "quasi-nonhydrostatic (QNH)" equations (Xue, 1989), but they should possibly rather be called "quasi-elastic (QE)". This equation set is filtered of some of the unwanted acoustic modes and can be used to simulate non-hydrostatic circulation while it remains applicable to large-scale circulation. Some characteristics of this equation set are discussed in the next Section.

6.3 QUASI-ELASTIC EQUATIONS

6.3.1 The Miller-Pearce Model

Miller (1974) and Miller and Pearce (1974) formulated a nonhydrostatic flow model in pressure, p, coordinates (a novel feature at that time). They introduced an interesting approximation of the vertical momentum equation, which in combination with approximations to the continuity and horizontal momentum equations ensured the absence of vertically propagating sound waves from the solution set. Buoyancy modes remain undistorted by the simplifications, and horizontally propagating sound waves (Lamb waves) may be removed by applying the lower boundary condition $\omega = 0$ at $p = p_0$ where p_0 is a constant. A firm theoretical basis for the equations (called the Miller-Pearce model (MP-model)) is provided by Miller and White (1984).

With the neglect of all forcing and cloud physics processes, the MP-model consists of the following approximate forms of the horizontal and vertical momentum equations (6.1) – (6.3) and continuity equation (6.4), and the exact thermodynamic energy equation (6.5) for a perfect gas:

$$\frac{Du}{Dt} - fv + \frac{\partial \phi'}{\partial x} = 0 \tag{6.1}$$

$$\frac{Dv}{Dt} + fu + \frac{\partial \phi'}{\partial y} = 0 \tag{6.2}$$

$$\frac{R}{g}\frac{D}{Dt}\left(\frac{\omega T_{ref}}{p}\right) + \frac{gT'}{T_{ref}} + \frac{gp}{RT_{ref}}\frac{\partial \phi'}{\partial p} = 0 \tag{6.3}$$

$$\frac{\partial u}{\partial x} + \frac{\partial v}{\partial y} + \frac{\partial \omega}{\partial p} = 0 \tag{6.4}$$

$$\frac{DT}{Dt} - \kappa\omega\frac{T}{p} = 0 \tag{6.5}$$

Here

$$\frac{D}{Dt} = \frac{\partial}{\partial t} + u\frac{\partial}{\partial x} + v\frac{\partial}{\partial y} + \omega\frac{\partial}{\partial p} \tag{6.6}$$

In equations (6.1)-(6.6) (and throughout this Chapter) u and v are the velocity components in the x and y directions, ϕ is the geopotential, T is the temperature, $\omega = \frac{Dp}{Dt}$, g is the gravitational acceleration, R is the gas constant for a unit mass of dry air and c_p is the specific heat at constant pressure. ϕ' and T' are perturbations of ϕ and T from the reference profiles $\phi_{ref}(p)$ and $T_{ref}(p)$. The reference state is chosen to be in hydrostatic balance, so that

$$\frac{d\phi_{ref}}{dp} = -\frac{RT_{ref}}{p} \tag{6.7}$$

Miller and White (1984) expanded this model to σ-coordinates. Lamb waves are present in the σ-coordinate formulation, where the lower boundary condition is $\dot{\sigma} = 0$ at $\sigma = 1$. This implies a computational penalty compared to the p-coordinate formulation.

The model described above (called the Miller-Pearce model (MP-model)) has been applied successfully in p - coordinates in numerous studies of systems where the initial state is rather homogeneous. These include numerous studies of cumulonimbus and other convective systems (Moncrieff and Miller, 1976; Miller and Bets, 1977; Thorpe and Miller, 1978; Thorpe et al., 1982; Brugge and Moncrieff, 1985). The MP-model in σ -coordinates was used to simulate mountain waves and deep orographic convection (Xue, 1989; Xue and Thorpe, 1991) and for studying gravity wave drag (Miranda and James, 1992).

The MP model is restrictive in the sense that it is formulated in terms of a reference temperature $T_{ref}(p)$. A single reference state may not be typical of different parts of the computational domain. This may be of particular importance if the model is applied in large-scale modelling or in mesoscale simulations of features such as frontal zones.

6.3.2 The extended QE-equations in p -coordinates

White (1989) modified the MP-model to be able to represent large temperature variations on pressure surfaces. With the neglect of all forcing and cloud physics processes, the extended quasi-nonhydrostatic model in p –coordinates consist of the following approximate forms of the horizontal and vertical momentum equations, continuity equation and the exact thermodynamic equation for a perfect gas:

$$\frac{Du}{Dt} - fv + \frac{\partial \phi'}{\partial x} = 0 \tag{6.8}$$

$$\frac{Dv}{Dt} + fu + \frac{\partial \phi'}{\partial y} = 0 \tag{6.9}$$

$$\frac{R}{g}\frac{D}{Dt}\left(\frac{\omega T}{p}\right) + \frac{gT'}{T} + \frac{gp}{RT}\frac{\partial \phi'}{\partial p} = 0 \tag{6.10}$$

$$\frac{\partial u}{\partial x} + \frac{\partial v}{\partial y} + \frac{\partial \omega}{\partial p} = 0 \tag{6.11}$$

$$\frac{DT}{Dt} - \kappa\frac{\omega T}{p} = 0 \tag{6.12}$$

The above equation set is free of sound waves (applying the lower boundary condition $\omega = 0$ at $p = p_0$ where p_0 is a constant) (White, 1989). Although the extended equations differ from the original only in the replacement of the reference state temperature $T_{ref}(p)$ by the true temperature T, it is not a trivial extension. In the quasi-geostrophic equations the use of a reference state profile is a necessary requirement if good conservation properties are to be retained (Hoskins and Pearce, 1983). The MP-model is not subject to such a restriction: White (1989) showed that the extended QE-equations imply a p-coordinate analogue of Ertel's potential vorticity conservation law and conserves energy. In 1994 Salmon and Smith showed that White's equations have a Hamiltonian structure and that the conservation properties follow from the symmetry properties of the relevant Hamiltonian.

6.3.3 Extended QE-equations in σ-coordinates

The explicit use of the reference temperature $T_{ref}(p)$ is avoided in the QE-equations in p-coordinates (6.8)-(6.12). White (1989) retained the use of the temperature and geopotential perturbations ϕ' and T' from the hydrostatic reference state, because of potential computational advantages during the numerical integration of the equations. However, it can easily be shown that the ϕ' and T' fields can be replaced in equations (6.8)-(6.12) with the full fields ϕ and T. With the aim of obtaining an extended set of QE-equations in σ-coordinates, the equations are written in terms of ϕ and T (in two dimensions for a start):

$$\frac{Du}{Dt} + \frac{\partial \phi}{\partial x} = 0 \tag{6.13}$$

$$\frac{R}{g}\frac{D}{Dt}\left(\frac{\omega T}{p}\right) + g + \frac{gp}{RT}\frac{\partial \phi}{\partial p} = 0 \tag{6.14}$$

$$\frac{\partial u}{\partial x} + \frac{\partial \omega}{\partial p} = 0 \tag{6.15}$$

$$\frac{DT}{Dt} - \kappa \frac{\omega T}{p} = 0 \tag{6.16}$$

Here the Coriolis effect has been neglected for simplicity. These equations imply a diagnostic equation for the geopotential:

$$\frac{\partial^2 \phi}{\partial x^2} + \frac{\partial}{\partial p}\left(r^2 \frac{\partial \phi}{\partial p} \right) = 2\left[\frac{\partial u}{\partial x}\frac{\partial \omega}{\partial p} - \frac{\partial \omega}{\partial x}\frac{\partial u}{\partial p} \right] - \frac{\partial}{\partial p}\left[rg - \frac{\omega^2}{\gamma p} \right] \tag{6.17}$$

where $r = \frac{gp}{RT}$.

Equations (6.13) to (6.17) can be transformed to σ-coordinates where

$$\sigma = \frac{p - p_T}{p_{surf} - p_T} = \frac{p - p_T}{p_s} \tag{6.18}$$

Here p represents the full pressure field, p_T is the pressure at the model top (a constant) and p_{surf} is the surface pressure. The transformation procedure is quite extensive and will not be described here. The extended QE-equations in σ-coordinates are:

$$\frac{Du}{Dt} = -\frac{\partial \phi}{\partial x} + \sigma \left(\frac{\partial \phi}{\partial \sigma} \right)\left(\frac{\partial \ln p_s}{\partial x} \right) \tag{6.19}$$

$$\left(\frac{R}{g} \right)\frac{D}{Dt}\left(\frac{\omega T}{p} \right) = -g - \frac{p}{p_s}\frac{g}{RT}\frac{\partial \phi}{\partial \sigma} \tag{6.20}$$

$$\frac{\partial u}{\partial x} + \frac{\partial \dot{\sigma}}{\partial \sigma} + \frac{D \ln p_s}{Dt} = 0 \tag{6.21}$$

$$\frac{DT}{Dt} = \kappa \omega \frac{T}{p} \tag{6.22}$$

$$\left(\frac{\partial^2 \phi}{\partial x^2} \right) + \frac{\partial}{\partial \sigma}\left[s^2 \frac{\partial \phi}{\partial \sigma} \right] - \frac{2\sigma}{p_s}\left(\frac{\partial p_s}{\partial x} \right)\frac{\partial^2 \phi}{\partial x \partial \sigma} + \left(\frac{1}{p_s}\frac{\partial p_s}{\partial x} \right)^2 \frac{\partial}{\partial \sigma}\left(\sigma^2 \frac{\partial \phi}{\partial \sigma} \right) - \frac{\sigma}{p_s}\left(\frac{\partial^2 p_s}{\partial x^2} \right)\frac{\partial \phi}{\partial \sigma} =$$
$$2\left[\left(\frac{\partial u}{\partial x} \right)_\sigma \frac{\partial}{\partial \sigma}\left(\Omega \frac{p}{p_s} \right) - \frac{\sigma}{p_s}\frac{\partial}{\partial x}(\Omega p_s)\frac{\partial u}{\partial \sigma} - \frac{1}{p_s}\frac{\partial}{\partial x}(\Omega p_T)\frac{\partial u}{\partial \sigma} \right] - \frac{\partial}{\partial \sigma}\left[(sg) - \frac{p}{p_s}\Omega^2 \frac{1}{\gamma} \right] \tag{6.23}$$

where the quantity Ω is defined by

$$\Omega = \frac{\dot{\sigma}}{\sigma} + \frac{1}{p_s}\frac{Dp_s}{Dt} \tag{6.24}$$

Note that $s = \frac{\sigma g}{RT}$ and $\gamma = \frac{c_p}{c_v}$.

These equations describe a dry, adiabatic atmosphere without rotation and friction. c_v is the specific heat of dry air at constant volume, $\dot{\sigma} = \frac{D\sigma}{dt}$ and $\omega = \frac{Dp}{dt}$. The total derivative of any variable A is defined as

$$\frac{D}{dt} = \frac{\partial}{\partial t} + u\frac{\partial}{\partial x} + \dot{\sigma}\frac{\partial}{\partial \sigma} \qquad (6.25)$$

Note that the equations are not formulated in terms of a reference temperature and geopotential profile, unlike the closely related equation sets used by Xue (1989), Xue and Thorpe (1991) and Miranda and James (1992).

Equations (6.19)-(6.24) form a closed set. Important to note is that in the set of equations (6.19)-(6.24) there are six variables: u, $\frac{\omega T}{p}$, $\dot{\sigma}$, T, ϕ and p_s, but only five independent equations as the diagnostic equation (6.23) is merely derived from the momentum equations and continuity equation. One more equation can be obtained by using information from the upper and lower boundary. We have that

$$\dot{\sigma} = 0 \text{ at } \sigma = 0 \text{ and } \sigma = 1$$

Manipulating the continuity equation and integrating from the surface to the top boundary provides a way to include this additional information and gives a seventh equation that closes the set and from which p_s can be calculated.

6.3.4 On the QE-assumption

The purpose of this Section is to provide some insight into the nature of the main assumption used in the QE-equations (following White, 1989). The unapproximated vertical component of the momentum equation (for motion on an f-plane) in Cartesian coordinates is

$$\frac{Dw}{Dt} + g + \frac{1}{\varphi}\frac{\partial p}{\partial z} \qquad (6.26)$$

in which w is the vertical velocity $\frac{Dz}{Dt}$. Equation (6.26) may be written as:

$$\frac{1}{g}\frac{\partial\phi}{\partial\sigma}\frac{Dw}{Dt}+\frac{\partial\phi}{\partial\sigma}+\frac{p_s}{p}RT \quad = 0 \tag{6.27}$$

After subtracting the reference state relation ($\frac{d\phi_{ref}}{d\sigma}+\frac{p}{p_s}RT_{ref} \ = 0$), and rearranging, equation (6.27) becomes:

$$\frac{Dw}{Dt}+g\frac{\partial\sigma}{\partial\phi}\left(\frac{\partial\phi'}{\partial\sigma}+\frac{p}{p_s}RT'\right)=0 \tag{6.28}$$

Substituting for $\frac{\partial\sigma}{\partial\phi}$ from equation (6.27) gives:

$$\frac{Dw}{Dt}=\frac{p}{p_s}\frac{g}{RT}\left(1+\frac{1}{g}\frac{Dw}{Dt}\right)\left(\frac{\partial\phi'}{\partial\sigma}+\frac{p_s}{p}RT'\right) \tag{6.29}$$

Equation (6.29) is equivalent to equation (6.26), and gives useful insight into the range and nature of possible approximations. With the approximations

$$\frac{Dw}{Dt}\prec g \quad \text{and} \quad w\approx-\frac{\omega RT}{gp} \tag{6.30}$$

equation (6.29) reduces to

$$\frac{R}{g}\frac{D}{Dt}\left(\frac{\omega T}{p}\right)+g+\frac{p}{p_*}\frac{g}{RT}\frac{\partial\phi}{\partial\sigma}=0 \tag{6.31}$$

This is the QE-vertical momentum equation.

6.4 THE SPLIT SEMI-LAGRANGIAN SOLUTION PROCEDURE

6.4.1 The purpose of splitting methods

Numerous different physical and dynamical factors are present in the system of atmospheric equations. It is often advantageous to use different numerical schemes during the integration of set of atmospheric equations, with each numerical scheme designed specifically for accurate and stable integrations of a given physical or dynamical process. For example, in atmospheric models it is computationally efficient to use the highly stable semi-Lagrangian technique to solve the advection terms in the horizontal momentum equations, but a high-order finite element scheme is more accurate for the simulation of the advection of a passive trace gas.

The idea of the splitting methods is to construct schemes for a complex system of equations so that within each time step this system is split into a number of simpler subsystems, which are then solved consecutively one at a time (Messinger and Arakawa, 1976). In this Section, a semi-Lagrangian scheme with a large time-step is used for the numerical integration of the advection terms in the QE-equations. The remaining processes, such as gravity and Lamb wave propagation, are incorporated during an adjustment process consisting of smaller adjustment time-steps.

6.4.2 Horizontal and vertical discretization

The horizontal and vertical discretization were carried out on an unstaggered grid.

6.4.3 Split semi-Lagrangian solution procedure

The governing equations are split into advective and non-advective terms, using a two time-level split semi-Lagrangian scheme. The integration procedure consists of a semi-Lagrangian advection step with time step Δt_s followed by N adjustment steps with time step $\Delta t_a = \frac{\Delta t_s}{N}$. In the discussion that follows it is assumed that the values of u, $\frac{\omega T}{p}$, $\dot{\sigma}$, T, ϕ and p_s are known at all grid points at time level τ. The split semi-Lagrangian procedure will be used to update all variables at time level $\tau + 1$.

Let τ^* be associated with variables evaluated at the previous time level, τ, at the departure points.

1) SPLITTING OFF THE ADVECTIVE PART

The horizontal momentum, continuity and thermodynamic energy equations are discretized the semi-Lagrangian way to obtain the "advection" values of variables at time level $\tau + 1$:

$$\frac{Du}{Dt} = 0 \tag{6.32}$$

$$\frac{D}{Dt}\left(\ln p_s\right) = 0 \tag{6.33}$$

$$\frac{DT}{Dt} = 0 \tag{6.34}$$

The D_3 semi-Lagrangian procedure (McGregor, 1993; Engelbrecht, 2000) is used to calculate the departure points. The values of u and T are evaluated at the departure points using bicubic interpolation (McDonald, 1984) for the two-dimensional case, and by using a high-order three-dimensional interpolation scheme for the three-dimensional case. Let the values of u and T obtained from the semi-Lagrangian procedure be denoted by u^* and T^*.

The "advection" value of $\ln p_s$ is found by solving equation (6.33) in the form:

$$\frac{\partial \ln p_s}{\partial t} = -u\frac{\partial \ln p_s}{\partial x} \tag{6.35}$$

The quantity $-u\frac{\partial \ln p_s}{\partial x}$ is calculated at each model level from the semi-Lagrangian procedure and stored, following Leslie and Purser (1991) and McGregor (1986). These values are then used in the vertical integration of equation (6.33), to obtain an expression from which the time rate of change of $\ln p_s$ due to advection at time level $\tau + 1$ can be calculated:

$$\left(\frac{\partial \ln p_s}{\partial t}\right)^{\tau+1} = -\int_0^1 \left(u\frac{\partial \ln p_s}{\partial x}\right)^{\tau^*} d\sigma \tag{6.36}$$

Let the "advection" value of the surface pressure obtained from equation (6.36) be denoted by p_s^*.

2) ADJUSTMENT STEP

After the "advection" values of variables have been found, an adjustment procedure is performed to incorporate the effect of non-advective processes. The adjustment equations are:

$$\frac{\partial \ln p_s}{\partial t} = -\int_0^1 \frac{\partial u}{\partial x} d\sigma \tag{6.37}$$

$$\dot{\sigma} = -\int_0^{\sigma_k} \left(\frac{\partial u}{\partial x}\right) d\sigma - \sigma \frac{\partial \ln p_s}{\partial t} \tag{6.38}$$

$$\frac{\omega T}{p} = \left(\frac{\dot{\sigma}}{\sigma} + \frac{\partial \ln p_s}{\partial t}\right) T \tag{6.39}$$

$$\frac{\partial T}{\partial t} = \kappa \left(\frac{\omega T}{p}\right) \tag{6.40}$$

$$\left(\frac{\partial^2 \phi}{\partial x^2}\right) + \frac{\partial}{\partial \sigma}\left[s^2 \frac{\partial \phi}{\partial \sigma}\right] - \frac{2\sigma}{p_s}\left(\frac{\partial p_s}{\partial x}\right)\frac{\partial^2 \phi}{\partial x \partial \sigma} + \left(\frac{1}{p_s}\frac{\partial p_s}{\partial x}\right)^2 \frac{\partial}{\partial \sigma}\left(\sigma^2 \frac{\partial \phi}{\partial \sigma}\right) - \frac{\sigma}{p_s}\left(\frac{\partial^2 p_s}{\partial x^2}\right)\frac{\partial \phi}{\partial \sigma} =$$
$$2\left[\left(\frac{\partial u}{\partial x}\right)_\sigma \frac{\partial}{\partial \sigma}\left(\Omega \frac{p}{p_s}\right) - \frac{\sigma}{p_s}\frac{\partial}{\partial x}(\Omega p_s)\frac{\partial u}{\partial \sigma} - \frac{1}{p_s}\frac{\partial}{\partial x}(\Omega p_T)\frac{\partial u}{\partial \sigma}\right] - \frac{\partial}{\partial \sigma}\left[(sg) - \frac{p}{p_s}\Omega^2 \frac{1}{\gamma}\right] \tag{6.23}$$

$$\frac{\partial u}{\partial t} = -\frac{\partial \phi}{\partial x} + \sigma \frac{\partial \ln p_s}{\partial x}\frac{\partial \phi}{\partial \sigma} \tag{6.41}$$

The values of u^*, T^* and $\ln p_s^*$ are used as initial conditions during the first adjustment time step. Forward time differencing is applied to solve equation (6.37) and backward differencing is used in equations (6.40) and (6.41). Equations (6.38), (6.39) and (6.23) are diagnostic equations that make use of the latest available values of the relevant variables. The adjustment step is repeated N times and the semi-Lagrangian procedure is applied again, and so on until the end of the integration period is reached.

3) EVALUATION OF VERTICAL INTEGRALS

The trapezium rule is used to calculate the integrals that need to be evaluated during the numerical integration procedure. Centred finite differences are employed to evaluate the relevant spatial derivatives. For example, the integral $\int_0^1 \left(\frac{\partial u}{\partial x}\right) d\sigma$ is evaluated as follows:

$$\int_0^1 \frac{\partial u}{\partial x} d\sigma = \left[\frac{u_{i+1,1} - u_{i-1,1}}{2\Delta x} + \sum_{j=2}^{j=A_s-1} \frac{u_{i+1,j} - u_{i-1,j}}{2\Delta x} + \frac{u_{i+1,As} - u_{i-1,As}}{2\Delta x}\right]\Delta\sigma \qquad (6.42)$$

4) NUMERICAL DIFFUSION

Diffusion terms need to be introduced in equations (6.40) and (6.41) to ensure numerical stability of the solution:

$$\frac{\partial u}{\partial t} = -\frac{\partial \phi}{\partial x} + \sigma\left(\frac{\partial \phi}{\partial \sigma}\right)\left(\frac{\partial \ln p_s}{\partial x}\right) + K_d \frac{\partial^2 u}{\partial x^2} + K_s \frac{\partial^2 u}{\partial \sigma^2} \qquad (6.43)$$

$$\frac{\partial T}{\partial t} = \kappa \frac{\omega T}{p} + K_d \frac{\partial^2 T}{\partial x^2} + K_s \frac{\partial^2 T}{\partial \sigma^2} \qquad (6.44)$$

K_d and K_s are the diffusion coefficients.

5) THE ELLIPTIC EQUATION

Equation (6.23) gives a diagnostic equation for the geopotential. The discretized version of this elliptic equation can be solved using a robust solver developed specifically for this model, based on the Jacobi relaxation method. Although this approach is numerically not very efficient, it is convenient to use during the development phase of such a complex numerical model because of its flexibility.

Also, the solver is symmetric, which is a most useful property when analysing symmetric numerical test results. A more efficient Successive Over Relaxation (SOR) technique has also been developed.

The need to solve the elliptic equation during each adjustment time step forms an expensive part of the integration procedure. However, all previous numerical solutions of the QE-equations (in p or σ- coordinates) were based on fully explicit methods that exploited an elliptic equation similar to equation (6.23) (White, 1989; Xue, 1989; Xue and Thorpe, 1992; Miranda and James, 1992). An advantage of the present approach is that the semi-Lagrangian procedure allows the use of a large advection time-step, which yields a significant computational advantage over the fully explicit methods.

An interesting and unique aspect of the split semi-Lagrangian solution procedure presented here is that the vertical momentum equation (6.20) is never solved explicitly during the integration procedure. However, as stated earlier, the elliptic equation (6.23) is derived from the momentum, continuity and thermodynamic energy equations. The important dynamical aspects of equation (6.23) are described implicitly in the elliptic equation (6.23). By avoiding the explicit use of equation (6.20) and by calculating the values of $\frac{\omega T}{p}$ at each adjustment step from equation (6.39), numerical consistency with the corresponding $\dot{\sigma}$ field is ensured. The split-semi-Lagrangian approach doesn't require linearization of any kind.

6.5 SEMI-IMPLICIT SEMI-LAGRANGIAN SOLUTION PROCEDURE

6.5.1 QE-equations in C-CAM

For application in C-CAM, the set of QE-equations have been expanded into three dimensions and written in a form that closely corresponds to the existing set of hydrostatic equations used in the model.

$$\frac{d_H u}{dt} + m\frac{\partial \phi}{\partial x} - m\sigma\left(\frac{\partial \phi}{\partial \sigma}\right)\left(\frac{\partial \ln p_s}{\partial x}\right) + \dot{\sigma}\frac{\partial u}{\partial \sigma} = \left(f + f_m\right)v + N'_u \tag{6.45}$$

$$\frac{d_H v}{dt} + m\frac{\partial \phi}{\partial y} - m\sigma\left(\frac{\partial \phi}{\partial \sigma}\right)\left(\frac{\partial \ln p_s}{\partial y}\right) + \dot{\sigma}\frac{\partial v}{\partial \sigma} = -\left(f + f_m\right)u + N'_v \tag{6.46}$$

$$\left(\frac{R^2 T}{g^2 \sigma}\right)\frac{D}{Dt}\left(\frac{\omega T}{\sigma p_s}\right) + \frac{\partial \phi}{\partial \sigma} + \frac{RT}{\sigma} = 0 \tag{6.47}$$

$$\frac{d_H \ln p_s}{dt} + D + \frac{\partial \dot{\sigma}}{\partial \sigma} = 0 \tag{6.48}$$

$$\frac{d_H T}{dt} + \dot{\sigma}\frac{\partial T}{\partial \sigma} - \frac{RT}{c_p \sigma}\frac{\omega}{p_s} = N'_T \tag{6.49}$$

Here

$$\frac{d_H}{dt} = \frac{\partial}{\partial t} + mu\frac{\partial}{\partial x} + mv\frac{\partial}{\partial y} \tag{6.50}$$

where m denotes the map factor of the conformal projection. N'_u, N'_v and N'_T represent physical forcing and the divergence D is given by

$$D = m^2\left\{\frac{\partial\left(\frac{u}{m}\right)}{\partial x} + \frac{\partial\left(\frac{v}{m}\right)}{\partial y}\right\} \tag{6.51}$$

6.5.2 Semi-implicit scheme

The existing semi-implicit semi-Lagrangian integration scheme in C-CAM has been modified to solve the QE-equations. Only a brief summary of the solution procedure is given here. More details are to follow in Engelbrecht (2005).

The semi-Lagrange discretization of the equations is given below. Values of variables at the current time level are denoted by the subscript τ and those at the subsequent time level by $\tau+1$. The values of variables at the departure points calculated from the semi-Lagrangian procedure are denoted by τ_*. Subscript $\bar{\tau}$ represents a time-average of the quantity in brackets, evaluated along a trajectory between time levels τ_* and $\tau+1$. Bicubic spatial interpolation is used to evaluate all quantities with subscript τ_* in the semi-Lagrangian discretization:

$$\left\{u+(1+\gamma)\frac{\Delta t}{2}\left(m\frac{\partial p}{\partial x}-fv\right)\right\}^{\tau+1}=\left\{u-(1-\gamma)\frac{\Delta t}{2}\left(m\frac{\partial p}{\partial x}-fv\right)\right\}^{\tau^*}+\Delta t\left(N_u-\dot{\sigma}\frac{\partial u}{\partial \sigma}\right)^{\bar{\tau}} \tag{6.52}$$

$$\left\{v+(1+\gamma)\frac{\Delta t}{2}\left(m\frac{\partial p}{\partial y}+fu\right)\right\}^{\tau+1}=\left\{v-(1-\gamma)\frac{\Delta t}{2}\left(m\frac{\partial p}{\partial y}+fu\right)\right\}^{\tau^*}+\Delta t\left(N_v-\dot{\sigma}\frac{\partial v}{\partial \sigma}\right)^{\bar{\tau}} \tag{6.53}$$

$$\left\{\frac{T}{\sigma}\frac{\omega}{p_s}+(1+\varepsilon)\frac{\Delta t}{2}\frac{g^2\sigma}{R^2T}\left(\frac{\partial \phi}{\partial \sigma}+\frac{RT}{\sigma}\right)\right\}^{\tau+1}=\left\{\frac{T}{\sigma}\frac{\omega}{p_s}-(1+\varepsilon)\frac{\Delta t}{2}\frac{g^2\sigma}{R^2T}\left(\frac{\partial \phi}{\partial \sigma}+\frac{RT}{\sigma}\right)\right\}^{\tau_*} \tag{6.54}$$

$$\left\{\ln p_s+(1+\varepsilon)\frac{\Delta t}{2}\left(D+\frac{\partial \dot{\sigma}}{\partial \sigma}\right)\right\}^{\tau+1}=\left\{\ln p_s-(1-\varepsilon)\frac{\Delta t}{2}\left(D+\frac{\partial \dot{\sigma}}{\partial \sigma}\right)\right\}^{\tau_*} \tag{6.55}$$

$$\left\{T-(1+\varepsilon)\frac{\Delta t}{2}\frac{R\bar{T}}{c_p\sigma}\frac{\omega}{p_s}\right\}^{\tau+1}=\left\{T+(1-\varepsilon)\frac{\Delta t}{2}\frac{R\bar{T}}{c_p\sigma}\frac{\omega}{p_s}\right\}^{\tau^*}+\Delta t\left(N_T-\dot{\sigma}\frac{\partial T}{\partial \sigma}\right)^{\bar{\tau}} \tag{6.56}$$

Here the constants γ and ε induces off-centring of the time averaged terms. This procedure helps to avoid spurious mountain wave resonance (Rivest et al., 1994)

The system of equations is then further rearranged, converted into eigenspace, and decoupled in the vertical. Eventually the process leads to a Helmholtz equation for the vertical mode $\mathbf{P}$ of the augmented geopotential

$$\mathrm{P} = \phi + \mathrm{R}\overline{\mathrm{T}}\ln \mathrm{p_s} : \tag{6.57}$$

$$\nabla_{\alpha}^{2}\mathbf{P} = \left(\mathbf{P} - \mathbf{X}_{\mathbf{p}}\right) / \left(m^2 \frac{\Delta t^2}{4}(1+\varepsilon)\lambda_k \right) + \mathbf{X}_{\mathbf{D}} / \left(m^2 \frac{\Delta t}{2} \right) \tag{6.58}$$

Here $\mathbf{P}$, $\mathbf{X}_{\mathbf{p}}$ and $\mathbf{X}_{\mathbf{D}}$ are NxN matrixes where N is the number of grid points used by the model in the horizontal. Equation (6.58) is solved by successive over-relaxation, applying Dirichlet boundary conditions. Having obtained values for $\mathbf{P}$, eigenvectors may be used to give $\mathrm{P}^{\tau+1}$. The velocity fields, surface pressure and temperature can then be calculated.

The semi-implicit solution procedure for the QE-equations allows the use of a time step about 10 times larger than that used in fully explicit methods. The splitting of the equations, and the use of a smaller adjustment time step, is avoided. However, the approach requires the use of a linearized temperature field $\overline{T}$, and the elliptic equation (6.58) is expensive to solve.

6.6 NUMERICAL TESTS

6.6.1 Introduction to numerical tests

The QE-equation set is dynamically consistent since it satisfies important energy and vorticity conservation laws (White, 1989). It seems as if the equation set can be used for large-scale modelling during long-term numerical integrations (for example climate simulations). The nonhydrostatic character of the equation set may, alternatively, allow the equations to be used for high-resolution mesoscale and microscale modelling where the hydrostatic assumption ceases to be valid. It remains to be shown that the assumptions made in obtaining the extended QE set of equations in σ- coordinates restrict the application of the model to very high horizontal and vertical resolutions. In this Section the performance of the model is tested at very high horizontal and vertical resolutions to investigate its ability to simulate nonhydrostatic circulation.

The model is applied to simulate bubble convection in an isentropic environment (e.g. Mendez-Nunez and Carroll, 1994; Straka et al., 1993; Robert, 1993; Droegemeier and Wilhelmson, 1987). Bubble convection tests have become a standard way of testing the performance of nonhydrostatic equaton sets. Another important factor that can be investigated with these tests is how the split semi-Lagrangian and semi-implicit semi-Lagrangian schemes will function under the test conditions when applied to the QE-equations. In order to remain stable, the semi-implicit technique must apparently satisfy a number of constraints. The most important constraint is related to the reference state used in the model for the application of the semi-implicit scheme (Robert, 1993). Simmons et al. (1978) and Côté et al. (1983) have shown that an isothermal reference state is a necessary condition for stability. The split-explicit semi-Lagrangian scheme completely avoids the use of reference states and the bubble experiments provide an interesting test to determine the effects of this formulation.

Finally, it is important to note at that although the semi-implicit semi-Lagrangian scheme in C-CAM provides unconditionally stable integrations when applied to the hydrostatic σ-coordinate equations, there is no guarantee that integrating the QE-equations with a modified semi-implicit approach will be equally successful. In fact, there is a possibility that both the semi-implicit and split-explicit schemes might run into difficulties if the static stability vanishes at some point in the atmosphere or if it becomes negative. Large-scale models use a parameterised convective adjustment scheme that constrains the static stability to positive values. This constraint is applied in all large-scale models, including those that use the classical integration algorithms (Robert, 1993). It is used to prevent a form of instability that will hopefully be well managed if the resolution of the model could be extended all the way to a few meters. To investigate these ideas the convective scale is examined, where the adjustment constraint on static stability is not needed (Robert, 1993).

6.6.2 Grid-converged solutions

Many different types of numerical schemes have been developed to simulate particular non-linear fluid flow problems. The reason why so many schemes are accepted widely is rooted in the proof of theorems such as those developed by Lax, which state that consistency and stability are the necessary and sufficient conditions for the convergence of discretized linear problems (Straka, 1993; Richtmeyer and Morton, 1967). Thus, given a stable and consistent discretised form of a continuous system, a grid-converged solution can be obtained as Δx and $\Delta t \to 0$. The term grid-converged is used to state that no meaningful improvement in a numerical solution could be obtained using higher resolution within the practical limits of finite precision, speed and memory of a computing machine (Straka et al., 1993). This implies that all stable and convergent difference equations for a given linear continuous system should approach the same grid-converged or analytic solution (Straka et al., 1993).

Computers now have enough speed and memory so that grid-converged numerical solutions can be found for non-linear problems with scale-limiting physics, such as diffusion, by using very high resolution. In the numerical simulation of diffusion-limited problems, the length scale of the smallest resolvable feature is determined by the length scale associated with the diffusion (Straka et al., 1993).

Researchers generally choose test problems that have relevance to their fields of study. While this has proven useful for individual disciplines, it makes comparisons of the behaviour of various numerical techniques and equation sets difficult (Straka et al., 1993). With this in mind Straka et al. (1993) studied the behaviour of a variety of numerical methods when applied to a particular diffusion-limited non-linear problem test problem of fluid flow for which a grid–converged solution could be generated. The selected test problem is described in the next Section.

6.6.3 The cold bubble test

Following Straka (1993), a two-dimensional problem is chosen because it is more computationally feasible to obtain a grid-converged solution for a two-dimensional problem than for a three-dimensional problem. In order to obtain a grid-converged solution, the problem has to be diffusion limited. To test the robustness of the numerical method, the test problem is designed to contain non-linear dynamics, transient features and fine-scale structures (Straka, 1993). The problem is solvable using both compressible and incompressible flow equations (Straka, 1993).

A density current problem in an otherwise homogeneous and isentropic fluid was chosen that is similar to that used by Droegemeier and Wilhelmson (1987). The density current is initiated as a cold blob of air that subsequently descends to the ground. As the density current spreads out laterally at the lower boundary, Kelvin-Helmhotz shear instability rotors form along the top of the cold air boundary.

The independent variables are horizontal (x) and vertic)al (σ) grid directions, and time (t). Constants include: R_d=287.0 J kg^{-1}K^{-1} (gas constant for dry air), C_p=1004 Jkg^{-1}K^{-1} (specific heat at constant pressure); C_v=717.0 Jkg^{-1}K^{-1} (specific heat at constant volume); p_0=100000.0 kgm^{-1}s^{-2} (reference pressure); g=9.81 ms^{-2} (gravitational parameter); K= 75.0 m^{2}s^{-1} (Diffusion coefficient).

6.6.4 Computational domain

The integration domain covered 40 km in the x direction with a free surface introduced at 442 hPa, that is, at about 6400 m. These are the same settings used by Straka (1993) and Janjc (2000). The horizontal resolution used is 100m, and the vertical resolution was 100 m on average (65 equally spaced σ-levels are used).

6.6.5 Cold bubble test in σ-coordinates

Setting up the cold bubble test in σ-coordinates is a bit trickier than in z-coordinates, and some details are given below. The procedure provides useful experience concerning the initialisation of a numerical model in a more general sense. The procedure described below allows for the inclusion of non-zero topography in the model, although experiments involving topography are not shown here.

6.6.5.1 Initial conditions

Surface pressure

The initial atmosphere is chosen to be isentropic, which means that the environmental temperature lapse rate is dry adiabatic:

$$\overline{T} = T_s - zgC_p^{-1}, \qquad (6.59)$$

where $\overline{\theta} = T_s = 300\ K$, with T_s the homogeneous surface temperature at $z = 0$.

The surface pressure can be calculated as a function of $z = z_s(x)$ by using the definition of potential temperature and assuming a dry adiabatic lapse rate to give:

$$p_{surf} = p_0 \left[1 - \frac{g z_s}{c_p T_s} \right]^{\frac{c_p}{R_d}}$$

Here p_0 is the reference pressure level, which is taken to be 1000 hPa, and $z_s(x)$ denotes topographic height.

Initial height of σ-levels and the geopotential

It is necessary to the find the initial geometric height of each of the σ-levels in order to specify the value of temperature at each of the grid points. By using the potential temperature definition under dry adiabatic conditions it follows that:

$$z = \frac{c_p T_s}{g} \left[1 - \left(\frac{\sigma p_s + p_T}{p_0} \right)^{\frac{R_d}{C_p}} \right]$$

The initial geopotential distribution is given by

$$\phi = gz$$

Temperature

The dry-adiabatic initial temperature distribution can now be found from equation (6.59).

To provide the negative buoyancy necessary to initiate a density current, the following function is used to specify a temperature perturbation:

$$\Delta\mathrm{T} = \begin{cases} 0^\circ\mathrm{C} & \text{if} \quad \mathrm{L} > 1 \\ -15^\circ\mathrm{C}[\cos(\pi\mathrm{L}) + 1]/2 & \text{if} \quad \mathrm{L} \leq 1 \end{cases}$$

Here $L = \left\{ \left[(x - x_c) x_r^{-1} \right]^2 + \left[(z - z_c) z_r^{-1} \right]^2 \right\}^{0.5}$, with $x_c = 20000\ m$, $z_c = 3000\ m$, $x_t = 4000\ m$ and $z_t = 2000\ m$.

Velocity field

An initial state of no motion is assumed:

$$u = 0 = \dot{\sigma}$$

From the diagnostic equation (6.24) it follows that Ω is initialised by

$$\Omega = 0$$

6.6.6 Boundary conditions

6.6.6.1 Lateral boundary conditions

The lateral boundary conditions for the test problem (following Straka et al., 1993), are $u = \frac{\partial \dot{\sigma}}{\partial x} = \frac{\partial \phi}{\partial x} = \frac{\partial \theta}{\partial x} = \frac{\partial p_s}{\partial x} = 0$

On the lateral boundaries the assumption $\frac{\partial \theta}{\partial x} = 0$ in combination with the assumption $\frac{\partial p_s}{\partial x} = 0$ implies that $\frac{\partial T}{\partial x} = 0$.

6.6.6.2 Vertical boundary conditions

Temperature

On the lower boundary it is assumed that $\frac{\partial \theta}{\partial \sigma} = 0$. This implies that, in terms of temperature, $T\big|_{\sigma=1} = T\big|_{\sigma=1-\Delta\sigma} \left(\frac{p_s + p_T}{\sigma p_s + p_T} \right)^{\frac{Rd}{C_p}}$.

On the top boundary the assumption $\frac{\partial \theta}{\partial \sigma} = 0$ implies that

$$T\Big|_{\sigma=1} = T\Big|_{\sigma=1-\Delta\sigma}\left(\frac{p_s + p_T}{\sigma p_s + p_T}\right)^{\frac{Rd}{C_p}}$$

Geopotential

At the lower boundary of the model the geopotential height is related to the surface topography. Since the lower boundary of the model is the ground surface, which has topography profile

$$z = z_s(x)$$

it follows that

$$\phi\Big|_{\sigma=1} = g z_s(x)$$

A hydrostatic geopotential distribution is assumed over the top layer of the model.

Velocity field

A free slip condition on the velocity components is imposed at the lower and top boundaries of the domain. This implies that $\dot{\sigma} = 0$ and $\frac{\partial u}{\partial \sigma} = 0$ at $\sigma = 1$ and $\sigma = 0$.

6.6.7 Two-dimensional bubble convection tests

In the two-dimensional cold bubble tests the split semi-Lagrangian scheme was applied to solve the QE-equations. The time step used is 0.4 s and the horizontal and vertical resolution about 100m. The CFL-criterion is exceeded with a factor of 1.3.

Figure 6.1 shows the evolution of the cold bubble in time. As the cold blob of air reaches the surface it spreads out horizontally as a gust front, and Kelvin-Helmholtz instability rotors develop. The results compare well to those of Janjic and Gerrity (2001) and Straka et al. (1993).

6.6.8 Three dimensional bubble convection on the C-CAM grid

In this experiment a three-dimensional cold bubble was introduced to the C-CAM grid. The model ran in highly-stretched mode, giving a horizontal resolution of about 1 km over the panel of maximum resolution. 35 σ-levels were used in the vertical. The time step was 10 s, which means that the CFL criterion is exceeded with a factor of 3. The same settings and boundary conditions were used as for the two-dimensional tests, except that the model top was located at $p_T = 0$ hPa with a constant in time isothermal atmosphere assumed above 442 hPa.

Figure 6.2 shows simulation results when the semi-implicit scheme is applied to the hydrostatic formulation of C-CAM. The integration remained stable and the bubble descended to the surface, but fine scale structures such as a rotor is not simulated in the absence of nonhydrostatic dynamics.

In Figure 6.3 the result obtained when the semi-implicit scheme is applied to the QE-equations is shown. The ω-field shows the presence of a rotor after 300 and 900 s with the associated lateral movement of a gust front. These results correspond well to two-dimensional tests performed at 1 km resolution (not shown). The results indicate the implementation of the QE-equations was successful and that the semi-implicit scheme performs well.

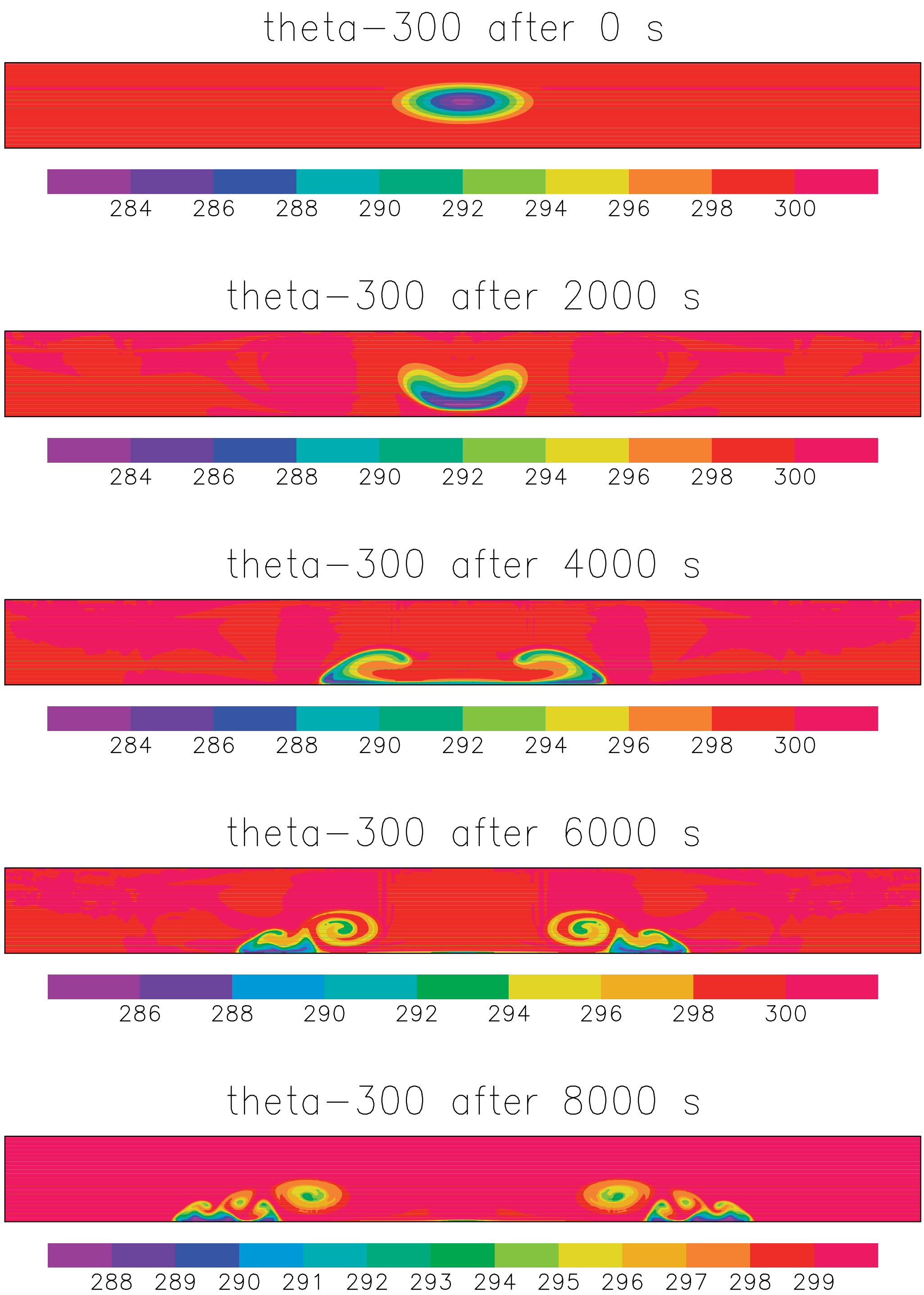

Figure 6.1 Two-dimensional cold bubble test with the split semi-Lagrangian scheme.

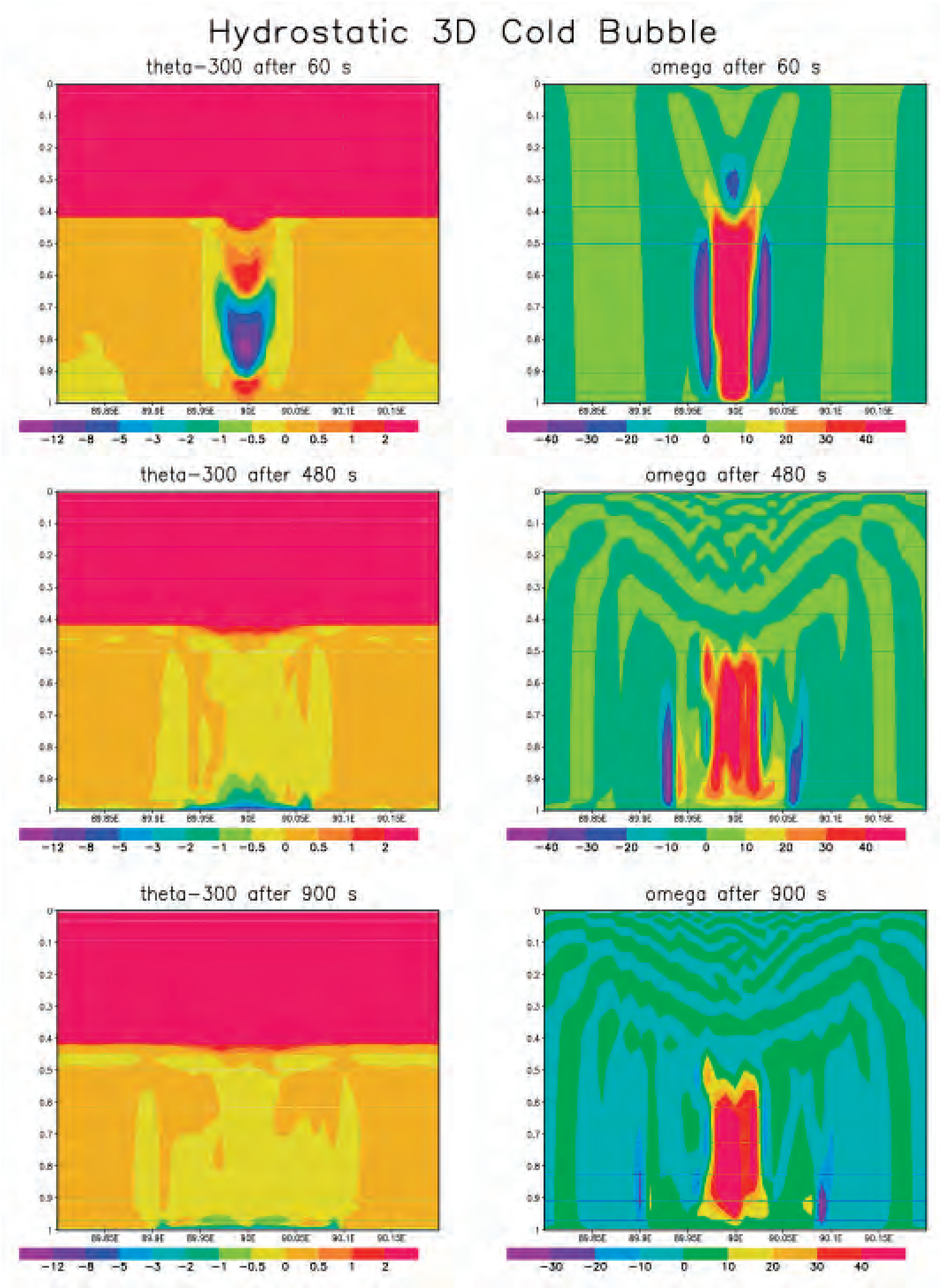

Figure 6.2 Hydrostatic cold bubble in C-CAM

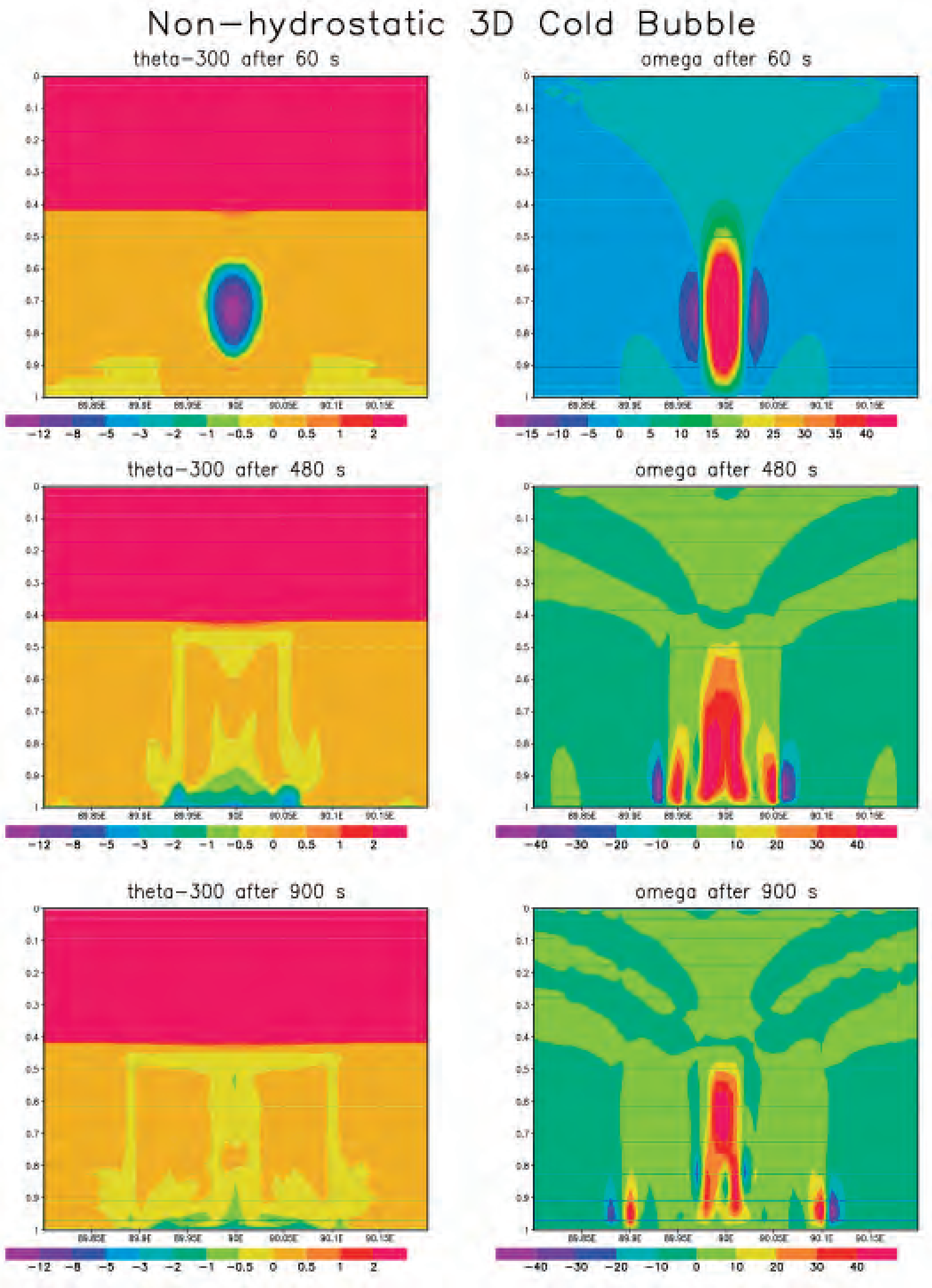

Figure 6.3 Nonhydrostatic cold bubble in C-CAM

CHAPTER 7

SHORT-RANGE WEATHER FORECASTING WITH C-CAM

7.1 INTRODUCTION

C-CAM's highly efficient numerical integration scheme makes it possible to run the model in real-time at high resolution on a powerful PC. C-CAM became operational in real time at the University of Pretoria on the 1st of December 2004. This chapter is a preliminary investigation into C-CAM's performance as a short-range weather forecasting model over southern Africa. Only one forecast of the model is analyzed, with the intention to do more extensive model verification during 2005. Some of the model forecast fields are verified by means of comparison to satellite imagery and observed station data obtained from the SAWS. In the final Section of this chapter the dynamic predictability of the weather event by C-CAM is investigated by means of a quantitative comparison between the 500 hPa geopotential fields of the model forecast and NCEP Reanalysis data.

7.2 THE C-CAM FORECASTING SYSTEM

C-CAM is initialized once a day at 00Z at C100 resolution. This means that the model has 100 x 100 grid points on each of the 6 panels. A Schmidt stretching factor of 0.3 is used, which implies that the horizontal resolution is approximately 15 km on the panel of highest resolution and approximately 60 km on the panel at the opposite side of the cube. The model has eighteen sigma levels in the vertical and output is interpolated to selected pressure levels between 1000 hPa and 100 hPa. The lowest sigma level is located approximately 30m above the surface.

The widely used AVN initial conditions are downloaded once a day for 00Z from the FTP site of the National Center for Environmental Prediction (NCEP).

Due to limited archiving space it has been decided to run C-CAM for only four days for each initialization. Model output is written at 0.3º resolution on a domain covering 70ºS to 10ºN and 10ºW to 60ºE, and at 0.15º resolution on a domain covering 36ºS to 20ºS and 12 ºE to 35ºE.

The model integration is performed on a PC with a 2000 MHz CPU and 512 MRAM. A four-day model simulation at C100 resolution takes 8.5 hours to complete on the present computing system.

7.3 SHORT-RANGE FORECASTS AND A SUBJECTIVE VERIFICATION

Short-term forecasts with CCAM are discussed for the model run of 3 December 2004 that was initialized at 00Z. A four-day forecast was produced. Variables are written out every 6 hours.

In this chapter, some of the basic fields that are used for short-term forecasting are discussed. Subjective verification is done by means of observations (SYNOP data obtained from the SAWS) and satellite imagery (METEOSAT 7 data obtained from the SAWS and the University of Dundee). Introductory statistical analysis is also done for the 500 hPa geopotential height. NCEP Reanalysis data was used as the observational data set.

7.3.1 The synoptic weather pattern as simulated by C-CAM (C100 resolution) where the model output is written at 0.3º resolution for the 3 December 2004 00Z run

7.3.1.1 Introduction

The weather system responsible for the rain event of 3 to 6 December 2004 over southern Africa is called a tropical-temperate trough. Tropical temperate troughs are responsible for about 80% of the rainfall that falls over the summer rainfall region of South Africa (Harrison, 1984). They occur when a tropical and mid-latitude trough connects, resulting in the development of a rain bringing cloud band that extends from Tropical Africa southwards over Angola, Namibia and Botswana to the western parts of South Africa. The connection between the tropics and the mid-latitude system, usually a cold front with good upper air support, is established over a few days. This usually happens when the mid-latitude system nears South Africa. The upper air trough that moves in over South Africa contributes to the southward flow of moist tropical air. As the mid-latitude system propagates eastward the cloud band follows until it exits South Africa.

7.3.1.2 Description of the synoptic weather pattern as simulated by C-CAM and subjective verification by means of satellite imagery

The mean sea level pressure (MSLP) and the height of the 500 hPa pressure field as simulated for 1200z on the 3rd, 4th, 5th and 6th of December 2004 are described in this Section. The satellite imagery is then utilized to verify the position of the most prominent synoptic scale features subjectively. These prominent synoptic scale features are in this case the cold front and the cloud band.

On Friday, 3 December 2004 a cold front was situated west to southwest of southern Africa while convective cloud occurred over the northern parts of South Africa extending further northwards into central Africa (Figure 7.2). C-CAM's simulation of the MSLP for the corresponding time (Figure 7.1) showed a frontal system west to southwest of southern Africa as well as a surface trough over central South Africa that extended northwards over Botswana and Namibia to central Africa. The position of the cold front and upper air trough (Figure 7.9) as simulated by C-CAM corresponds well to the position seen on the satellite image. The surface trough (Figure 7.1) reflects the true western boundary of the convective cloud development over South Africa (Figure 7.2) very satisfactorily.

The frontal system and upper air trough moved closer to southern Africa on Saturday the 4th of December 2004 (Figures 7.3 and 7.10). The surface trough intensified and is very prominent over the western to central parts of southern Africa (Figure 7.3). This corresponds very well with the satellite image (Figure 7.4). A good defined cloud band is now clearly seen. The C-CAM simulated position of the cold front corresponds very well with the position seen on the satellite image.

A second frontal system can be seen on Sunday, 5 December 2004 while the main frontal system is situated just west of South Africa (Figures 7.5 and 7.6). Both these systems are well captured by C-CAM. However, the vortex of the second system is simulated further southwards than seen on the satellite image. It is possible that there is a slight misinterpretation of the position of the vortex on the satellite image due to the curvature of the Earth. The presence of the second frontal system is reflected in the upper air as well (Figure 7.11). The surface trough that extends southwards from central Africa to form a connection with the main frontal system has shifted eastwards. The cloud band with embedded convective activity shifted accordingly (Figure 7.6).

On Monday, 6 December 2004, the upper air trough (Figure 7.12) started to move in over South Africa while the surface trough extended eastwards (Figure 7.7). As a consequence, the cloud band moved eastwards as well (Figure 7.8). Convective activity took place over most of the eastern and southeastern parts of South Africa. The initial cold front was situated south east of the land (Figure 7.8), extending its tail along the southern coastal belt. The C-CAM simulation of this front indicated that it had not made landfall yet in comparison to the satellite image. It can therefore be assumed that the 'timing' of the front was out by a few hours. However, considering that this model prognosis is the fourth day of this specific model run, it performed satisfactorily.

7.3.1.3 The jet stream

An important feature in short-term weather forecasting is the jet stream. A jet stream is a region of locally concentrated fast moving air. It occurs in regions of strong horizontal temperature gradient and near the top of the troposphere. For this weather event it was found that the jet stream occurred at approximately 300 hPa. Per definition, this stream of air must exceed 80 KT to qualify as a jet stream. During this weather event of 3 to 6 December 2004 this criteria was met once according to C-CAM (Figure 7.13). This was on the 3rd of December 2004. Jet streams can be identified on satellite imagery. A distinct characteristic of a jet stream that is associated with a mid-latitude frontal system is a cloud formation with a sharp poleward edge. This is seen on the infrared satellite image of 3 December 2004 1200z (Figure 7.14). During the remainder of this weather event the poleward edge of the cloud associated with the frontal system became more diffused (Figures 7.4, 7.6 and 7.8). This is an indication that the wind strength decreased. This was simulated by C-CAM as well. The position of the core of maximum winds as simulated by C-CAM and the position of the poleward edge of the cloud associated with the frontal system compared very well during this weather event.

7.3.1.4 Description of the rainfall pattern as simulated by C-CAM

The rainfall pattern that occurred during this rain event is described in this Section. A quantitative verification of the rainfall totals or the rainfall pattern will not be attempted here since the rainfall data that is suitable for research purposes was not available yet. However, rainfall Figures of some SYNOP stations have been obtained for the 6th of December. A qualitative verification of the simulated rainfall for the 6th of December is done in Section 7.3.2.2

As the cold front neared southern Africa the cloud band over continental southern Africa intensified and moved southwards until it exited South Africa over the southern coastal areas. The cloud band then moves eastwards in association with the movement of the cold front (see Figuress 7.2, 7.4, 7.6, 7.8). By visual inspection of the daily rainfall (Figures 7.15, 7.16, 7.17 and 7.18) it is observed that the typical rainfall pattern associated with tropical-temperature troughs is captured well. The rain band associated with the cold front is captured as well as the southward propagation of the rain band over central Africa until these two rain bands merge to move further eastwards into the Indian Ocean.

7.3.2 C-CAM model fields (C100 resolution) where the model output is written at 0.15º resolution

7.3.2.1 Introduction

The goal of this Section is merely to show some of the C-CAM forecasts at 15 km horizontal resolution, and to point out their potential value for operational weather forecasting. All the fields shown in this Section are for day four of the model run, that is, for 6 December 2004. High-resolution 15 km forecasts 4 days ahead are still a relatively unexplored field in numerical weather prediction. It is therefore necessary to investigate the models accuracy and reliability for high-resolution forecasts of this length in time, and much more extensive work along these lines is intended.

7.3.2.2 Low-level winds

The 10m winds for 12:00Z on December 6th can be seen in Figure 7.19. Important areas of onshore flow are simulated for the coastal areas of the

Eastern Cape and southern KwaZulu-Natal, with northeasterly winds simulated over the eastern part of the Northern Province. Westerly to northwesterly winds were simulated for most of the remainder of the country. Low-level winds are a very useful forecasting tool for thundershower development during the summer months. An area of surface convergence is seen over the southeastern part of the country. Thunderstorms did indeed develop in this area (Figure 7.25).

Qualitative comparison of the simulated 12:00Z winds for December 6th (Figure 7.19) to the observed field (Figure 7.20), reveals that there was indeed onshore flow over the Eastern Cape and southern KwaZulu-Natal coasts, with northeasterly winds over the eastern part of Limpopo Province. The observed westerly winds over the west coast and northwesterly winds over the central interior (Figure 7.20), are also well captured in the model forecast (Figure 7.19). This favorable comparison suggests that the model managed to predict low level circulation and wind flow well for the 4th day of the model integration.

7.3.2.3 Maximum screen temperature

The maximum screen temperature simulation can be seen in Figure 7.21. Cool conditions are indicated over the far western as well as the southwestern part of the country while warm to hot conditions are indicated elsewhere except over parts of KwaZulu-Natal where very hot conditions are indicated.

A qualitative comparison of the simulated maximum screen temperature to the observed maximum temperatures is done for the Western Cape (Figure 7.23), Eastern Cape (Figure 7.24) and KwaZulu-Natal (Figure 7.22). These areas were chosen since they were expected to be affected by the frontal system and a ridging high-pressure system.

Over the Western Cape C-CAM underestimated the maximum temperature over the far western areas as well as over some of the places in the northern part of the province. Along the southern coastal belt C-CAM fared well. C-CAM did not fare very well over the Eastern Cape. Observed maximum temperatures were in most instances underestimated. This could be because C-CAM simulated the movement of the cold front and ridging high-pressure system slower than it actually was. Over KwaZulu-Natal C-CAM generally performed very well. The extreme high temperatures were predicted, although their location was slightly misplaced.

7.3.2.4 Relative humidity

The simulated relative humidity fields for 500 hPa (Figure 7.27) and 850 hPa (Figure 7.28) are shown. On the 500 hPa (approximately 5000 m above sea level) field, a thin moisture band is shown over the central interior of the country. This corresponds reasonably with the cloud band seen on the infrared satellite image (Figure 7.2) for the corresponding time although it seems that the actual cloud band is somewhat to the east of the simulated moisture band.

At 850 hPa (approximately 1500 m above sea level) very moist conditions are simulated over most of the Eastern Cape and parts of the Western Cape. This abundance of low-level moisture is due to the ridging of the surface high-pressure system (Figure 7.7). This area of maximum low-level moisture corresponds very well with an area of low-level stratus clouds as seen on the visible wavelength satellite image (Figure 7.26).

Convective cloud development can be seen over the central and eastern interior on the visible wavelength satellite image while the western interior has very limited cloud development (Figure 7.26). The synoptic weather pattern favors cloud development over the central and eastern part of the country, considering the position of the surface trough (Figure 7.7). C-CAM's simulation of the low-level relative humidity for the corresponding time shows higher values of relative humidity over the western interior compared to the eastern parts of the country. At first, this seems to be the wrong way around considering the cloud development as seen on the satellite image. However, this might be explained by the presence of the cloud band and rainfall over the western parts of the country the previous days.

The lowest simulated values of relative humidity are seen over KwaZulu-Natal (Figure 7.28). This area has very little cloud as seen on the visible satellite image (Figure 7.26).

7.3.2.5 Rainfall pattern

The simulated rainfall totals for December 6th are shown in Fig 7.29. Rainfall was predicted to occur in a band stretching from Namibia and Botswana over the central interior of South Africa to the eastern Cape. Much detail can be seen in the simulation, most importantly the higher rainfall totals simulated for the eastern Cape and southern KwaZulu-Natal. The high simulated rainfall totals south-east of Lesotho and over Limpopo show typical orographic alignments, and is the result of the high-resolution topography of the 15-km model run.

The 12:00Z infrared (Figure 7.25) and visible wavelength (Figure 7.26) satellite images show a cloud band stretching from Botswana over the central and eastern interior of South Africa to the Eastern Cape and southern KwaZulu-Natal. The positioning of the cloud band at midday suggests that there is much merit in the model forecast of accumulated rainfall for December 6th (Figure 7.29). There are big convective cells to be seen over the Eastern Cape and southern KwaZulu-Natal, which probably developed through the dynamic processes within the cloud band, while interaction with moist onshore flow was taking place.

Observed rainfall Figures (Table 7.1) have been obtained from the SAWS to aid with the qualitative verification of the simulated rainfall field (Figure 7.29). The data used are for the 24 hour period between 06:00Z on December 6th and 06:00Z on December 7th, which doesn't overlap perfectly with the period of simulated rainfall totals for December 6th. From Table 7.1 it can be seen that widespread rain occurred over much of South Africa during this period. Quite a number of stations over the central interior reported rainfall totals between 20 and 45 mm. Heavy falls of rain (> 50 mm in 24 hours) were reported by a number of stations in the Eastern Cape, as well as by a few coastal stations over the Western Cape. A comparison of Table 7.1 with Figure 7.29 reveals that the C-CAM simulated rainfall pattern for the 4th day of the model integration is quite similar to the observed pattern. However, the model underestimated rainfall totals over the central interior. The model also failed to predict the heavy falls of rain that occurred over the Eastern Cape, although the model successfully predicted these areas to be the most favorable for rainfall on December 6th. The model simulated rainfall for the south coast, but not the heavy falls that occurred at a few stations.

Place	Amount (mm)	Place	Amount (mm)
Gauteng		**North West Province**	
Carletonville	3	Mafikeng	11
Heidelberg	26	Pilanesberg	16
Irene	9	Potchefstroom	12
Johannesburg	17	Rustenburg	26
Nigel	22	Taung	5
Pretoria	7	Vryburg	4
Sandton	23	**Limpopo Province**	
Springs	5	Potgietersrus	2
Unisa	3	Warmbad	1
Vereeniging	4	**Freestate**	
Mpumalanga		Bethlehem	5
Bethal	9	Bloemfontein/Diere	47
Carolina	9	Bloemfontein	26
Delmas	2	Clarens	8
Ermelo	5	Cornelia	26
Standerton	17	Dealesville	29
North West Province		Dewetsdorp	3
Bloemhof	4	Ficksburg	3
Klerksdorp	1	Goedemoed	25
Lichtenburg	44	Heilbron	25
Northern Cape		**Free State**	
Britstown	21	Hertzogville	8
De Aar	2	Kestell	8
Hopetown	18	Kroonstad	3
Kuruman	5	Reddersburg	4
Petrusville	3	Senekal	8
Postmasburg	3	Thaba Nchu	5
Western Cape		Trompsburg	21
Beaufort-Wes	28	Vaaldam	11
Cape Columbine	1	Verkeerdevlei	6
De Rust	16	Warden	41
George	44	Winburg	8
Heidelberg	15	Zastron	28

Hermanus	4	**Eastern Cape**	
Kleinmond	11	Addo	37
Knysna	136	Alexandria	18
Ladismith	9	Aliwal-Noord	14
Langebaanweg	2	Barkly-East	11
Oudshoorn	20	Burgersdorp	31
Piketberg	2	Cape St Francis	63
Plettenberg Bay	65	Cradock	13
Riversdal	11	Dohne	45
Robertson	4	Elliot	16
Stilbaai	41	Fort Beaufort	33
Swellendam	25	Graaff-Reinet	5
Tsitsikamma	84	Grahamstown	20
Vredenburg	3	Humansdorp	118
Vyeboom	6	Jamestown	23
Worcester	1	Joubertina	43
KwaZulu-Natal		Kareedouw	50
Cedara	5	Middelburg	2
Durban	4	Oos Londen	63
Estcourt	6	Patensie	65
Giants Castle	3	Port Elizabeth	45
Greytown	17	Port St Johns	26
KwaZulu-Natal		**Eastern Cape**	
Ixopo	51	Queenstown	42
Margate	15	Uitenhage	36
Matatiele	7	Umtata	29
Mtunzini	4	Willowmore	27
Pietermaritzburg	16		
Pongola	3		
KwaZulu-Natal			
Port Edward	3		
Sezela	31		
Virginia	2		

Table 7.1: Observed rainfall figures obtained from the SAWS

7.4 SOME THOUGHTS ON THE PREDICTIVE ABILITY OF C-CAM

Some introductory statistical analysis was done on the 500 hPa geopotential heights. The 500 hPa geopotential heights are a very useful variable for weather forecasting. Once the geopotential height (any pressure level) is known, the wind, temperature and vorticity fields of that specific pressure level can be determined if hydrostatic and geostrophic balance are assumed. All of these variables are very important in weather forecasting.

In this chapter the absolute difference (|C-CAM – NCEP|) as well as the Root Mean Square Error (RMSE) is determined for the 500 hPa C-CAM prognosis over a domain covering 45ºS-10ºS and 10ºW-45ºE. NCEP Reanalysis data was used to determine this. The NCEP Reanalysis data has a resolution of 2.5ºX 2.5º, whereas the C-CAM data is written on a 0.3º grid. A bi-cubical reduction scheme was used to reduce the C-CAM data to a 2.5º grid.

The results of |C-CAM – NCEP| for the 17 integration times (00 h to 96 h) can be seen in Figures 7.30, 7.31 and 7.32. The absolute error is the smallest for the initial field used by C-CAM (t = 0, Figure 7.30). As the model integration progresses in time, larger errors enter the domain from the west (Figures 7.30, 7.31 and 7.32). This can probably be explained by the fact that the model resolution decreases progressively away from the area of interest. These errors are propagated into the area of interest by the prevailing westerly winds. This situation is similar to that which occurs using a traditional nested modeling approach, where errors of the low-resolution GCM enter the limited area model domain at the lateral boundaries. It is therefore important to determine how long these errors take to reach the area of interest. From the absolute errors shown in Figure 7.31 and from the RMSE (Figure 7.33), it can be seen that the error started to grow at t = 60 h (step 11 in Figure 7.33). More case studies are required to determine with more certainty the integration time at which errors from the low-resolution part of the domain reach the area of interest. This preliminary experiment suggests that the model simulation is relatively free of these errors for at least 2 days of integration. Thereafter, model prediction should be interpreted with more caution. It is important to mention that the model-simulated upper trough was trailing the NCEP Reanalysis field in the southern part of the domain shown. This contributed significantly to the absolute errors shown in Figures 7.31 and 7.32. In the previous Sections it was also mentioned that the satellite imagery indicates that the model rainfall field trailed the observed cloud bands in time. To which extent the slower propagating model fields are caused by systems traveling from a low to a high resolution domain still needs to be determined.

7.5 CONCLUSIONS

The mostly subjective verification of the 3 December 2004 00Z C100 C-CAM run led to the following conclusions:

- It seems that the simulated position of the cold front was lagging by a few hours behind the true position of the cold front. This was also reflected in the simulated maximum screen temperatures compared to the observed maximum temperatures.
- The simulated rainfall band was situated further west than the cloud band seen on the satellite images. Even though this comparison of simulated 24 hour accumulated rainfall to cloud development as seen on satellite images (6 hourly over the 24 hour period) was done carefully, such comparisons need to be done more objectively since cloud development does not necessarily imply that precipitation reaches the ground.
- Although the position of the simulated rainfall band was situated further west than the actual cloud band, the area of simulated precipitation was generally captured quite well during this rain event.
- A huge concern is the fact that heavy rainfall was not simulated explicitly by C-CAM on more than one occasion, e.g. on the 6th of December when heavy rainfall occurred along parts of the Eastern Cape coast.
- The RMSE of the 500 hPa geopotential heights suggests that the model simulation is relatively free of errors (|C-CAM - NCEP|) for at least 2 days of integration time.
- This preliminary study shows that although there is still work that needs to be done to improve the present C100 C-CAM forecasting system for southern Africa, it is very useful for short-range weather forecasting over southern Africa.

The C100 C-CAM forecasting system has been utilized to do short-term weather forecasts (four-day precipitation forecasts) from 1 December 2004 to 13

December 2004 on nearly a daily basis at the University of Pretoria. The model fields that were utilized to produce these forecasts were: mean sea level pressure, 700 hPa heights and winds, 500 hPa heights and winds, 300 hPa heights and winds, maximum screen temperature and relative humidity (850 hPa, 700 hPa and 500 hPa). Initially some of the fields were very noisy, but this problem was reduced by using a model time-step of 5 minutes instead of 10 minutes as used initially. Generally, the precipitation forecasts that were produced from these fields captured the areas of cloud development and possible precipitation very well.

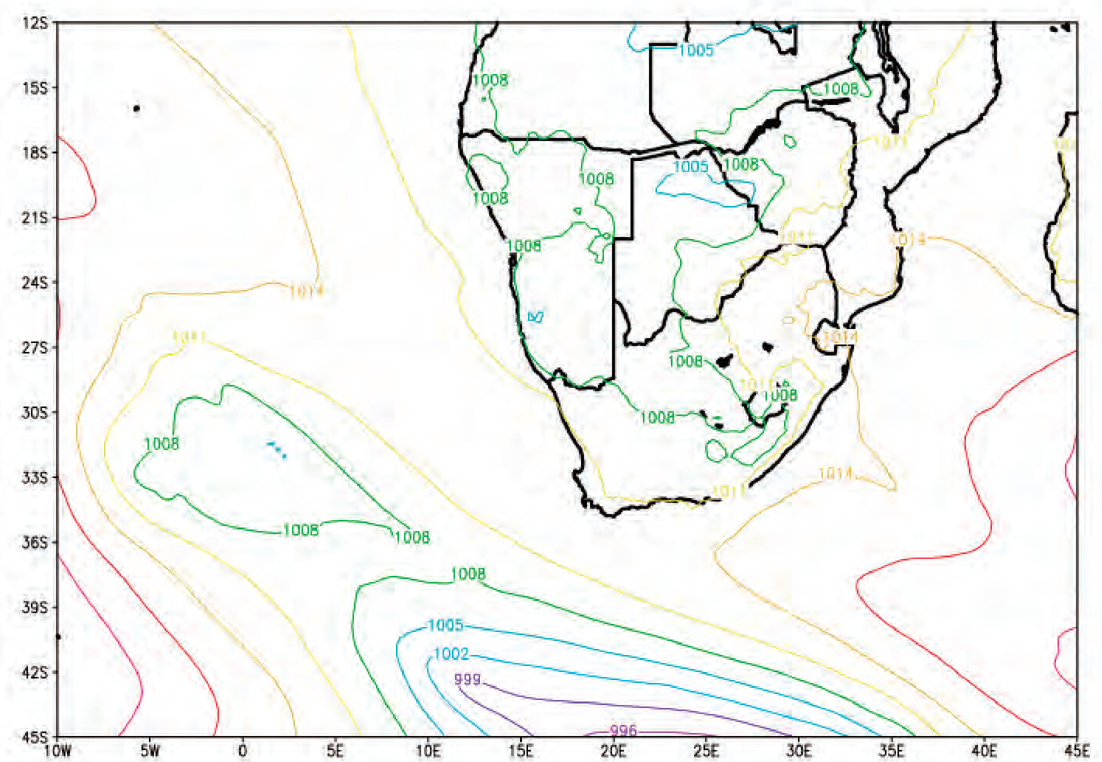

Figure 7.1 Mean Sea Level Pressure (MSLP), 3 December 2004 1200Z

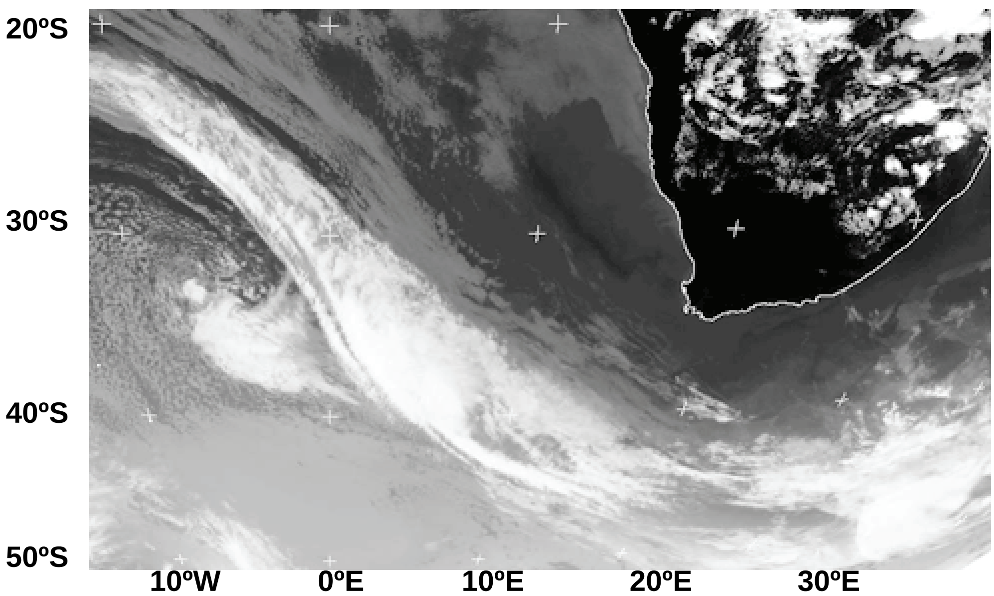

Figure 7.2 Infrared Satellite image (copyright 2004 EUMETSAT), 3 December 2004 1200Z

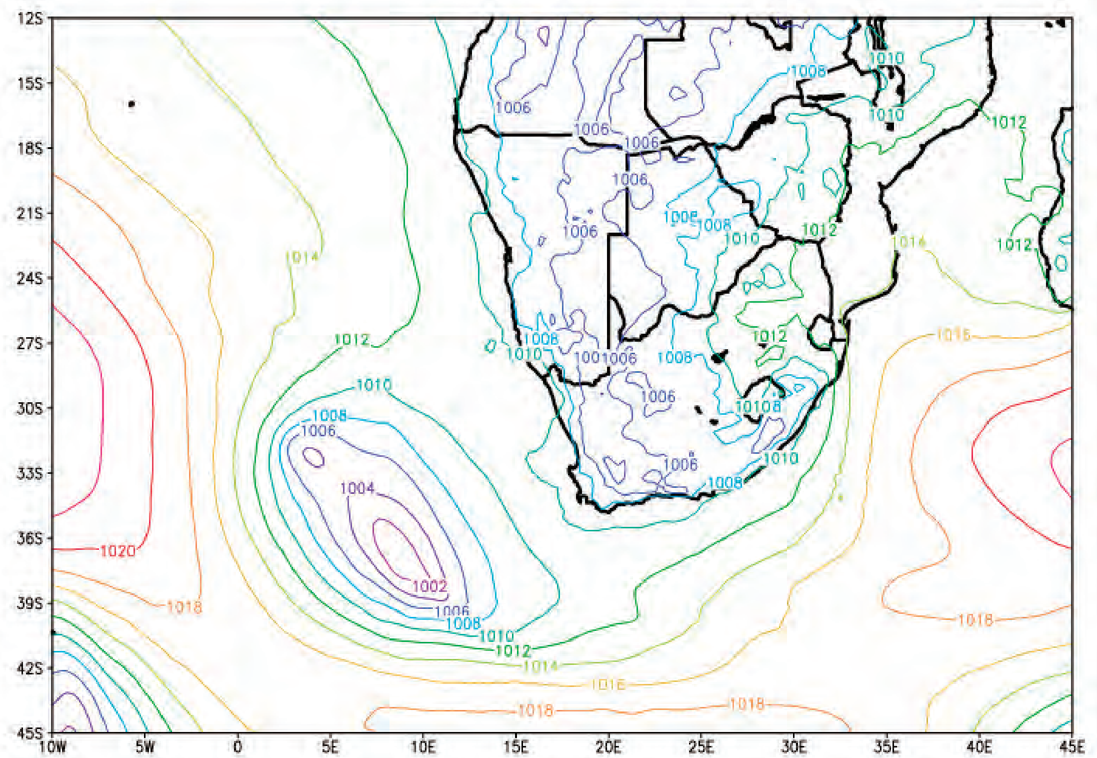

Figure 7.3 Mean Sea Level Pressure (MSLP), 4 December 2004 1200Z

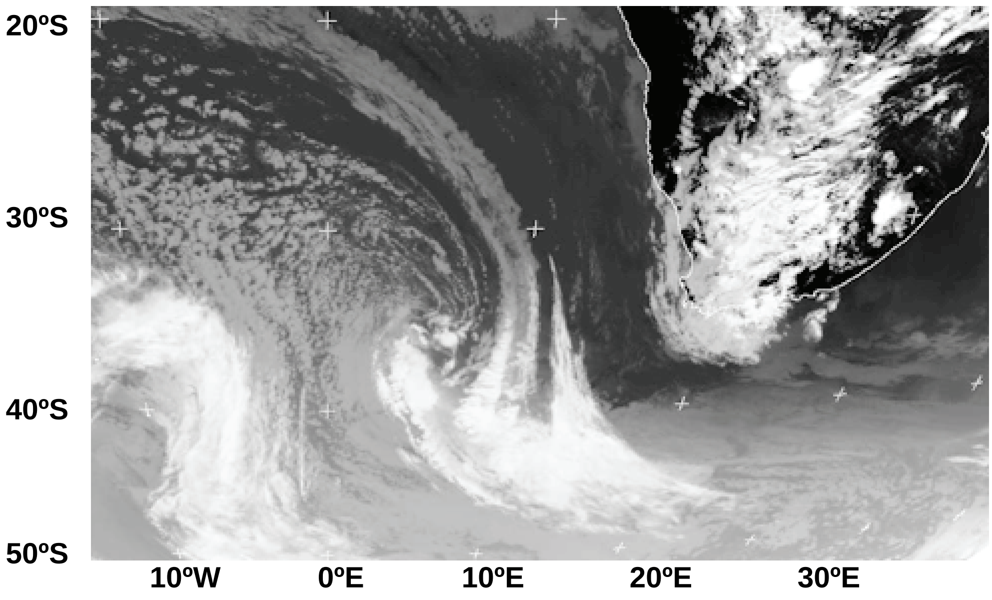

Figure 7.4 Infrared Satellite image (copyright 2004 EUMETSAT), 4 December 2004 1200Z

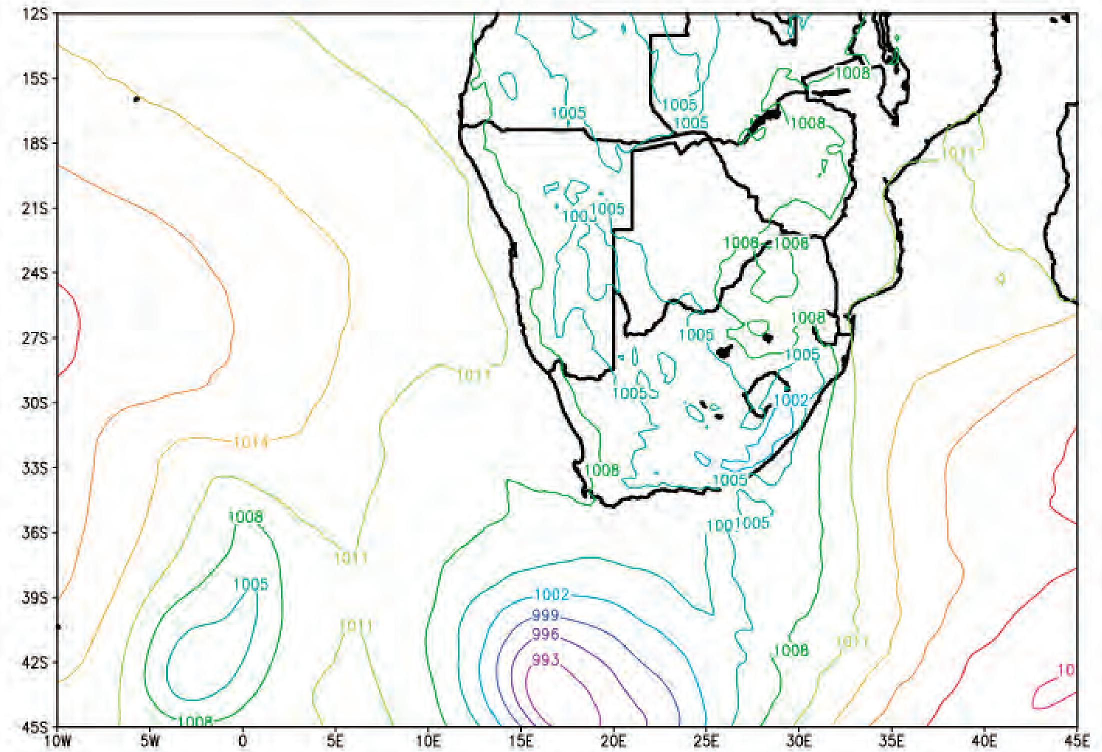

Figure 7.5 Mean Sea Level Pressure (MSLP), 5 December 2004 1200Z

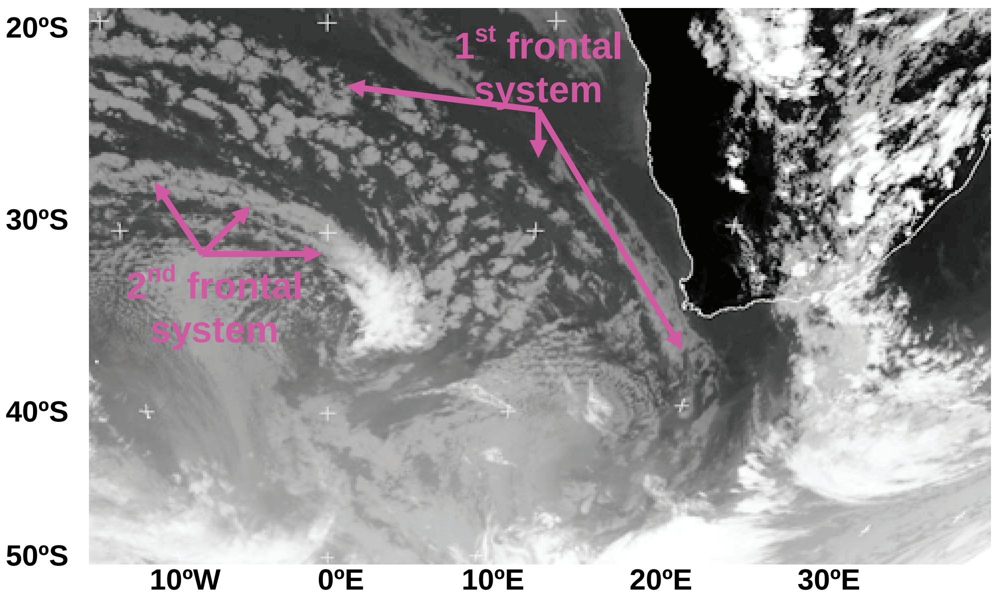

Figure 7.6 Infrared Satellite image (copyright 2004 EUMETSAT), 5 December 2004 1200Z

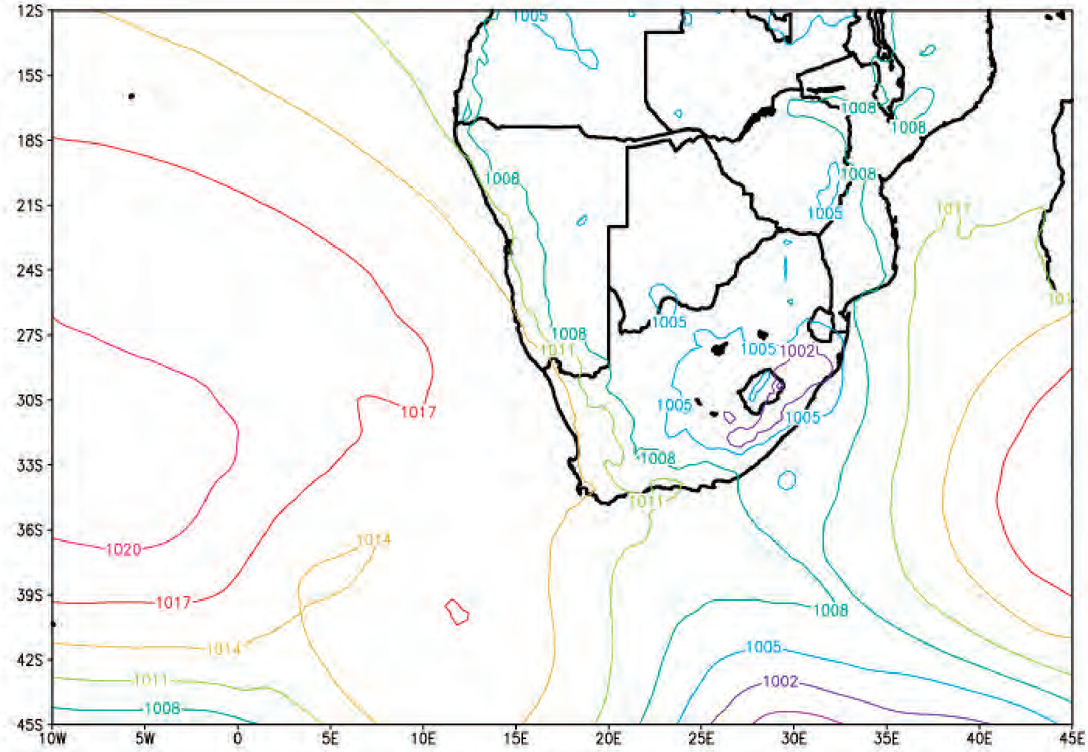

Figure 7.7 Mean Sea Level Pressure (MSLP), 6 December 2004 1200Z

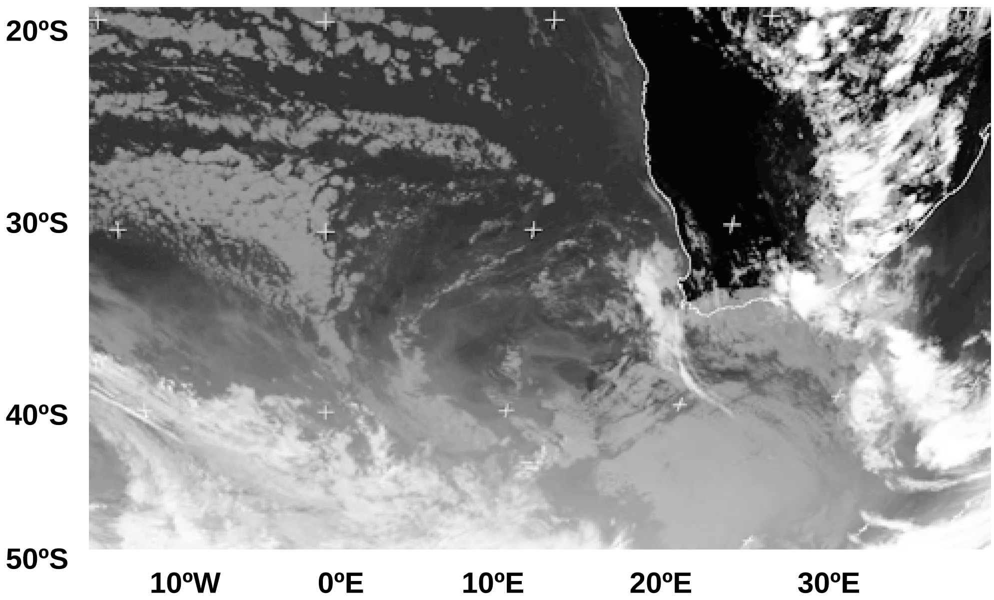

Figure 7.8 Infrared Satellite image (copyright 2004 EUMETSAT), 6 December 2004 1200Z

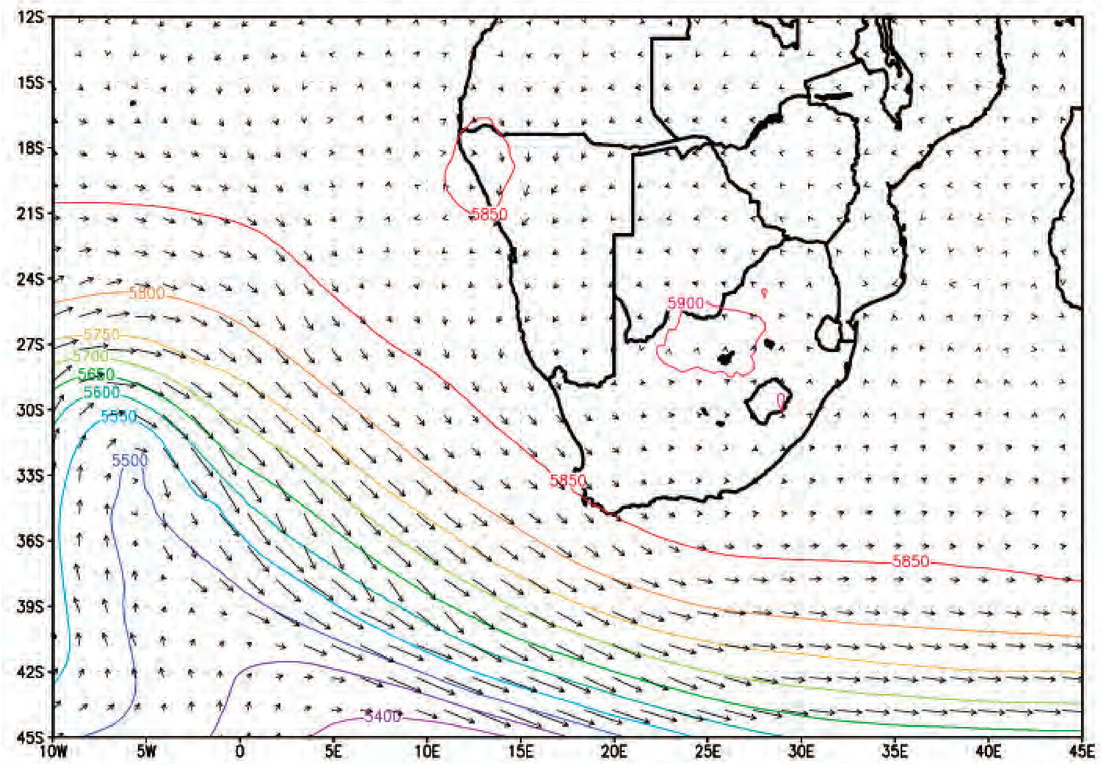

Figure 7.9 500 hPa heights, 3 December 2004 1200Z

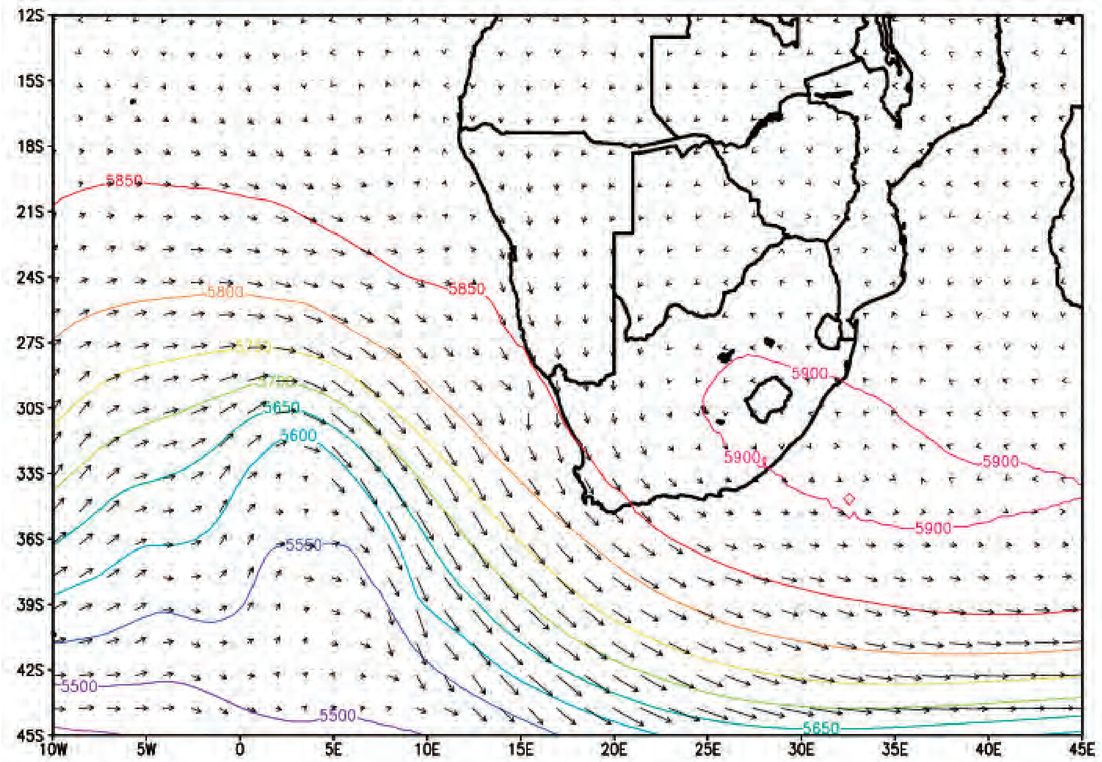

Figure 7.10 500 hPa heights, 4 December 2004 1200Z

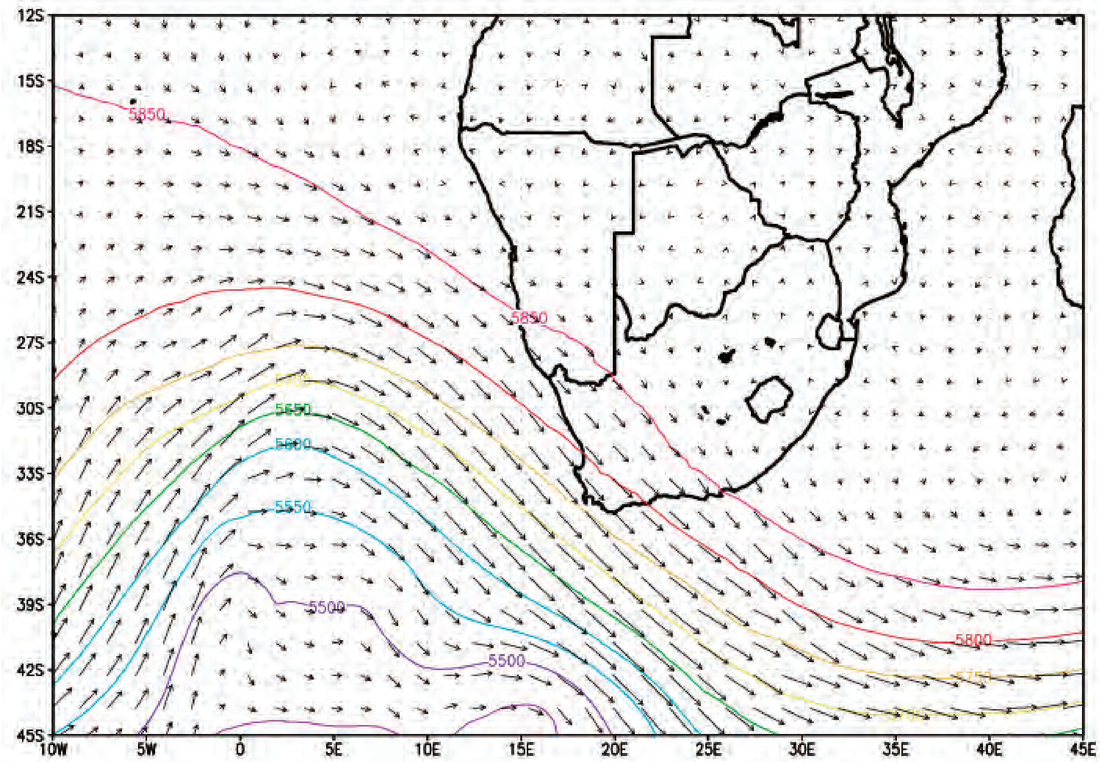

Figure 7.11 500 hPa heights, 5 December 2004 1200Z

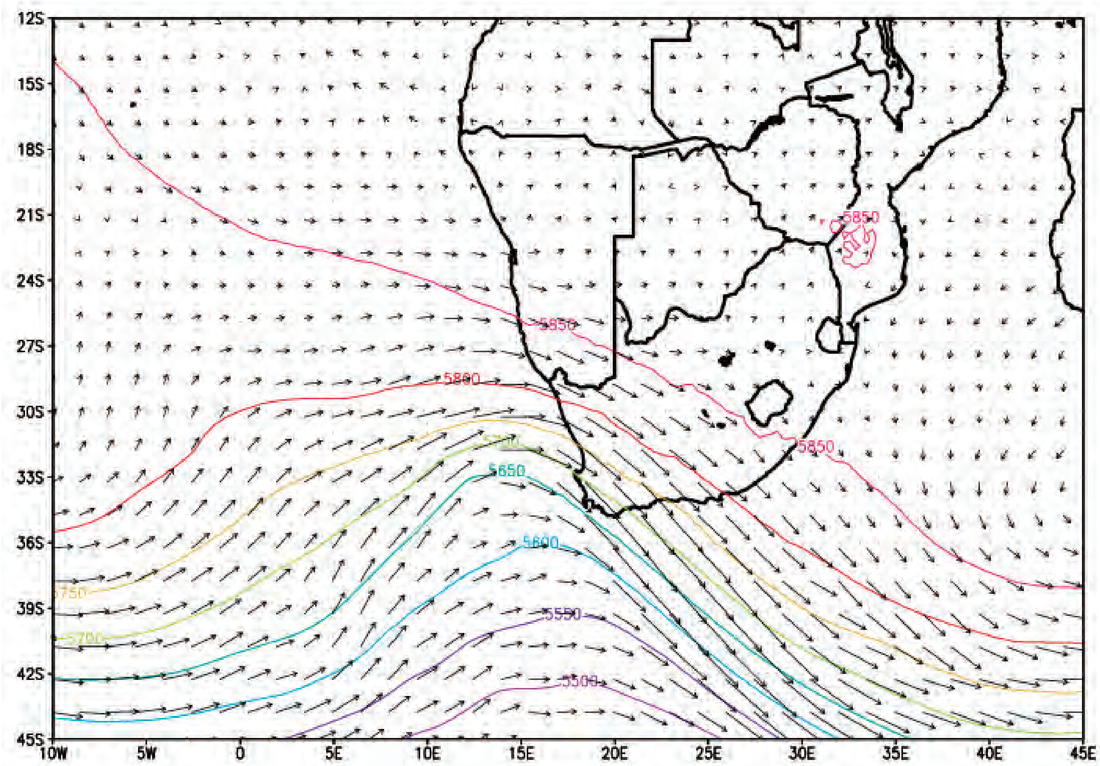

Figure 7.12 500 hPa heights, 6 December 2004 1200Z

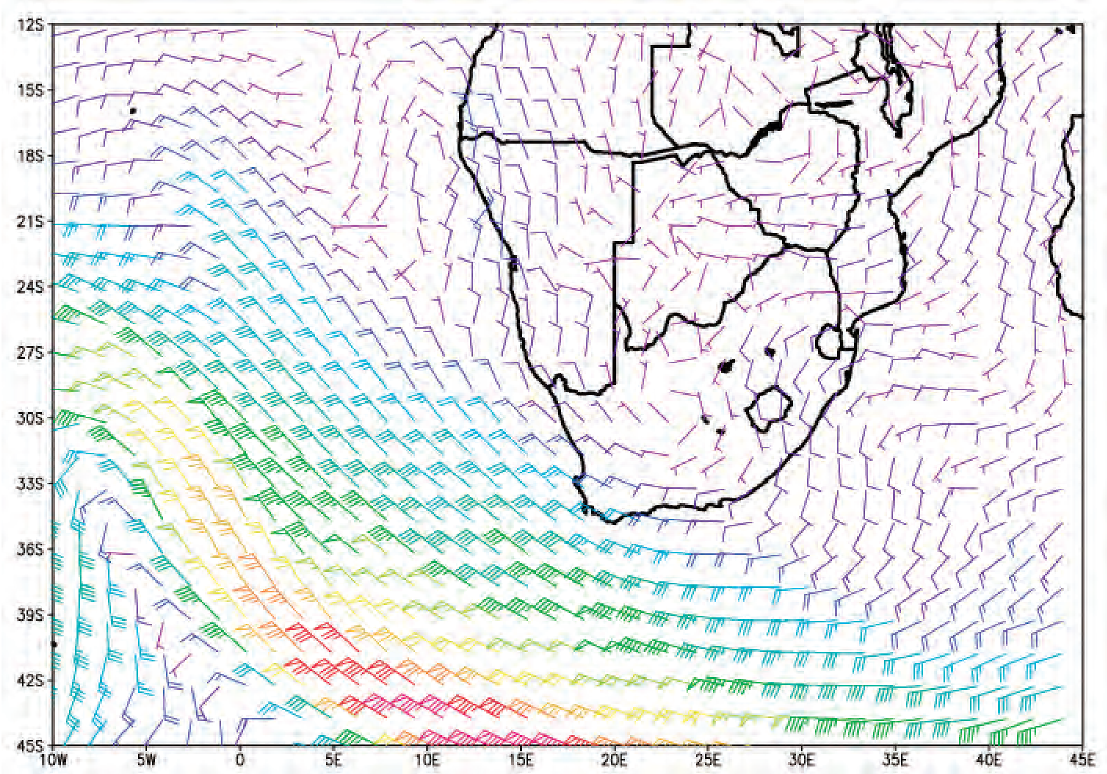

Figure 7.13 300 hPa winds, 3 December 2004 1200Z

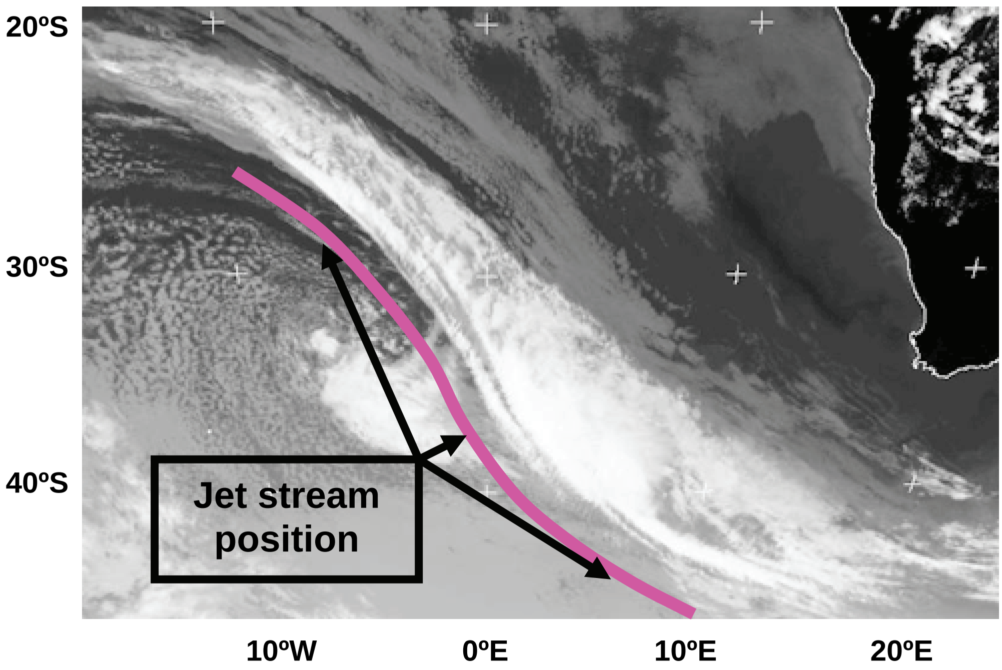

Figure 7.14 Infrared satellite image (copyright 2004 EUMETSAT), 3 December 2004 1200Z

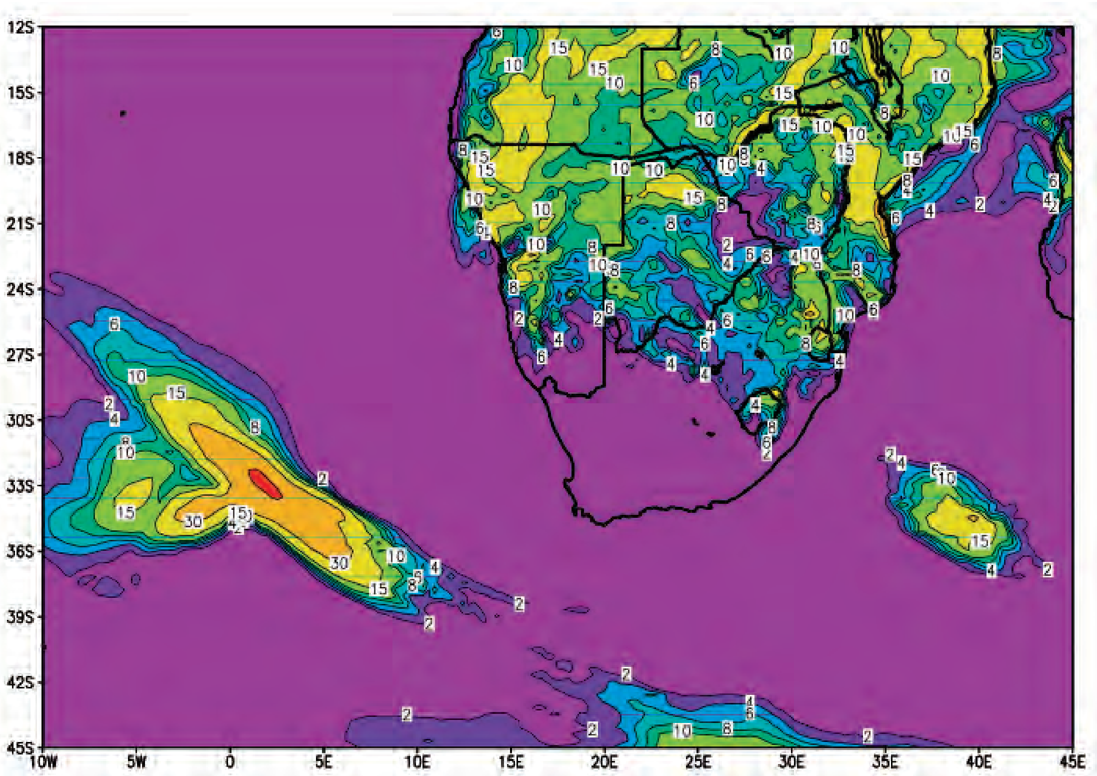

Figure 7.15 Accumulated rainfall, 3 December 2004

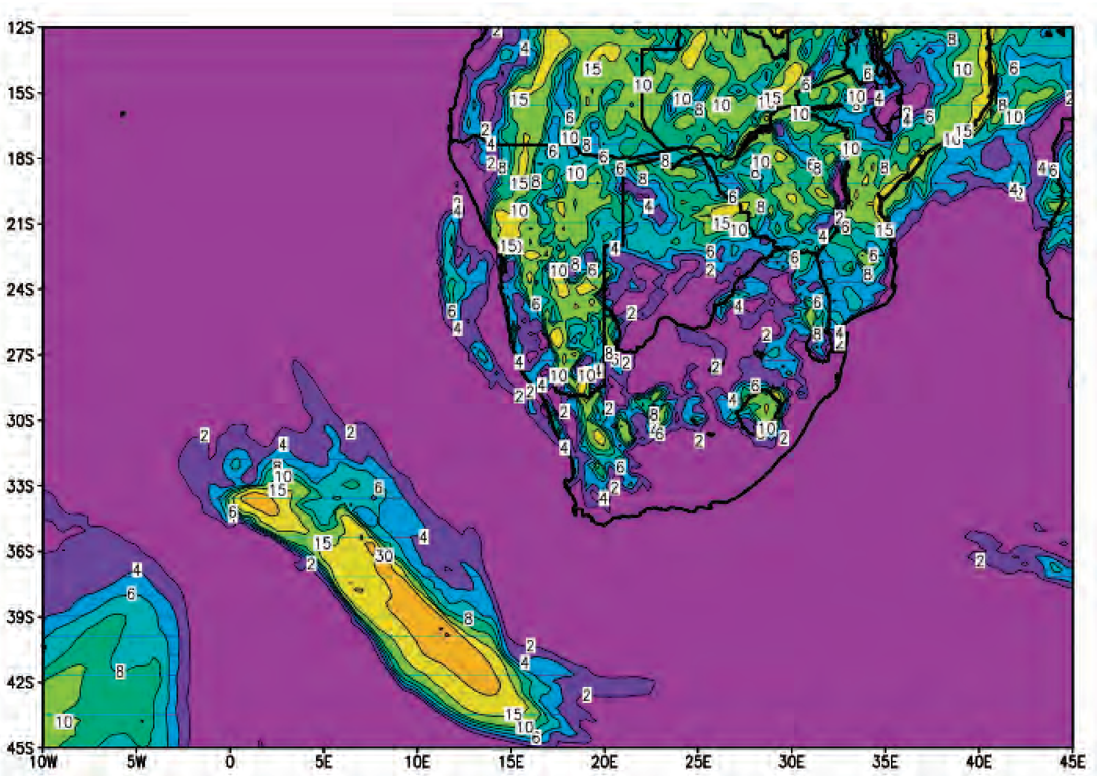

Figure 7.16 Accumulated rainfall, 4 December 2004

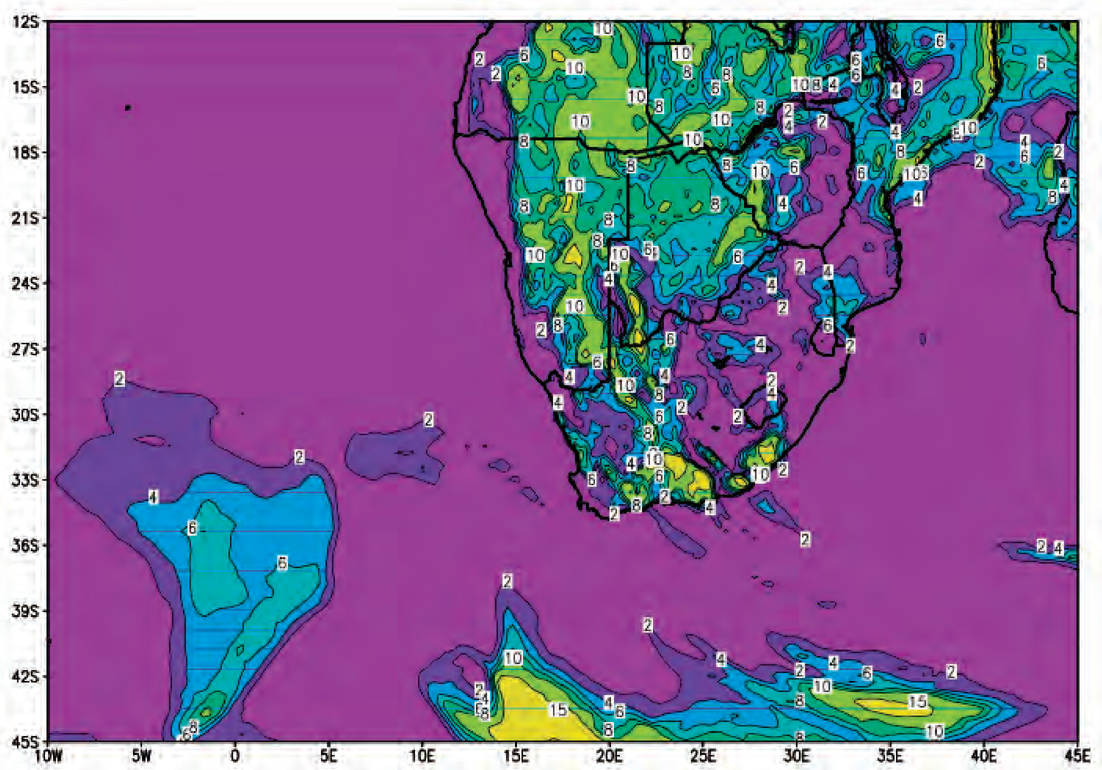

Figure 7.17 Accumulated rainfall, 5 December 2004

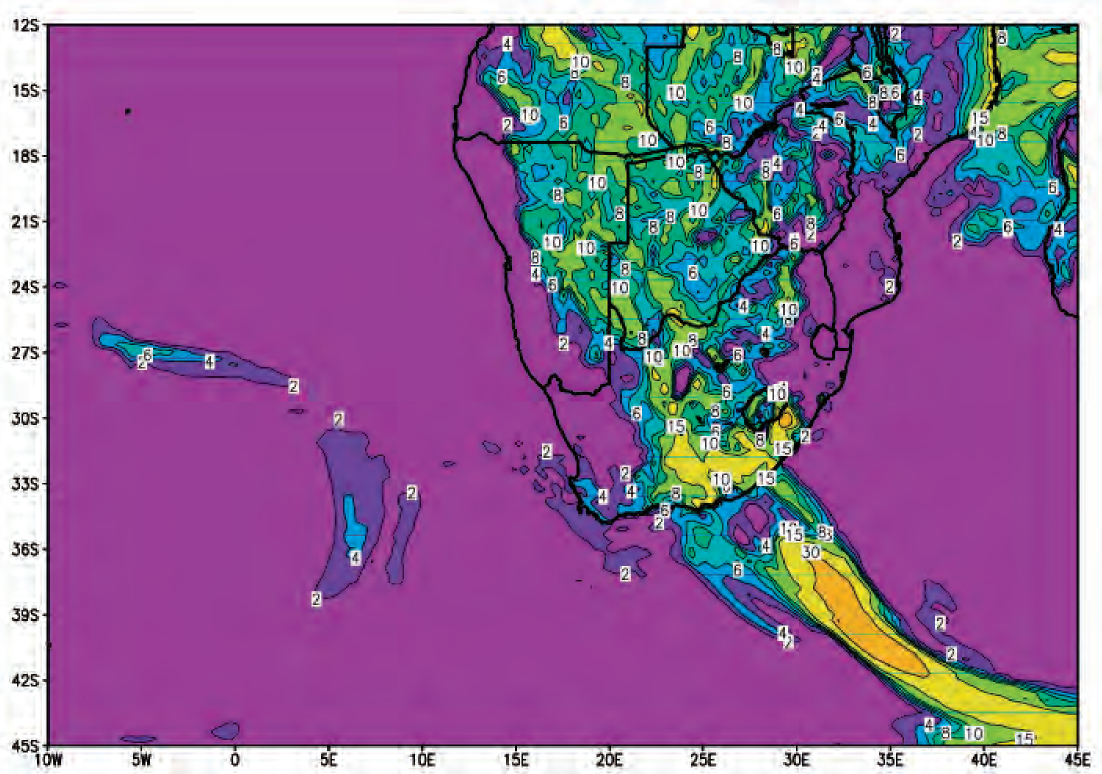

Figure 7.18 Accumulated rainfall, 6 December 2004

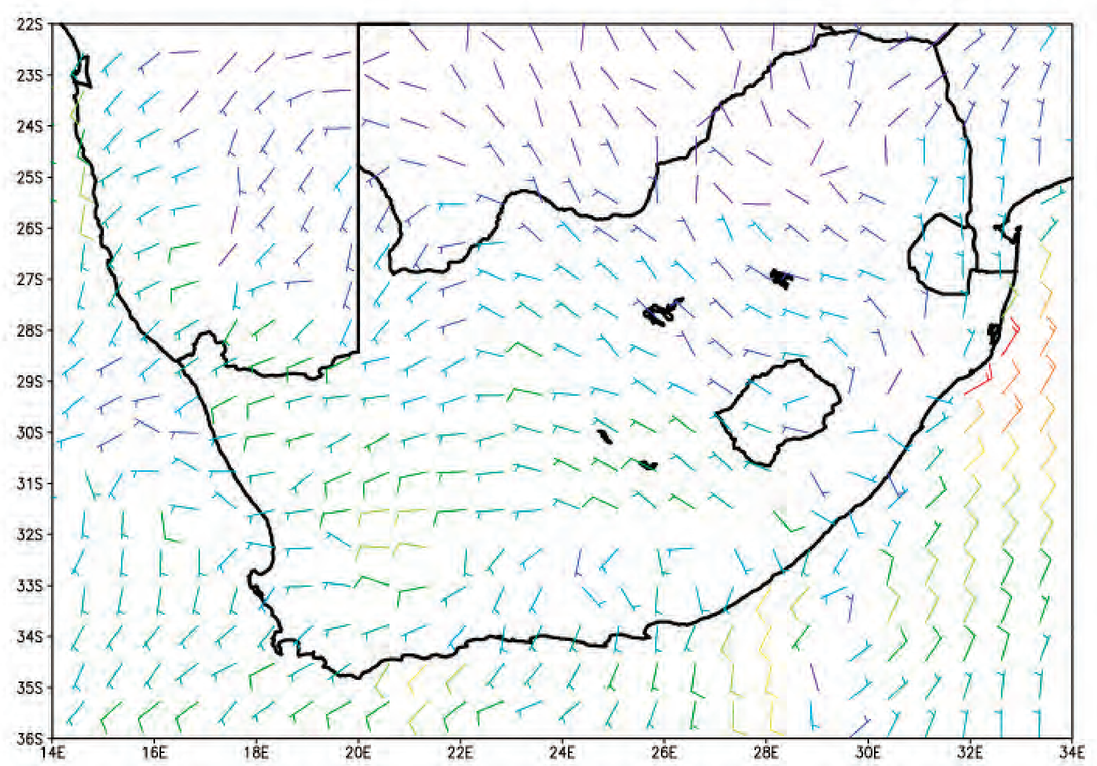

Figure 7.19 10m wind, 6 December 2004 1200Z

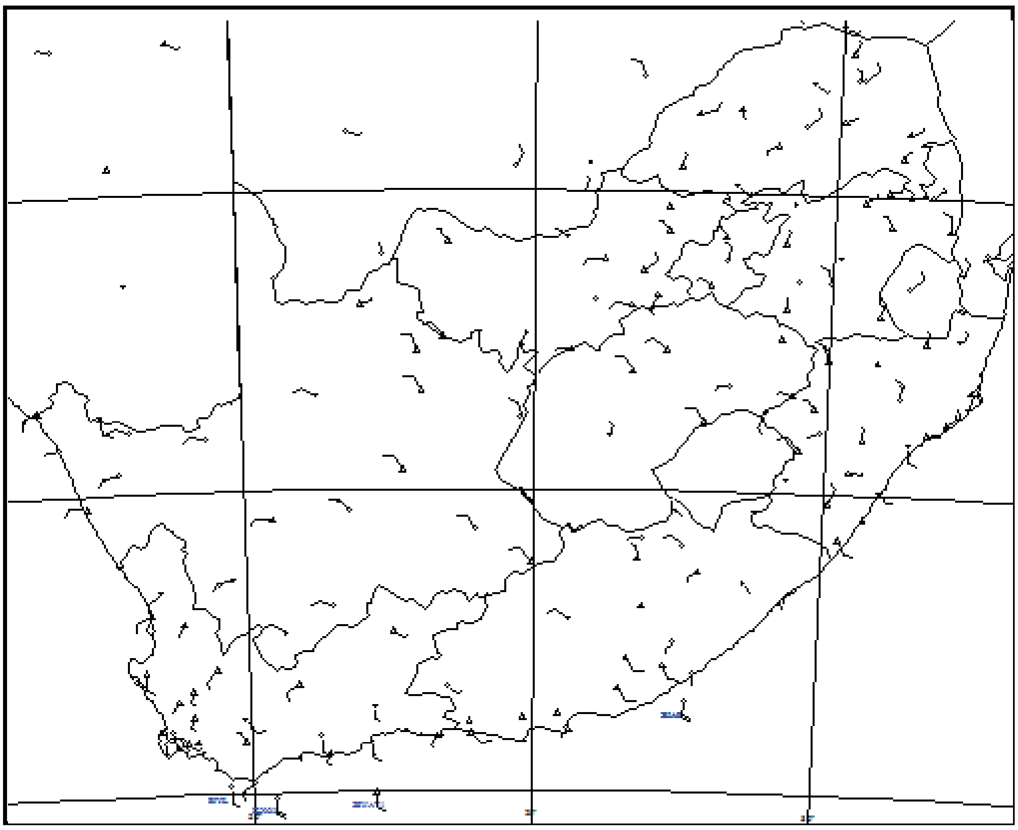

Figure 7.20 Surface wind observations obtained from the South African Weather Service valid at 6 December 2004 1200Z

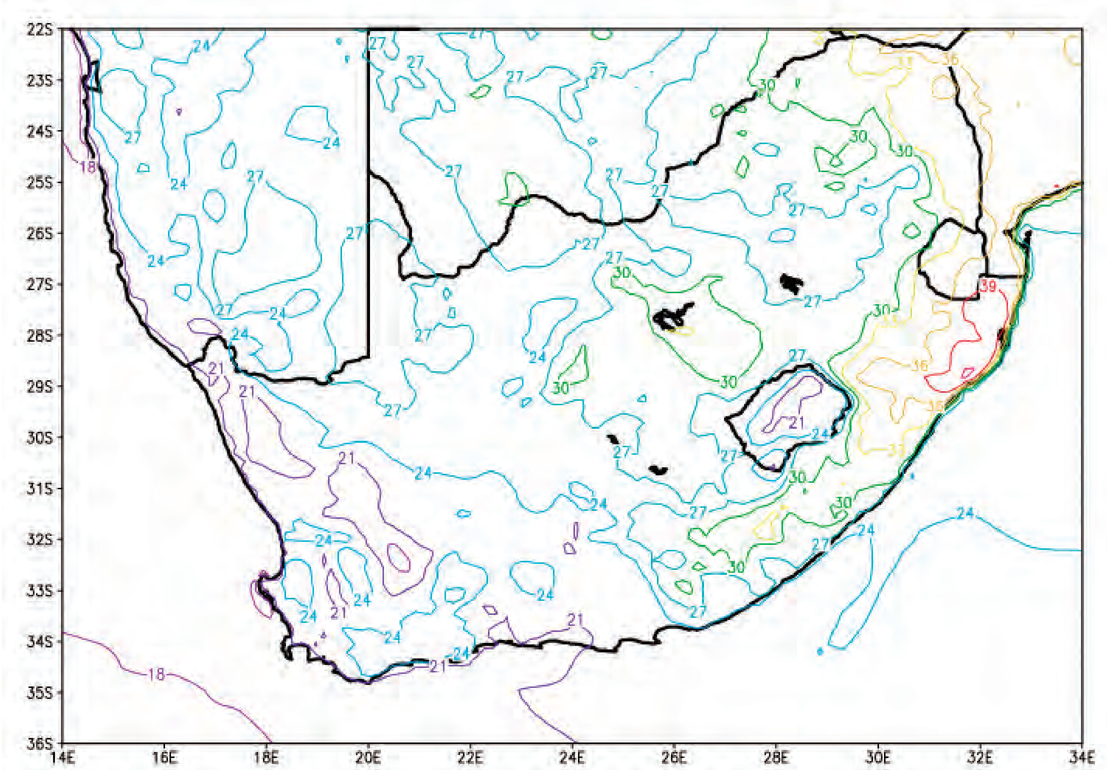

Figure 7.21 Maximum screen temperature, 6 December 2004

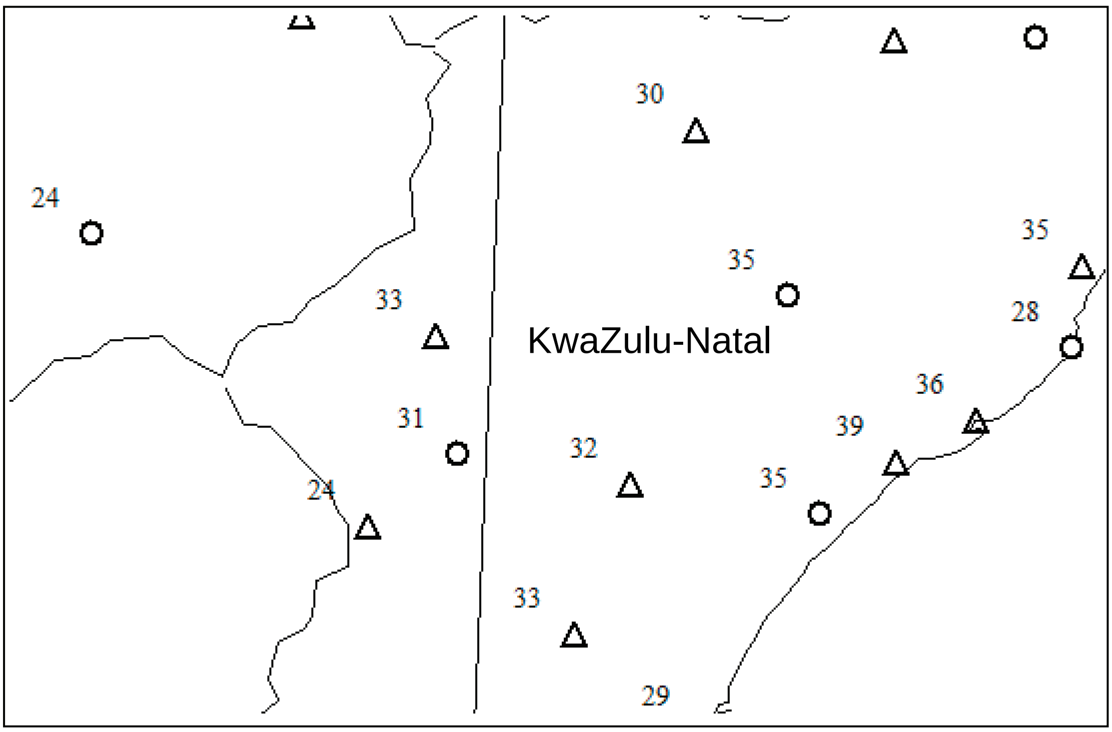

Figure 7.22 Observed maximum surface temperature, 6 December 2004

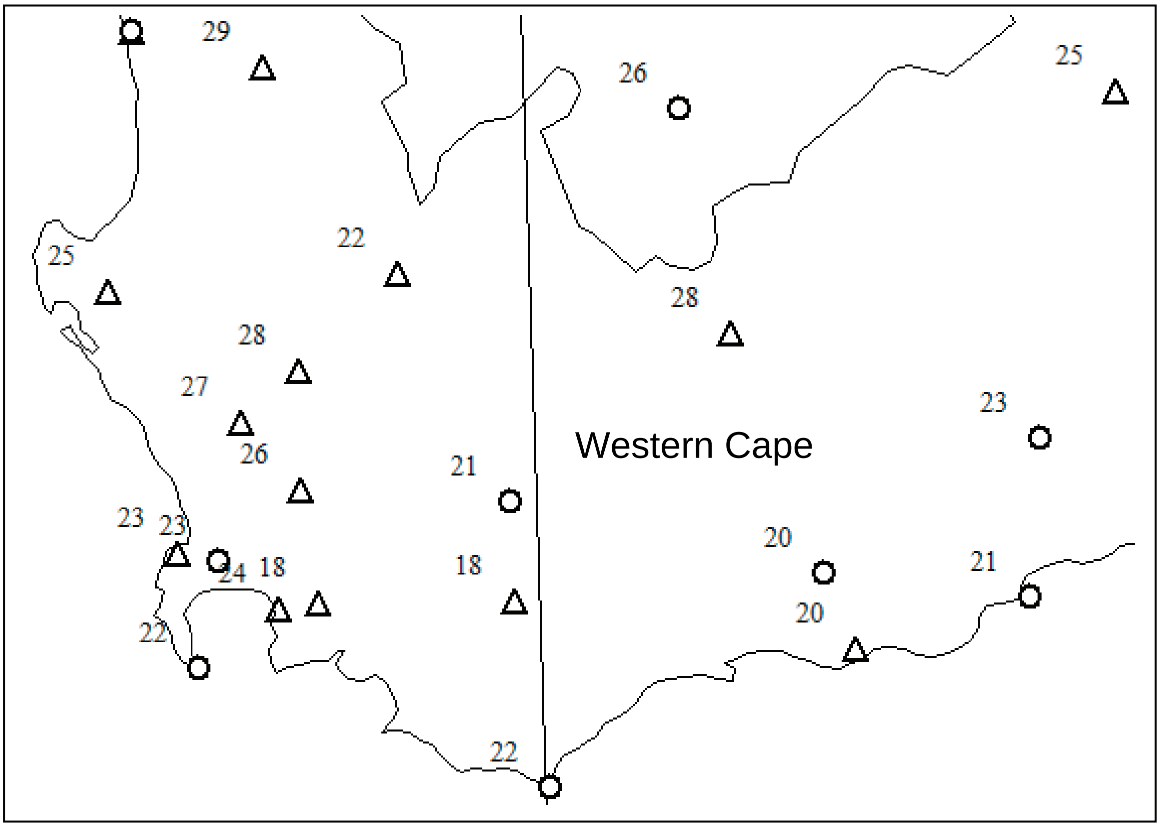

Figure 7.23 Observed maximum surface temperature, 6 December 2004

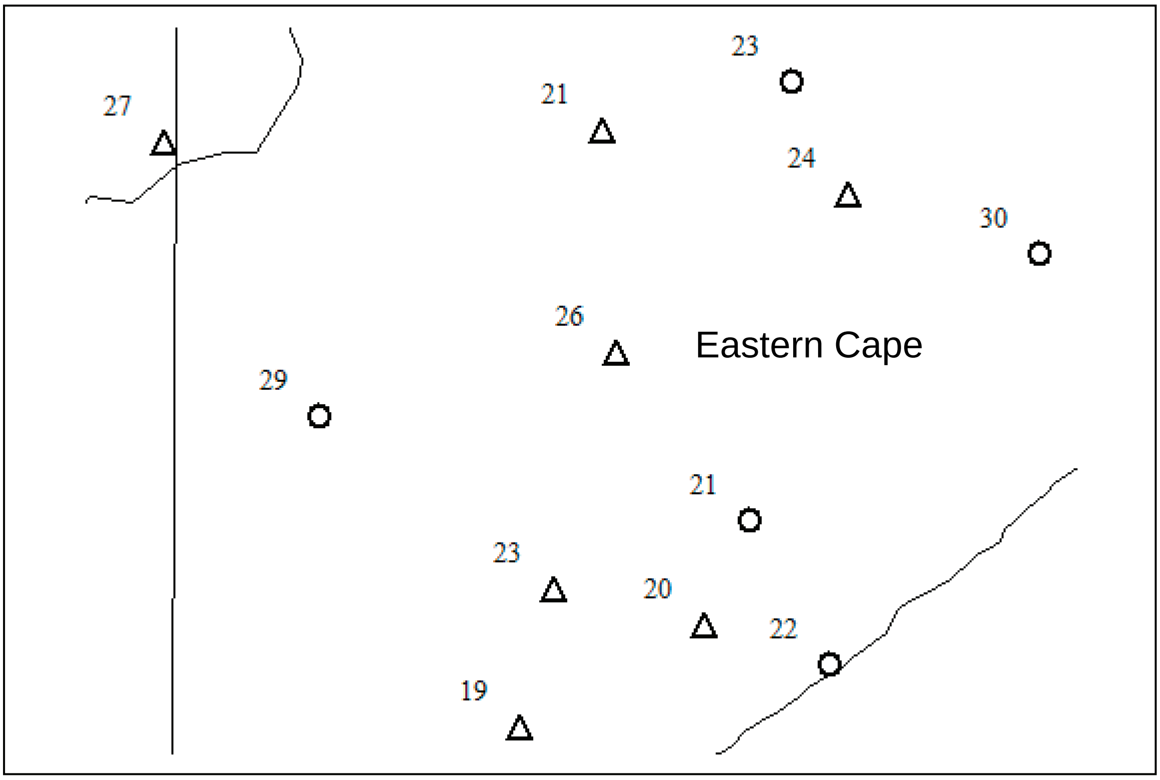

Figure 7.24 Observed maximum surface temperature, 6 December 2004

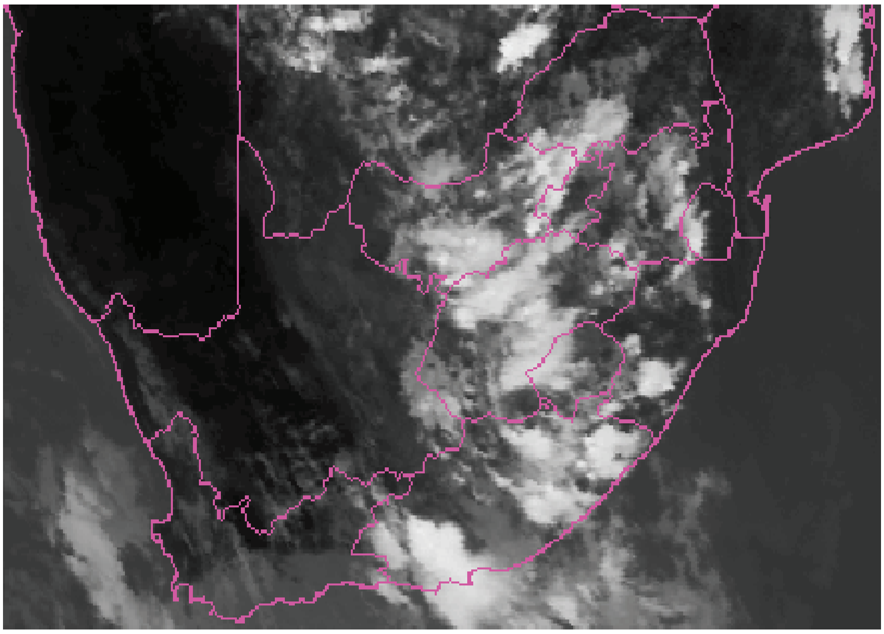

Figure 7.25 Infrared satellite image (copyright 2004 EUMETSAT), 6 December 2004 1200Z

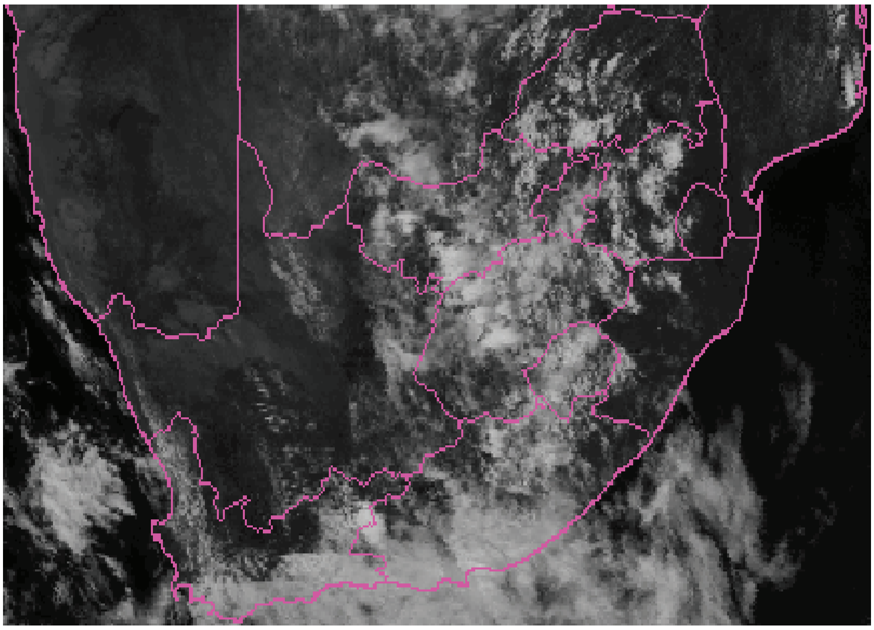

Figure 7.26 Visible satellite image (copyright 2004 EUMETSAT), 6 December 2004 1200Z

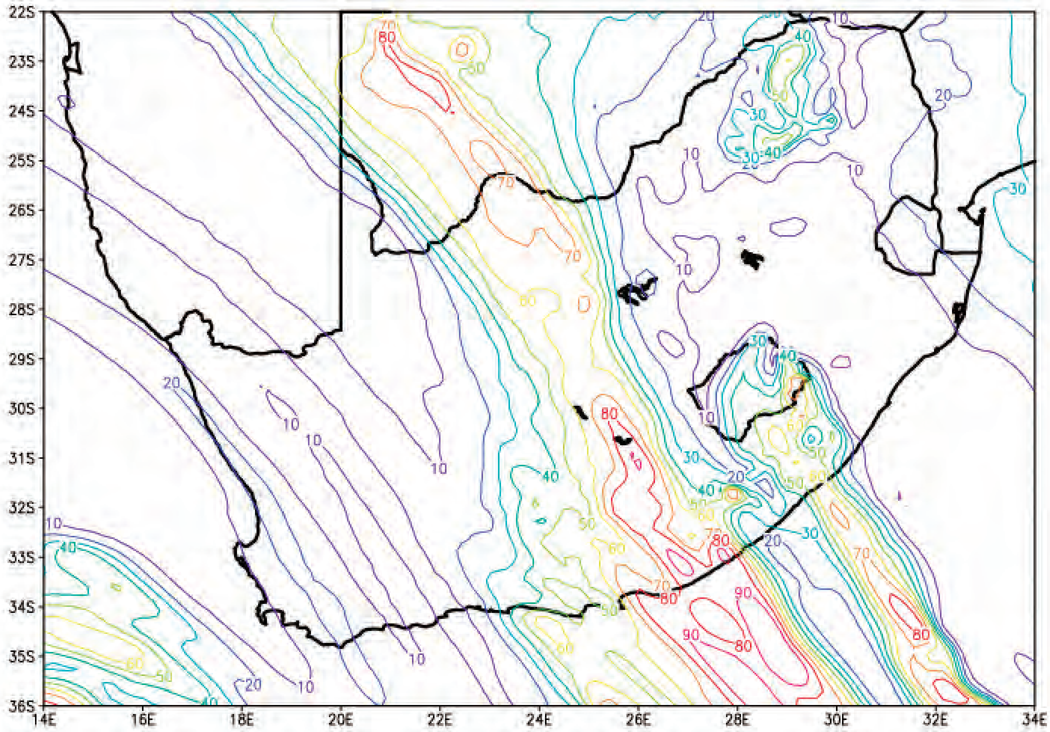

Figure 7.27 500 hPa relative humidity, 6 December 2004 1200Z

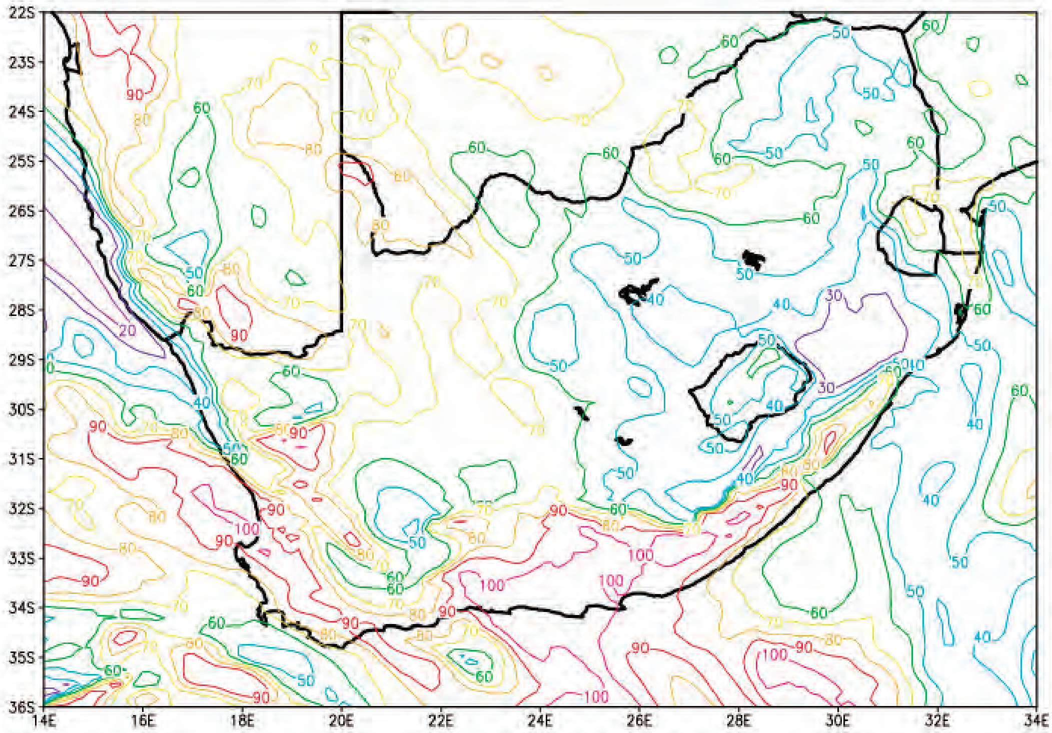

Figure 7.28 850 hPa relative humidity, 6 December 2004 1200Z

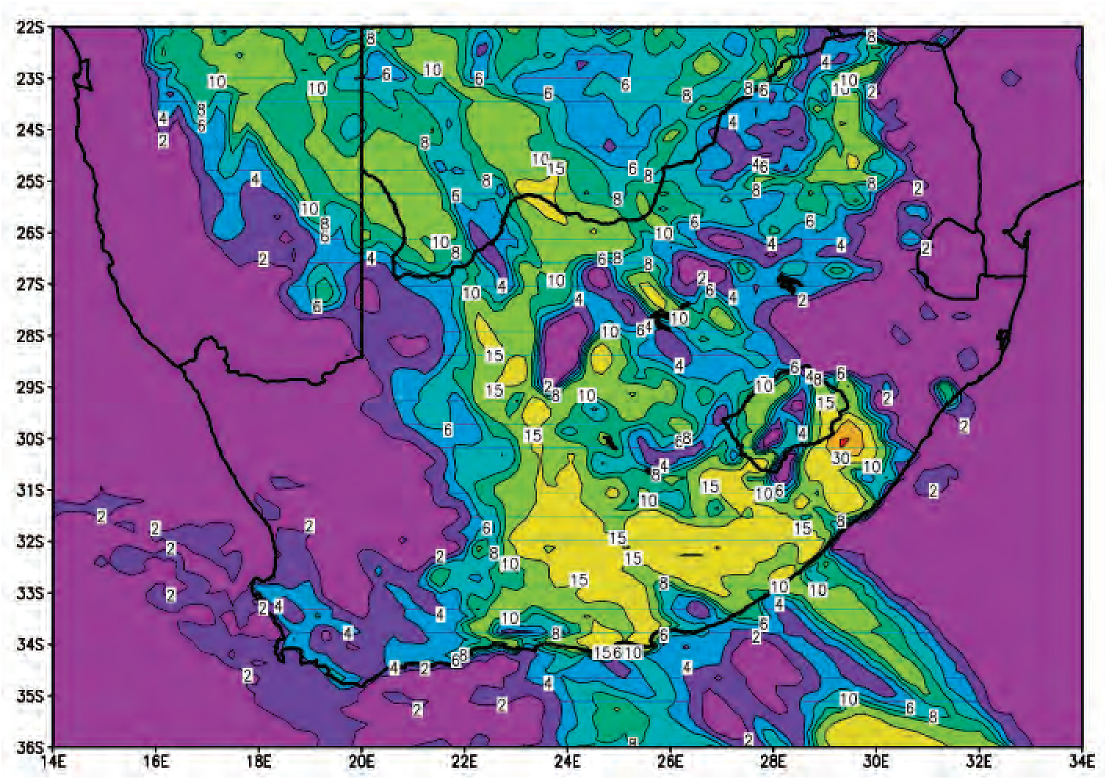

Figure 7.29 Accumulated rainfall, 6 December 2004

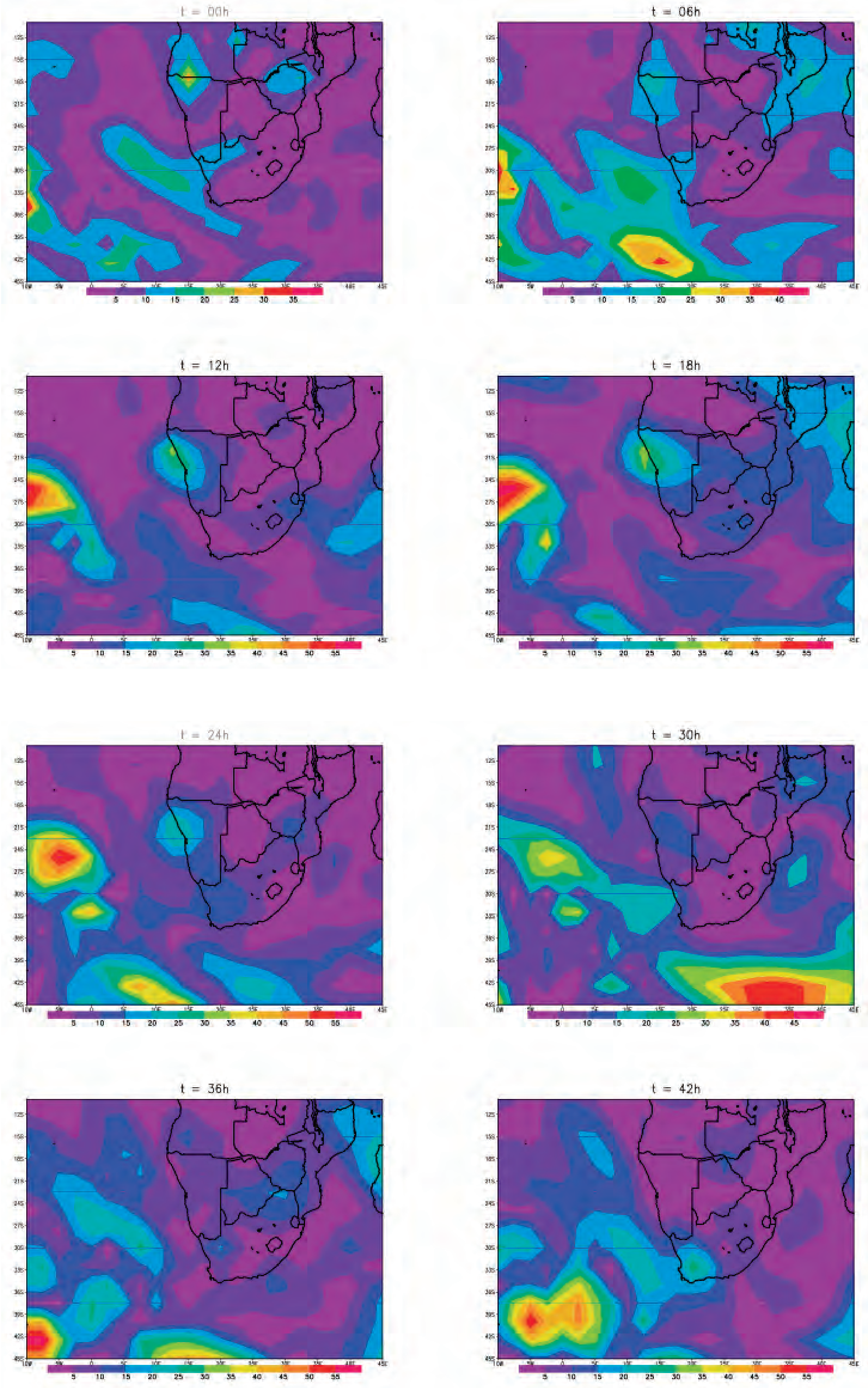

Figure 7.30 Absolute difference of 500 hPa, C-CAM – NCEP for t = 00 h to t = 42 h

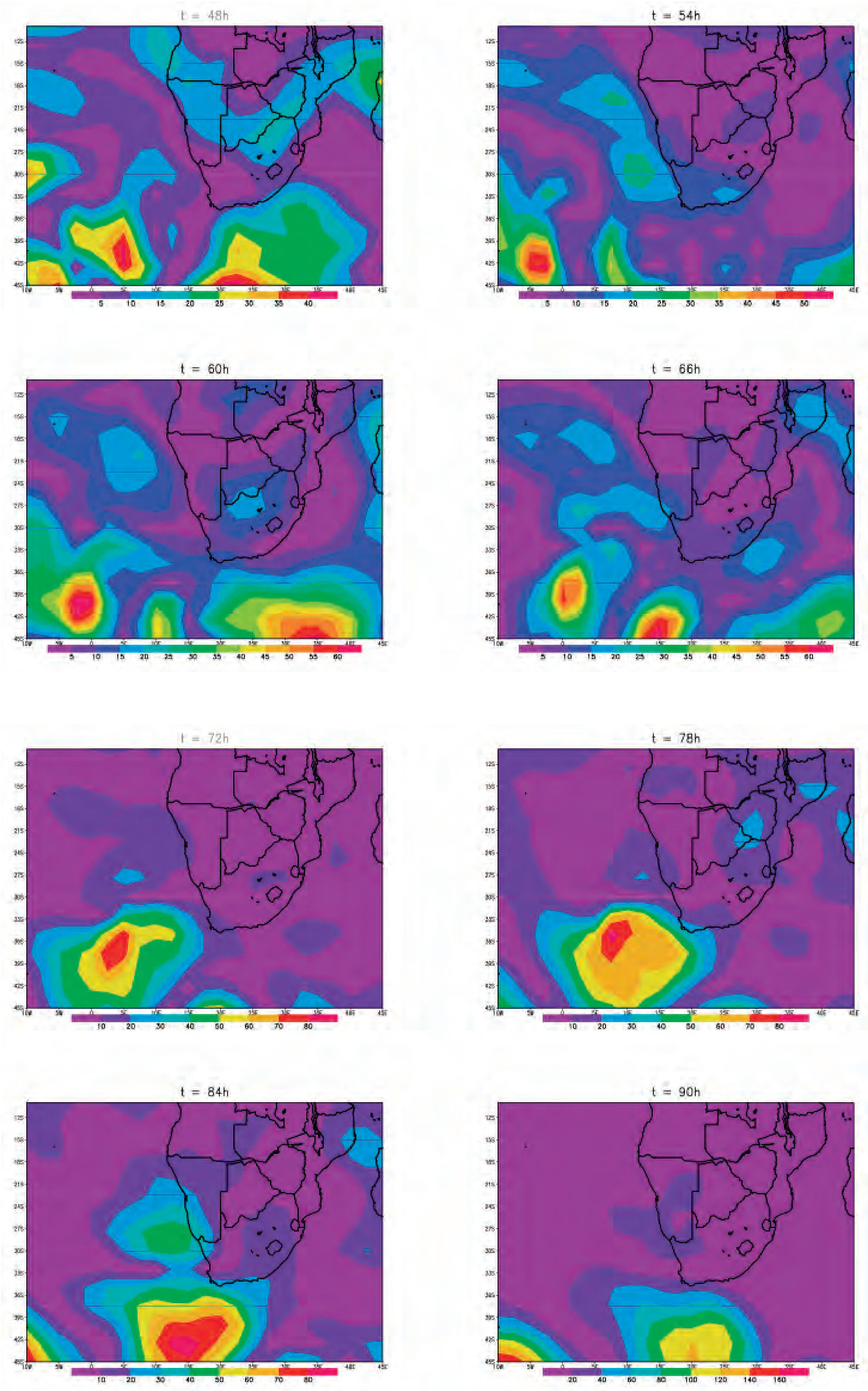

Figure 7.31 Absolute difference of 500 hPa, C-CAM – NCEP for t = 48 h to t = 90 h

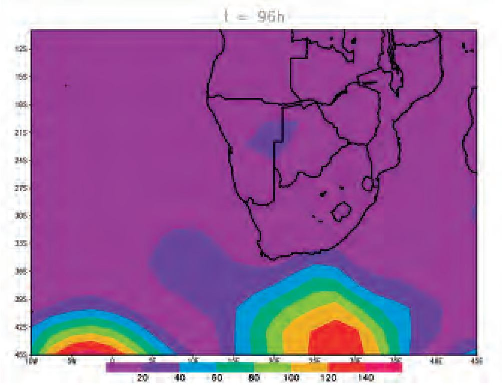

Figure 7.32 Absolute difference of 500 hPa, C-CAM – NCEP for t = 96 h

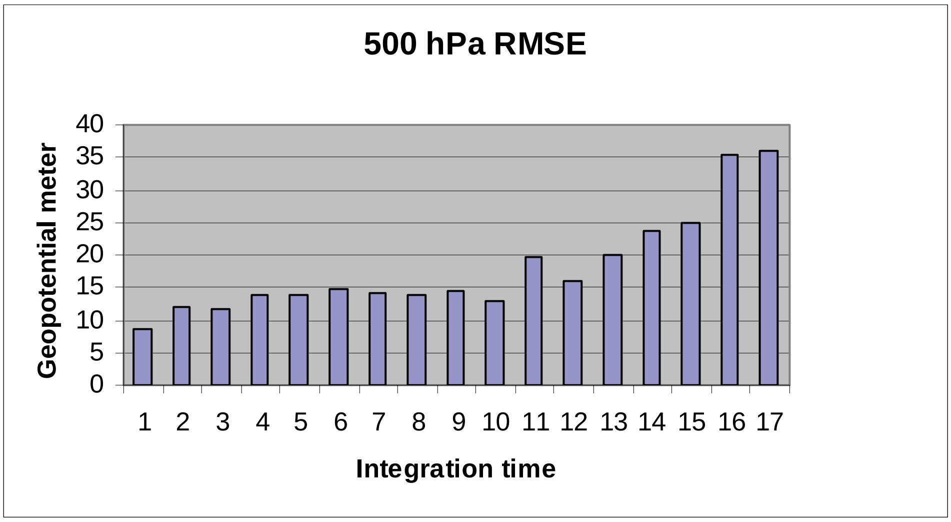

Figure 7.33 Root Mean Square Error (RMSE) of the 500 hPa geopotential height C-CAM prognosis

CONCLUSIONS

1. Overview of achievements

The main objectives of the project were to improve the simulation of water-related variables over South Africa by applying a sophisticated local-scale atmospheric model and, simultaneously, to equip African scientists with knowledge and skills to develop, maintain and use atmospheric models.

As a result of the project, strong international research links have been established with the CSIRO-AR. Both DARLAM and the more advanced C-CAM regional atmospheric models were obtained from the CSIRO-AR for use in the research. The CSIRO-AR not only provided the research team with the source code of both models, but also assisted the team considerably in improving model simulations over southern Africa. Noticeable inputs by researchers and students in the South African team contributed to these improvements. Furthermore, bilateral research activities between the research team and the CSIRO-AR contributed significantly to knowledge transfer and even encouraged some local researchers to start developing code for a unique South African model. Although the WRC project was constrained by a time limit, the capacity gained through the project established a strong platform for further sustainable research and development. Many years of atmospheric simulation completed by using both DARLAM and C-CAM have strengthened skills in running models and interpreting model output. Model development, following the initial opportunities provided by this project, has become an ongoing exercise, which promises numerous new challenges for the future.

The two very successful workshops on regional-scale atmospheric modelling that were presented in Pretoria brought the modeling community of Africa (south of the Sahara) and of the island Mauritius closer together. The majority of the participants attended both workshops and many remain in close contact with the project team. The links established with local researchers as a result of the project have already resulted in other, similar, collaborative research projects.

The Laboratory for Research and Training in Atmospheric Modelling (LRAM) is a facility that emanated from the project. It provides the foundation for research and development in atmospheric modeling at the University of Pretoria (UP) and is the focus of growing interest being shown by other research institutions and industry.

2. Research advances

To ensure a world-class approach to addressing the above-mentioned research objectives three criteria were set for the atmospheric model(s) to be employed as the point of departure, namely excellence, accessibility and applicability.

C-CAM is certainly one of the leading regional-scale models in the world, and ongoing work on model development and improvement is widely regarded as amongst the best in the world. Final results of this project have vindicated this choice of model, with C-CAM outscoring many other models in simulating rainfall over South Africa. Working with C-CAM, the UP research team managed to significantly reduce the overestimation of rainfall over the eastern parts of South Africa, typically seen in previous simulations obtained with the original versions of DARLAM and C-CAM. The numerical formulation of C-CAM's dynamics is at the leading edge of development in the world, making this model an excellent one for use in a project requiring further model improvement, as did the current WRC project. The strong international research links established through the project gave the SA research team necessary access to both the source code for C-CAM and access also to much assistance from the C-CAM development team. The collaboration between CSIRO-AR and the UP research teams in the research leading to the further development of C-CAM ensured both the accessibility and optimal use of the C-CAM model for the WRC project. C-CAM's numerical formulation and computational efficiency are of such a nature that the model can run on a standard workstation. Project achievements (particularly with regard to the improvement of rainfall simulation) and the applicability of the model with respect to the project objectives, prompted the research team to look further into using the model as a numerical weather prediction (NWP) tool – a process that has already proved successful.

The meeting of all the quality criteria for model choice set at the beginning of the project certainly contributed to the excellent model performance reflected in the results of the project.

3. New development

Much progress has been made in the development of a new dynamic kernel of a uniquely South African atmospheric model. This model will form the basis for further model development after the project. Other researchers and industry have already shown interest, particularly in the application of wind fields for air pollution modelling. The project enabled the research team to run the first NWP system independently from the SAWS, which is a major achievement. Forecasts can be viewed on the following web page: http://www.up.ac.za/academic/geog/meteo

4. Archived data

More than 200 years of atmospheric model simulations were completed during the project. All relevant data have been archived and are available from UP by contacting

hannes.rautenbach@up.ac.za or francois.engelbrecht@up.ac.za.

Four-day weather forecast results from 1 December 2004 have also been archived.

REFERENCES

1. Arakawa, A. (1966) Computational design for long-term numerical integration of the equations of fluid motion. Part I. *J. Comput. Phys*., 1, 119-143.
2. Brugge R and Moncrieff MW (1985) The effect of physical processes on numerical simulations of two-dimensional cellular convection. *Beitr. Phys. Atmos.* 58, 417-440.
3. Côté J, Beland M and Staniforth A (1983). Stability of vertical discretization schemes for semi-implicit primitive equation models. *Mon. Wea. Rev.* 1111189-1207.
4. Coffin, J. (1857) *The winds of the globe: Or the laws of the atmospheric circulation over the surface of the earth*. In "Smithsonian Contribution to knowledge 268", Vol 20, Smithsonian Institution, Washington DC.
5. Crimp, S.J., Lutjeharms, J.R.E., Mason, S.J. (1989) Sensitivity of tropical-temperate trough to sea-surface temperature anomalies in the Agulhas retroflection region. Water SA, 24 (2), 93-100.
6. Droegemeier KK and Wilhelmson RB (1987) Numerical simulation of thunderstorm outflow dynamics. Part I: outflow sensitivity experiments and turbulence dynamics. *J. Atmos. Sci.* 44 1180-1210.
7. Eliassen A (1949) The quasi-static equation of motion with pressure as independent variable. *Geophs. Publ.* 17 1-44.
8. Engelbrecht FA (2000) *Nested Climate Modelling over Southern Africa with a Semi-Lagrangian Limited Area Model.* MSc Thesis, University of Pretoria, 134 pp
9. Engelbrecht FA (2005) *Theory and application of quasi-elastic nonhyydrostatic equations in sigma-coordinates.* PhD Thesis, University of Pretoria. *To be sumitted.*
10. Engelbrecht, F.A. and Rautenbach, C.J.deW. (2000). Perspective for nested climate modeling over southern Africa. *SA Tydskrif vir Wetenskap en Tegnologie*, 19 no 2, 47-51.
11. Engelbrecht, F.A., Rautenbach, C.J.deW, McGregor, J.L. and Katzfey, J.J. (2002). January and July climate simulations over the SADC region using the limited-area model DARLAM. *Water SA*, **28** no **4**, 361-374.
12. Ferrel, W. (1859) The motion of fluids and solids relative to the earth's surface. *Math. Mon*., 1, 140-147, 210-216, 300-307, 366-372, 397- 406.
13. Haltiner, G.J. (1971) Numerical Weather Prediction. John Wiley & Sons, Inc. ISBN: 0471345806, 317pp.

14. Haltiner, G.J. and Williams, R.J. (1980) *Numerical prediction and dynamic meteorology*, Second Edition, p 119, John Wiley and Sons, Inc. New York, Chichester, Brisbane, Toronto.
15. Hoskins BJ and Pearce RP (1983) *Large-scale dynamical processes in the atmosphere.* London Academic Press.
16. Janjic ZI and Gerrity JP Jr. An Alternative Approach to Nonhydrostatic Modeling. *Mon. Wea. Rev.* 129 1164-1178.
17. Jury, M.R.,Pathack, B., Rautenbach, C.J.deW. and van Heerden, J. (1996). Drought over South Africa and Indian Ocean SST: Statistical and GCM results. *The Global Atmosphere and Ocean System*, 4, 47-63.
18. Kalnay, E. (2003) *Atmospheric modeling, data assimulation and predictability*. Cambridge University Press, ISBN: 0-521-79179-0, 341pp.
19. Todd MC, Washington R and Palmer PI (2004). Water vapour transport associated with tropical-temperate trough systems over southern Africa and the southwest Indian ocean. *Int. J. Climatol.* 24 555-568.
20. McDonald, A. (1984) Accuracy of multiply upstream semi-Lagrangian advective scheme. *Monthly Weather Review,* Vol. 112, pp 1267-1275.
21. McGregor (1986) Accuracy and initialization of a two-time level split semi-Lagrangian model. *Short- and Medium-Range Numerical Weather Prediction,* T. Matsuno, Ed, Tokyo100, Meteor. Soc. Jpn, 233-246.
22. McGregor JL (1993) Economical determination of departure points for semi-Lagrangian Models. *Mon. Wea. Rev.* **121** 221-230.
23. McGregor, J.L. (1996a) Semi-Lagrangian advection on a cubic gnomonic projection of the sphere. *Atmospheric-Ocean*, in press.
24. McGregor, J.L. (1996b) Semi-Lagrangian advection on Conformal-Cubic grids *Monthly Weather Review,* Vol. 124, 1311-1322.
25. McGregor,J.L. and Nguyen,K.L. (2003) *Simulation of the East Asian and Australian monsoons using a variable-resolution model*, CSIRO Atmospheric Research PBI, Australia.
26. McGregor, J.L. and Dix, M.R. (2001) The CSIRO conformal-cubic atmospheric GCM. In *AUTAM Symposium on Advances in Mathematical Modelling of Atmosphere and Ocean Dynamics.* P.F. Hodnett (Ed.), Kluwer, Dordrecht 197-202.
27. Mendez-Nunez LR and Carroll JJ (1994) Application of the MacCormack scheme to atmospheric nonhydrostatic models. Mon. Wea. Rev. **12**2 984-1000.

28. Mesinger F and Arakawa A (1976) *Numerical Methods used in Atmospheric Models.* Volume 1.GARP Publications series No. 17 64 pp.
29. Miller (1974) On the use of pressure as vertical coordinate in modelling convection. *Q.J.R. Meteorol. Soc.* 100, 155-162.
30. Miller MJ and Pearce RP (1974) A three-dimensional primitive equation model of cumulonimbus convection. *Q.J.R. Meteorol. Soc.* 100 133-154.
31. Miller MJ and Bets AK (1977) Travelling convective storms over Venezuela. *Mon. Weather Review.* 105 833-848.
32. Miller and White (1984) On the nonhydrostatic equations in pressure and sigma coordinates. *Quart. J. Roy. Meteor. Soc.* **110** 515-533.
33. Miranda PMA and James IN (1992) Non-linear three-dimensional effects on gravity-wave drag: Splitting flow and breaking waves. *Q.J.R. Meteorol. Soc.* 118 1057-1081.
34. Moncrieff MW and Miller MJ (1976) The dynamics and simulation of tropical cumulonimbus and squall lines. *Ibid.* 102 373-394.
35. New M.G., Hulme M., and Jones P.D. (2000) Representing twentieth-century space-time climate variability. Part II: Development of 1901-1996 monthly grids of terrestrial surface climate. *J. Climate, **13**, 2217-2238.*
36. Ogura Y and Charney JC (1962): A numerical model of thermal convection in the atmosphere. *Proc. Int. Symp. Numerical Weather Prediction,* Tokyo, Japan, Meteor. Society of Japan, 431-451.
37. Rancic', M., Purser, R.J. and Mesinger, F. (1995) A global shallow-water model using an expanded spherical cube: Gnomonic versus Conformal coordinates. *Quarterly Journal of the Royal Meteorological Society,* 122, 959-982.
38. Randal, D.A. (2000) *General circulation model development: past, present and future*. International Geophysics Series: Volume 7, Academic Press, ISBN: 0-12-578010-9, 807 pp.
39. Rautenbach, C.J.deW (1996) The construction of a data point concentration dependant weight function for interpolation to rainfall grid fields. SA Tydskrif vir Wetenskap en Tegnologie, 15 (4), 168-171.
40. Rautenbach, C.J.deW. (2003) Seasonal climate predictions with a coupled atmosphere-ocean general circulation model. *Water Research Commission Report*, 82pp
41. Richardson, L.F. (1922) *Weather prediction by numerical process*. Cambridge University Press, reprinted Dover, New York, 1965, 410pp.

42. Richtmeyer RD and Morton KW (1967) *Difference Methods for Initial Value Problems.* Interscience, New York.
43. Rivest C, Staniforth A and Robert A (1994) Spurious Resonant Response of Semi-Lagrangian Discretizations to Orographic Forcing: Diagnosis and Solution. *Mon. Wea. Rev.* 122 366-376.
44. Robert A (1993) Bubble Convection Experiments with a Semi-implicit Formulation of the Euler Equations. *J. Atmos. Sci.* 50 1865-1873.
45. Rõõm R (1998) Acoustic Filtering in Nonhydrostatic Pressure Coordinate Dynamics: A Variational Aproach. *J. Atmos. Sci.* **55** 654-668.
46. Sadourny, R. (1972) Conservative finite-difference approximations of the primitive equations on qausi-uniform spherical grids. *Monthly Weather review,* Vol.100, pp 136-144.
47. Salmon R and Smith LM (1994) Hamiltonian derivation of the nonhydrostatic pressure-coordinate model. *Quart. J. Roy. Meteor. Soc.*, 120, 1409-1413.
48. Simmons AJ, Hoskins BJ and Burridge D (1978) Stability of the semi-implicit method of time integration. *Mon. Wea. Rev.* 106 405-412.
49. Staniforth, A. and Cote', J. (1991) Semi-Lgrangian integration schemes for atmospheric models – a review. *Monthly Weather Review.* Vol. 19, 2206-2223
50. Straka JM, Wilhelmson RB, Wicker LJ, Anderson RJ and Droegemeier KK (1993) Numerical Solutions of a non-linear density current: A benchmark solution and comparisons. *Int.J. Numer. Methods fluids* 17 1-22.
51. Tanguay M, Robert A and Laprise R (1990) A semi-implicit semi-Lagrangian fully compressible regional forecast model. *Mon. Wea. Rev.* 118 1970-1980.
52. Tanguay, M., Simard, A., and Staniforth, A. (1991) A three dimensional semi-Lagrangian scheme for the Canadian regional finite-element forecast model. *Monthly weather Report.* Vol. 17, pp 1861-1871
53. Temperton, C. and Staniforth, A., 1987: An efficient two-time level semi-Lagrangian semi-implicit scheme. *Quarterly Journal of Royal Meteorological Society 113,* 1025-1039
54. Thorpe AJ and Miller MJ (1978) Numerical simulations showing the role of the downdraught in cumulonimbus motion and splitting. *Q.J.R. Meteorol. Soc.* 104 873-893.
55. Thorpe AJ, Miller MJ and Moncrieff MW (1982) Two-dimensional convection in non-constant shear: a model of mid-latitude squall lines. *Ibid.* 108 739-762.
56. Washington, W.M. and Parkinson, C.L. (1992) An introduction to three-dimansional climate modelling. University Science Books, 20 Edgehill Road, Mill Valley, California, 422pp.

57. White AA (1989) An extended version of a nonhydrostatic, pressure coordinate model. *Quart. J. Roy. Meteor. Soc.* 115 1243-1251.
58. Xue M (1989) *A Nonhydrostatic Numerical Model in Sigma-coordinates and Simulations of Mesoscale Phenomena.* PhD Thesis, Reading University, 258 pp.
59. Xue M and Thorpe AJ (1991) A mesoscale numerical model using the non-hydrostatic pressure-based σ-coordinate equations: Model experiments with dry mountain flow. *Mon. Weather. Rev.* 119 1168-1185.
60. Xie and Arkin (1996) Analyses of Global Monthly Precipitation using gauge observations, satellite estimates, and numerical model outputs. *J. Climate*, 840-858.
61. Xie and Arkin (1997) Global Precipitation: A 17-Year Monthly Analysis Based on Gauge Observations, Satellite Estimates and Numerical Model Outputs. BAMS, 78, (in press).